UILU-ENG-95-2543

EFFECTIVE CALCULATION OF LOW-VOLTAGE SOLUTIONS USING THE NEWTON-RAPHSON LOAD FLOW

RAYMOND PETER KLUMP

Power Affiliates Program

Department of Electrical and Computer Engineering

University of Illinois at Urbana-Champaign

Urbana, Illinois 61801

PAP-TR-95-7

May 1995

FOREWARD

This technical report is a reprint of the thesis written by Raymond Peter Klump as partial fulfillment of the requirements for the degree of Master of Science in Electrical and Computer Engineering at the University of Illinois.

T. J. Overbye

Thesis Advisor

May 1995

ACKNOWLEDGEMENTS

I would like to thank Professor Thomas Overbye for his guidance and encouragement. It has been an immense pleasure working with him as research assistant, and I look forward to continued graduate study with him. I am grateful also for the financial support provided by the Power Affiliates Program and its members. Finally, I would like to thank my parents, Ray and Louise; my sister, Cathy; my grandparents, Albert and Ann Orlando; my girlfriend, Karen Petit; and my friends, Mike Andrejek and Murali Venugapalan, for their constant encouragement and prayers. Most importantly I would like to thank God for placing such wonderful people in my life.

TABLE OF CONTENTS

CHAPTER 1

INTRODUCTION

1.1 The Power Flow Problem

Viewed from the standpoint of circuit analysis, the typical power system, a mammoth interconnected system of passive elements, linear and nonlinear loads, and var-limited generating units, poses a quite challenging computational problem. Linear circuit techniques presented in introductory circuit analysis classes cannot be applied to the analysis of power systems because of nonlinearities introduced through a variety of mechanisms. The nonlinearities surface not only in the characteristics of the various components of the system, including tap-changing and phase-shifting transformers, synchronous generators with saturation and var limitations, loads with nonlinear voltage dependence, and induction machines, but also in the formulation of the problem itself. Unlike other types of circuits, where voltages and currents are most likely the known quantities, real and reactive power injections are often all that are given at the system's nodes. Because power is the product of voltage and current, it is an inherently nonlinear quantity. Therefore, in its very essence, the study of power systems in steady state is a nonlinear circuit analysis problem and is thus resistant to the use of linear circuit analysis techniques, most notably superposition.

The analysis of power systems in steady state seeks the voltage magnitudes and angles and the real and reactive power injections at all nodes in the system. In power system parlance, a node is referred to as a bus, and the process of analyzing the circuit to find these quantities is known as performing a load flow or power flow. The constraints

that govern the problem and thus give rise to the system of equations to be solved are that the real power injected at each bus must balance the real power demanded from that bus, and that at all buses that are not sources of generation, the reactive power injected at the bus must balance the reactive power demanded from it. Again, because power is an inherently nonlinear quantity, these constraints constitute a set of nonlinear algebraic equations whose unknowns are the voltages at each bus, which may be expressed in either polar or rectangular form.

As is always the case when solving sets of nonlinear equations, multiple solutions, a single solution, or no solution may exist, depending upon how the system parameters have varied. Furthermore, because an iterative routine must be used to solve systems of order greater than three, even if a solution exists, it may not be found; when multiple solutions exist, any one of them may be found. It turns out that the convergence of iterative routines applied to solving systems of nonlinear algebraic equations is highly sensitive to changes in initial conditions, particularly near the boundaries of the regions of attraction of the various solutions. This is a characteristic of chaotic systems [1] and results from the fact that the boundaries of the regions of attraction of each of the solutions are fractal [2]. Thus, both the parameter variation and the location in voltage space of the initial guess affect the convergence properties of iterative nonlinear algebraic equation solvers. This characteristic has notable consequences on load flow studies, particularly when the goal is to find multiple solutions.

Given all system parameters, including line admittances, load models, generator powers, and shunt elements at all buses, a load flow study seeks to find the voltages at all

buses and the real and reactive power flowing through all the lines in the system by solving the set of nonlinear equations written with real and reactive power balances in mind. In a system with n+1 buses, there may be as many as $2n$ nonlinear equations to solve for $2n$ unknowns, and as many as 2^n solutions are possible [3]. The basis for these statistics will be discussed when the formulation of the power flow equations is detailed in the next section. Moreover, from the foregoing discussion, there may be but one solution to the set of equations, or it may be that the system has lost a solution entirely, a case that may suggest the system cannot be operated with the specified real and reactive power injections. However, this conclusion cannot be made without further investigation, for it is possible that the iterative solver failed to obtain a solution, even though one existed, due to an initial guess that lies outside the region of attraction of the solution. Because the boundaries of these regions are fractal, the likelihood of this event occurring is not terribly remote. Since the two situations are indistinguishable to the person performing the power flow (who notes only that no solution was found), it is difficult to discern the cause for the divergent behavior of the results. Fortunately, a tool has been developed to address this problem, and it will be discussed later.

More interesting from a research point of view is that an unexpected or unwanted solution may be obtained. This solution, though not the one at which the system would normally operate, is nevertheless valid in that it satisfies the mathematical constraints of the problem. Although this problem can be mitigated somewhat through proper choice of the initial guess for the iterative solver, the fractal boundaries of the region of attraction infuse a certain amount of guesswork into this approach, for there is no guarantee that the

desired solution, which traditionally has been the high-voltage solution or the "stable" solution from the standpoint of voltage stability, will be found. Traditionally, this problem has been adequately addressed by adopting the flat-start initial guess, which entails setting the voltage magnitudes at all buses to unity and the phase angles at all buses to zero. However, this approach is not foolproof. Consider a simple two-bus system with bus 1, the slack bus, connected through a phase-shifting transformer to the load bus, bus 2. Figure 1.1, which plots the boundary of the convergence regions of the high- and low-voltage solutions in the space of bus 2 real and imaginary voltage components as the phase shifter angle is changed, shows that as the phase of the transformer increases beyond 60°, the flat-start initial guess no longer yields the high-voltage solution. (Note that those guesses that converge to the high-voltage solution lie above and to the right of the plotted boundary in each case.) Although the topology of this system is not terribly realistic, as power systems evolve to incorporate more electronic controls, there likely will be an increasing number of cases for which a flat start initial guess will be inadequate.

For years, the assumption of the flat-start initial guess adequately addressed the problem of finding the desired solution. However, as researchers have become more interested in analyzing the stability of power systems, particularly as increased load demands stress power systems to the point where both their angular and voltage stability become real concerns, the "desired" solution and the high-voltage solution are now no

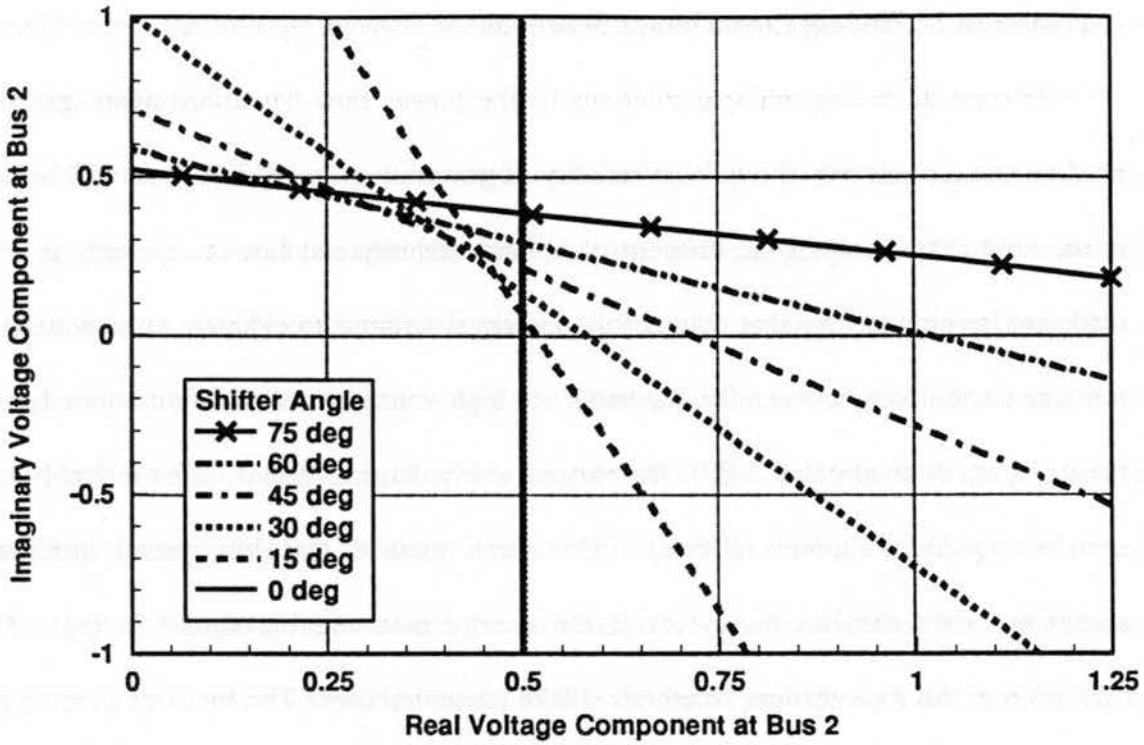

Figure 1.1: Variation of convergence region boundary with phase angle

longer synonymous. Much attention has been paid to identifying the various alternative, often termed low-voltage, solutions to the power balance equations because these are of key importance in assessing the voltage and transient stability of power systems. A simple approach, such as assuming a flat-start initial guess, will generally not work for finding the many low-voltage solutions. Proper conditioning of the initial guess to achieve the desired solutions is complicated by the complex nature of the fractal regions of convergence of each of the solutions. As a result, developing a convenient approach for finding some or all of the low-voltage solutions has become an active research area. Thus far, the results have been mixed.

1.2 Interest in Finding Low-Voltage Solutions

Interest in finding multiple solutions to the power flow equations stems from the need to assess accurately the voltage stability of power systems. While more will be said in the next chapter about the concept of voltage stability and how to quantify it, it is sufficient for now to note that many of the indices developed to evaluate voltage stability measure the distance between the "operable" or high-voltage solution, often referred to as the stable equilibrium point (SEP), and various low-voltage solutions, often referred to as unstable equilibrium points (UEPs). One such method that has gained increasing acceptance over the last few years is the energy measure, introduced in [4]. The derivation of this tool via direct methods will be presented later. The first step in using the energy measure is to perform the load flow to calculate the SEP. Then, one or more low-voltage solutions are calculated. Each UEP is then assigned its own energy measure which gauges the distance in voltage space between the SEP and that particular UEP. The smaller the energy measure for a particular UEP, the closer that solution is to the SEP and the closer the system is said to be to voltage instability. Finally, when any low-voltage solution's energy measure has become zero, that low-voltage solution and the operable solution have coalesced. Studies of the eigenvalues of the power flow Jacobian matrix [5] have shown that this union occurs through a saddle-node bifurcation, with one eigenvalue associated with each solution coalescing at the origin. This saddle-node bifurcation causes the system to incur a voltage instability, resulting in an uncontrollable collapse in the voltage profile in a portion of the system which, if not isolated through protection devices,

could infect the voltage profiles throughout the system. This process constitutes a voltage collapse.

The challenge in using the energy measure technique is not the calculation of the energy measure itself, but rather the determination of the appropriate set of low-voltage solutions. As already emphasized, a given set of power balance constraints may have a large number of different solutions, only one of which is the operable solution and the rest of which are UEPs, any one of which may be of critical interest in assessing voltage stability. Computing all of these low-voltage solutions and their associated energy measures for large systems would be an intractable problem given that no stringent guidelines exist for how to condition the initial guesses to provide each of the low-voltage solutions. Moreover, if the decision is made to find and investigate only a subset of the possible low-voltage solutions, it is unclear which solutions should be considered and which should be ignored, for it is important that the most critical low-voltage solutions not be omitted. Here, too, is the difficulty that convergence to the desired low-voltage solutions will be problematic. Computational expense, coupled with the fractal nature of the boundaries of the region of attraction, which renders conditioning of initial guesses an ineffective tool for finding many UEPs, has made the use of the energy measure concept somewhat problematic. Although some techniques have been introduced during the past few years to find critical UEPs reliably, most of them have either shown a tendency to miss solutions or proven too computationally expensive for use in an online environment.

1.3 Overview

Although knowledge of how contingencies and control actions may affect a system's voltage stability can be helpful in the planning stage, accurate voltage stability assessment can be most helpful only when performed in an online setting. When a contingency occurs in a system, rapid evaluation of voltage stability can indicate which areas are at the highest risk and which control actions should be pursued. Achieving this performance, however, requires that some rapid and reliable means of determining the most critical low-voltage solutions be developed. The goal of this research has been to advance such a method.

This thesis explores the development of a method suitable for reliable, online evaluation of the voltage stability of typical power systems. The method, developed from the structure of the power flow equations, introduces little additional computation and has been tested on a number of systems. Numerical studies have shown that the performance of this method, which shall be called the midpoint method for convenience, compares favorably with that of the most popular alternative methods.

In order to provide the proper background for understanding the mechanics of the midpoint method and the motivation for deploying it, this document will address a number of introductory topics. It will first review techniques for solving systems of nonlinear algebraic equations, with particular emphasis placed on the Newton-Raphson method. It will then describe the application of the Newton-Raphson method to the load flow problem and thus derive the set of power balance equations to be solved. Methods of improving convergence, particularly the optimal multiplier method, will also be discussed. The discussion will then turn to the concept of voltage stability and voltage collapse,

where strong emphasis will be placed on the relationship between voltage stability and load modeling and variations. This treatment will help to underscore the need for finding multiple solutions. Previous attempts at addressing this need, notably those of Tamura et al. [3], Iba et al. [6], and Ma and Thorp [7], will be presented. With this background in place, the midpoint method will be derived and demonstrated on a number of systems of various sizes. Its performance will be compared to that of its most popular predecessor on the basis of computational expense and reliability, and some conclusions will be drawn regarding its applicability. Furthermore, a useful tool for deciding at which buses to apply the midpoint method will be introduced and evaluated. Finally, a number of seemingly fruitful paths for future research in this area will be identified.

CHAPTER 2

LOAD FLOW FORMULATION AND LOW-VOLTAGE SOLUTIONS

2.1 Introduction

This chapter will first survey the techniques commonly used to solve systems of nonlinear algebraic equations in a general setting. It will then identify the techniques traditionally used in power flow studies while emphasizing the formulation of the Newton-Raphson load flow procedure. The important topic of var limit enforcement will be discussed in this setting, as well as an enhancement of the Newton-Raphson algorithm designed to prevent divergence. Finally, the concept of voltage stability will be addressed from a static generator model framework so that voltage collapse can be investigated purely from the power flow equations. The way in which static voltage stability hinges on load models and varies with loading levels and participation will be outlined to demonstrate the need for identifying and tracking multiple low-voltage solutions.

2.2 Nonlinear dc Analysis

A system of linear algebraic equations $\mathbf{Ax} = \mathbf{b}$ has a unique solution unless $\mathbf{A}$ is singular, in which case the equations are dependent. The situation in which nonlinearities are introduced is considerably more complicated, as systems of nonlinear equations may have no solution, one solution, multiple solutions, or an infinite number of solutions for a given value of the independent variable, as shown for the scalar case in Figure 2.1. The task involved in solving systems of nonlinear algebraic equations is illustrated in Figure 2.2

and can be summarized as follows: given $\mathbf{y} \in \Re^n$, find $\mathbf{x} \in \Re^n$ such that $\mathbf{f}(\mathbf{x}^*) = \mathbf{y}$.

Many techniques exist for solving this problem, and a few will now be discussed.

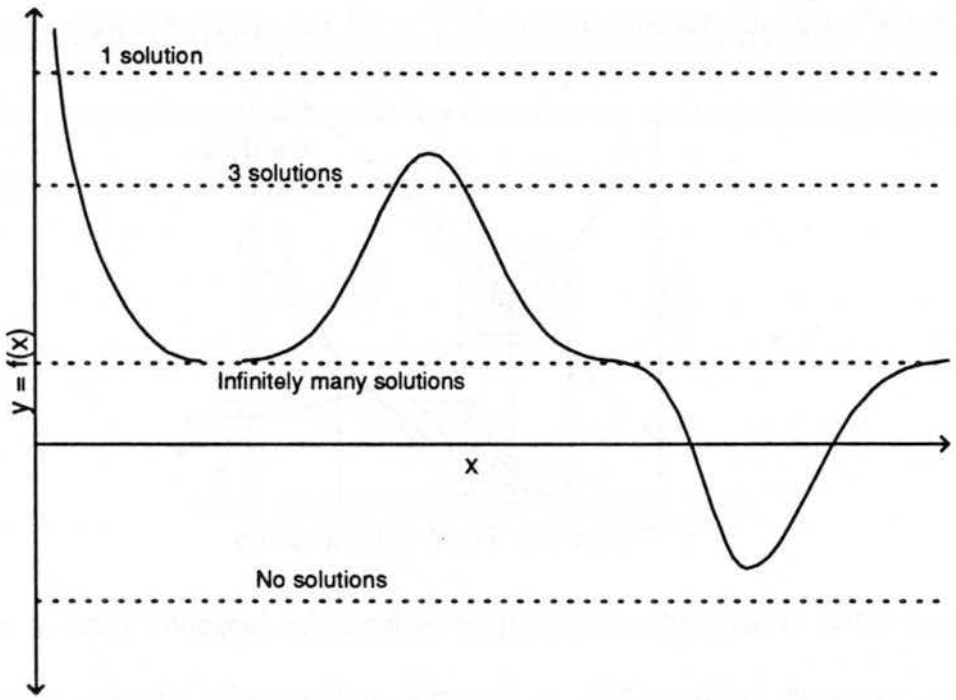

Figure 2.1: Solutions to nonlinear equations

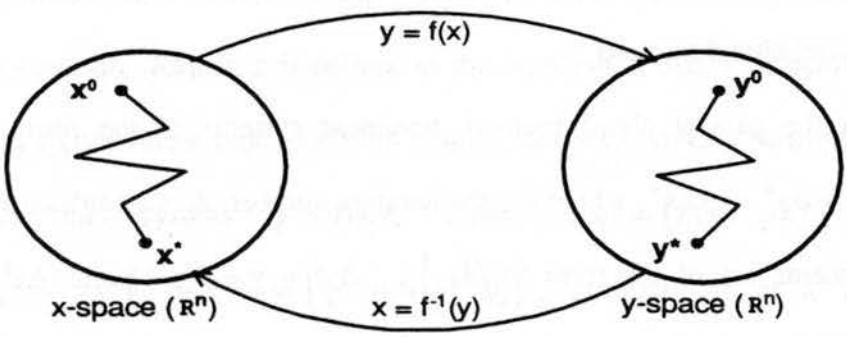

Figure 2.2: Solving nonlinear algebraic equations

2.2.1 Fixed-point iteration

When fixed-point iteration is used, a problem of the form $\mathbf{y} = \mathbf{f}(\mathbf{x})$ is recast as $\mathbf{x} = \mathbf{g}(\mathbf{x})$ through some simple algebraic manipulation. Each iteration then calculates $\mathbf{x}^{k+1} = \mathbf{g}(\mathbf{x}^k)$ until the stopping criterion $\|\mathbf{x}^{k+1} - \mathbf{x}^k\| < \varepsilon$, where ε is some small positive

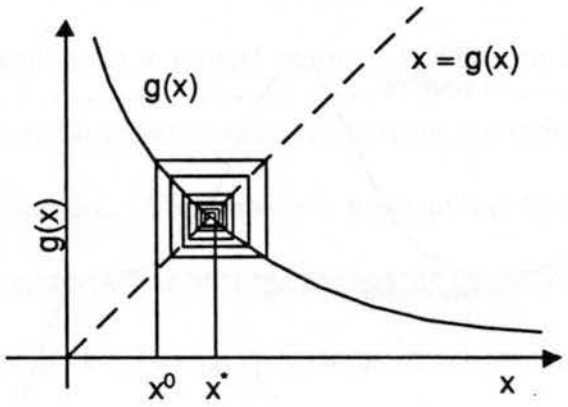

Figure 2.3: Fixed-point iteration

tolerance value, is satisfied. With this procedure, the iterations spiral in toward the solution, as shown in Figure 2.3. A limitation of fixed-point iteration, which is easily interpreted in the scalar case, is that the process will diverge if the slope of $g(x)$ at any iteration is greater than one.

2.2.2 Parallel chord method

With the parallel chord method, nonlinear systems of the form $\mathbf{y} = \mathbf{f}(\mathbf{x})$ are linearized as $\Delta\mathbf{y}^k = \mathbf{A}\Delta\mathbf{x}^k$, where k is the iteration number, $\mathbf{A}$ is a constant matrix for all k whose elements are of the form $\partial f_i/\partial x_j\big|_{\mathbf{x}^0}$, $\Delta\mathbf{y}^k = \mathbf{y} - \mathbf{f}(\mathbf{x}^k)$, and $\Delta\mathbf{x}^k = \mathbf{x}^{k+1} - \mathbf{x}^k$. These definitions may be manipulated to describe each iteration through the formula $\mathbf{x}^{k+1} = \mathbf{x}^k + \mathbf{A}^{-1}(\mathbf{y} - \mathbf{f}(\mathbf{x}^k))$. The iterations are repeated until $\mathbf{x}^k \rightarrow \mathbf{x}^{k+1}$. The constant nature of $\mathbf{A}$ indicates that, for each subsequent iteration, the solution trajectory in the

domain space is always parallel to the original trajectory. This statement is illustrated for the scalar case in Figure 2.4. The parallel chord method converges well when nonlinearities in the original system are minor, which for the scalar case suggests that the parallel chord trajectory closely resembles the actual shape of the function. However, this method has convergence problems with functions that are not monotonically increasing or decreasing.

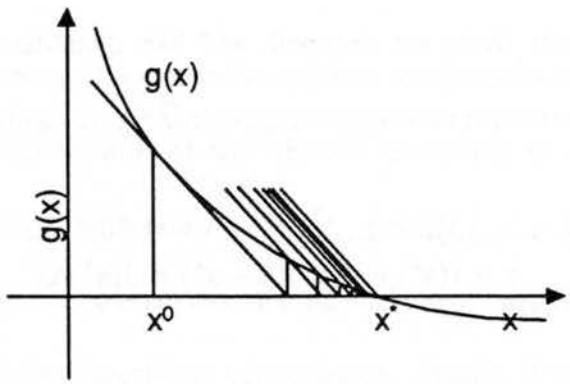

Figure 2.4: Iterations of parallel chord method

2.2.3 Newton's method

The iterative method most often applied to solving systems of nonlinear equations, Newton's method is similar in formulation to the parallel chord method except that the **A** matrix is not constant. Rather, it is defined as the Jacobian, a matrix of partial derivatives of the system's component functions with respect to its variables. Newton's method is derived for the system $\mathbf{y} = \mathbf{f}(\mathbf{x})$, where $\mathbf{f}(\mathbf{x}) = \begin{bmatrix} f_1(\mathbf{x}) & f_2(\mathbf{x}) & \cdots & f_n(\mathbf{x}) \end{bmatrix}^T$, $\mathbf{x} = \begin{bmatrix} x_1 & x_2 & \cdots & x_n \end{bmatrix}^T$, and $\mathbf{y} = \begin{bmatrix} y_1 & y_2 & \cdots & y_n \end{bmatrix}^T$, through use of a Taylor series expansion about the current iteration point $\mathbf{x}^k$. The current iteration point is related to the actual solution point $\mathbf{x}$ through the relation $\mathbf{x} = \mathbf{x}^k + \Delta\mathbf{x}$. The derivation of Newton's method proceeds as follows. The first step is to expand the system in a Taylor series:

$$\mathbf{y} = \mathbf{f}(\mathbf{x}) = \mathbf{f}(\mathbf{x}^k + \Delta\mathbf{x}) = \mathbf{f}(\mathbf{x}^k) + \mathbf{J}(\mathbf{x}^k)\Delta\mathbf{x}^k + h.o.t. \tag{2.1}$$

where *h.o.t.* denotes higher-order terms and $\mathbf{J}(\mathbf{x})$ is the Jacobian matrix defined as

$$\mathbf{J}(\mathbf{x}) = \begin{bmatrix} \frac{\partial f_1}{\partial x_1} & \frac{\partial f_1}{\partial x_2} & \cdots & \frac{\partial f_1}{\partial x_n} \\ \frac{\partial f_2}{\partial x_1} & \frac{\partial f_2}{\partial x_2} & \cdots & \frac{\partial f_2}{\partial x_n} \\ \vdots & \vdots & \ddots & \vdots \\ \frac{\partial f_n}{\partial x_1} & \frac{\partial f_n}{\partial x_2} & \cdots & \frac{\partial f_n}{\partial x_n} \end{bmatrix}. \tag{2.2}$$

Then, the higher-order terms are dropped, and like quantities are consolidated. The vector $\Delta\mathbf{x}^k$, the current iteration's approximation for $\Delta\mathbf{x}$, is identified as the variable to be solved. Then,

$$\mathbf{y} - \mathbf{f}(\mathbf{x}^k) = \mathbf{J}(\mathbf{x}^k)(\mathbf{x} - \mathbf{x}^k) = \mathbf{J}(\mathbf{x}^k)\Delta\mathbf{x}^k \tag{2.3}$$

so that

$$\Delta\mathbf{x}^k = \left[\mathbf{J}(\mathbf{x}^k)\right]^{-1}(\mathbf{y} - \mathbf{f}(\mathbf{x}^k)). \tag{2.4}$$

Then, since $\mathbf{x}^{k+1} = \mathbf{x}^k + \Delta\mathbf{x}^k$,

$$\mathbf{x}^{k+1} = \mathbf{x}^k + \left[\mathbf{J}(\mathbf{x}^k)\right]^{-1}(\mathbf{y} - \mathbf{f}(\mathbf{x}^k)). \tag{2.5}$$

This calculation is performed at the end of each iteration until the stopping criterion $\left\|\mathbf{x}^{k+1} - \mathbf{x}^k\right\| < \varepsilon$ is met. Optionally, an additional stopping constraint may be placed on the dependent variable. The important thing to note is that the Jacobian is recalculated at every iteration. The implications of this are illustrated for the scalar case in Figure 2.5.

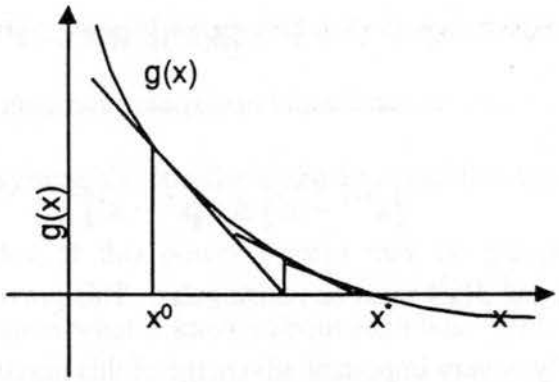

Figure 2.5: Iterations of Newton's method

An important property of any iterative solution routine is its rate of convergence. If the distance to the actual solution at any iteration is defined as $e_k = \|\mathbf{x}^* - \mathbf{x}^k\|$, then a method is said to converge with rate r if $\lim_{k\to\infty}\|e_{k+1}\| \le C\|e_k\|^r, C \neq 0$. If $r = 1$, then the routine is said to have linear convergence; the parallel chord method is such a routine. If $r > 1$, then the method has superlinear convergence. Finally, if $r = 2$, then the method converges quadratically. It can be shown that if Newton's method converges, then it does so quadratically. First, consider the Taylor expansion of $\mathbf{y} = \mathbf{f}(\mathbf{x}^*)$ about $\mathbf{x}^k$ where, instead of ignoring higher-order terms, one includes them in a remainder function $\mathbf{R}$ as follows:

$$\mathbf{y} = \mathbf{f}(\mathbf{x}^*) = \mathbf{f}(\mathbf{x}^k) + \mathbf{J}(\mathbf{x}^k)(\mathbf{x}^* - \mathbf{x}^k) + \mathbf{R}(\mathbf{x}^* - \mathbf{x}^k). \tag{2.6}$$

If the derivative of $\mathbf{J}(\mathbf{x}^k)$ is bounded, then, because $\mathbf{R}(\mathbf{x}^* - \mathbf{x}^k)$ is quadratic,

$$\|\mathbf{R}(\mathbf{x}^k - \mathbf{x}^*)\| \le \alpha\|\mathbf{x}^k - \mathbf{x}^*\|^2. \tag{2.7}$$

Using this fact together with (2.5), the following can be shown:

$$\mathbf{J}(\mathbf{x}^k)(\mathbf{x}^{k+1} - \mathbf{x}^k) = \mathbf{y} - \mathbf{f}(\mathbf{x}^k) = \mathbf{J}(\mathbf{x}^k)(\mathbf{x}^* - \mathbf{x}^k) + \mathbf{R}(\mathbf{x}^* - \mathbf{x}^k) \tag{2.8}$$

or

$$\mathbf{x}^{k+1} - \mathbf{x}^{k} = \mathbf{x}^{*} - \mathbf{x}^{k} + \left[\mathbf{J}(\mathbf{x}^{k})\right]^{-1}\mathbf{R}(\mathbf{x}^{*} - \mathbf{x}^{k}) \tag{2.9}$$

so that

$$\left\|\mathbf{x}^{k+1} - \mathbf{x}^{*}\right\| \leq C\left\|\mathbf{x}^{*} - \mathbf{x}^{k}\right\|^{2}, \tag{2.10}$$

where C is a constant and $\mathbf{J}(\mathbf{x}^{k})$ must be nonsingular. This proves that Newton's method converges quadratically, a very important advantage of this iterative method provided that it does, in fact, converge for a particular case.

2.3 Techniques of Power Flow Analysis

As discussed in the introduction, performing a load flow for a particular power system is tantamount to analyzing the circuit that models that system. The complication in this process is that the equations that describe the power system's equivalent circuit are nonlinear and thus do not lend themselves to convenient application of linear circuit theorems such as superposition. Furthermore, the elements that comprise the power system, particularly the loads, are constantly changing because they are affected by a number of factors, including consumer demand. In other words, the power system has no true "steady state." The nonlinearities of the problem are addressed by using one of the iterative routines discussed in the preceding section to solve the system of equations. The transient nature of the system's components is handled by restricting attention to the system at a single instant of time, effectively creating a steady state for the purpose of analysis. Thus, power flow analysis amounts to taking a snapshot of the nonlinear power system at a certain instant of time and using an iterative solution routine to solve the nonlinear equations that describe the system. The known quantities are various

parameters describing the system topology and the voltages at select buses. The unknown quantities are the remaining bus voltages and line flows.

A typical power system, the familiar Stagg-El Abiad five-bus system [8], is shown in Figure 2.6. The nodes of this power system may be grouped into three different categories, depending upon what is known about each bus. With reference to Figure 2.6, bus 1 is called the slack bus (also known as the swing or reference bus), bus 2 is a PV or generator bus, and buses 3, 4, and 5 are PQ or load buses. The known quantities are typically given in terms of real and reactive power injection or voltages at each bus, where the power injection $S_i = P_i + jQ_i$ at bus i is defined as $S_i = S_{gi} - S_{di}$ or equivalently as

$$S_i = (P_{gi} - P_{di}) + j(Q_{gi} - Q_{di}) \tag{2.11}$$

where the subscripts gi and di denote power supplied by the generators and power demanded by the loads at bus i, respectively. At the load buses, the known quantities are the real and reactive power injections which, because $P_{gi} = Q_{gi} = 0$ at such buses, are given by $P_i = -P_{di}$ and, $Q_i = -Q_{li}$, respectively. At the generator buses, real power injection $P_i = P_{gi} - P_{di}$ and voltage magnitude V_i are given, as well as limits on the amount of reactive power injection that can be supplied by the generators, a topic whose important implications will be discussed shortly. Finally, one node is designated as the slack bus for the system. The tasks of the slack bus are to provide an angle reference and to ensure that the net power injection calculated over all the buses in the system is zero. It does this by absorbing power if there is a net surplus of injection and generating power if there is a net shortage of injection.

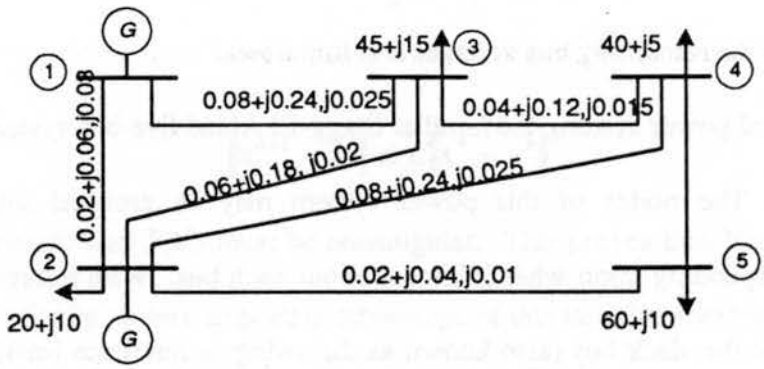

Figure 2.6: Stagg five-bus system

Traditionally, the power flow problem has been formulated using two different approaches, the Gauss-Seidel method and Newton's method, both of which may be derived by expressing the complex power injection at each bus in terms of the transfer admittances of the lines and the bus voltages. The net current injection at each bus i, defined as $I_i = I_{gi} - I_{li}$, may be expressed in terms of the admittances Y_{ik} of the lines linking bus i to each bus k and bus voltages V_k using nodal circuit analysis as $I_i = \sum Y_{ik} V_k$. Then, since complex power injection is defined as $S_i = V_i I_i^*$, it may be expressed as

$$S_i = S_{gi} - S_{di} = V_i \left(\sum_{k=1}^{n} Y_{ik} V_k \right)^* \tag{2.12}$$

so that

$$S_i^* = V_i^* \sum_{k=1}^{n} Y_{ik} V_k . \tag{2.13}$$

Equation (2.13) is the starting point for deriving both the Gauss-Seidel and Newton's methods.

2.3.1 Gauss-Seidel load flow

To derive the Gauss-Seidel method, divide both sides of (2.13) by V_i^* to obtain

$$\frac{S_i^*}{V_i^*} = \sum_{k=1}^{n} Y_{ik} V_k = Y_{ii} V_i + \sum_{k=1, \neq i}^{n} Y_{ik} V_k , \tag{2.14}$$

which may be rewritten as

$$V_i = \frac{1}{Y_{ii}} \left[\frac{S_i^*}{V_i^*} - \sum_{k=1, \neq i}^{n} Y_{ik} V_k \right] = h_i(V_2, \ldots, V_n), \tag{2.15}$$

where it has been assumed that the slack is numbered as bus 1 so that V_1 is not a variable. Equation (2.15) is an implicit formula for V_i and may be viewed as an implementation of fixed-point iteration. Similar equations may be written for all unknown bus voltages $\mathbf{x} = [V_2 \ldots V_n]$ so that the following system of equations is formed:

$$\begin{aligned} x_1^{k+1} &= h_1(x_1^k, x_2^k, \ldots, x_{n-1}^k) \\ x_2^{k+1} &= h_2(x_1^k, x_2^k, \ldots, x_{n-1}^k) \\ &\vdots \\ x_{n-1}^{k+1} &= h_{n-1}(x_1^k, x_2^k, \ldots, x_{n-1}^k) . \end{aligned} \tag{2.16}$$

The fixed-point iteration scheme used to solve this system is called Gauss-Jacobi iteration. A variation on this formulation involves using the current iteration's values of variables already found to solve for the current iteration's values of the remaining variables. This method is called Gauss-Seidel iteration and is expressed mathematically as

$$\begin{aligned} x_1^{k+1} &= h_1(x_1^k, x_2^k, \ldots, x_{n-1}^k) \\ x_2^{k+1} &= h_2(x_1^{k+1}, x_2^k, \ldots, x_{n-1}^k) \\ &\vdots \\ x_{n-1}^{k+1} &= h_{n-1}(x_1^{k+1}, x_2^{k+1}, \ldots, x_{n-1}^k) . \end{aligned} \tag{2.17}$$

The Gauss-Seidel method is fairly easy to code, and each iteration converges relatively

fast. However, this method is essentially a fixed-point iteration scheme and thus tends to converge slowly and to miss solutions. For these reasons, most load flow studies are conducted using the Newton-Raphson method.

2.3.2 Newton-Raphson load flow

The Newton-Raphson load flow equations may be derived from (2.13) using either polar or rectangular coordinates. Both forms are frequently used and will thus be derived in this section.

Derivation of Polar Form

The first task in deriving the polar form of the Newton-Raphon load flow equations is to let $\mathrm{V}_i = V_i\angle\theta_i = V_i\cos\theta_i + jV_i\sin\theta_i$ and $\mathrm{Y}_{ik} = g_{ik} + jb_{ik}$ in (2.13) to obtain

$$\begin{aligned}\mathrm{S}_i^* = P_i - jQ_i = \sum_{k=1}^{n} V_iV_k\begin{bmatrix} g_{ik}(\cos\theta_i\cos\theta_k + \sin\theta_i\sin\theta_k) + \\ b_{ik}(\sin\theta_i\cos\theta_k - \cos\theta_i\sin\theta_k)\end{bmatrix} \\ + j\left\{\sum_{k=1}^{n} V_iV_k\begin{bmatrix} g_{ik}(\cos\theta_i\sin\theta_k - \sin\theta_i\cos\theta_k) + \\ b_{ik}(\cos\theta_i\cos\theta_k + \sin\theta_i\sin\theta_k)\end{bmatrix}\right\}.\end{aligned} \tag{2.18}$$

By equating the real and imaginary parts of both sides and using the trigonometric identities

$$\begin{aligned}\cos(a-b) &= \cos a\cos b + \sin a\sin b \\ \sin(a-b) &= \sin a\cos b - \cos a\sin b\end{aligned}, \tag{2.19}$$

two real equations are obtained:

$$P_i = \sum_{k=1}^{n} V_iV_k\left[g_{ik}\cos(\theta_i - \theta_k) + b_{ik}\sin(\theta_i - \theta_k)\right] \tag{2.20}$$

$$Q_i = \sum_{k=1}^{n} V_iV_k\left[g_{ik}\sin(\theta_i - \theta_k) - b_{ik}\cos(\theta_i - \theta_k)\right]. \tag{2.21}$$

These equations express the Newton-Raphson power flow in polar coordinates.

Derivation of Rectangular Form

The first task in deriving the load flow equations in rectangular coordinates is to define $V_j = u_j + w_j$ for all j and $Y_{ik} = g_{ik} + jb_{ik}$. These expression are substituted into (2.13) which, after all multiplications have been performed, can be rewritten as

$$S_i^* = P_i - jQ_i = \sum_{k=1}^{n} \begin{matrix} (u_i u_k g_{ik} - u_i w_k b_{ik} + w_i w_k g_{ik} + w_i u_k b_{ik}) + \\ j(u_i w_k g_{ik} + u_i u_k b_{ik} - u_k w_i g_{ik} + w_i w_k b_{ik}) . \end{matrix} \tag{2.22}$$

By collecting terms and equating the real and imaginary parts on both sides, the rectangular form of the Newton-Raphson equations is obtained:

$$P_i = \sum_{k=1}^{n} \left[g_{ik}(u_i u_k + w_i w_k) + b_{ik}(u_k w_i - u_i w_k) \right] \tag{2.23}$$

$$Q_i = \sum_{k=1}^{n} \left[g_{ik}(u_k w_i - u_i w_k) - b_{ik}(u_i u_k + w_i w_k) \right]. \tag{2.24}$$

Problem Formulation

Define $\mathbf{x}$ as the set of unknowns and $\mathbf{f(x)}$ as the set of constraints at all buses in the system. Functionally,

$$\begin{aligned} \mathbf{x} &= \begin{bmatrix} \boldsymbol{\theta} \\ |\mathbf{V}| \end{bmatrix} = \begin{bmatrix} \mathbf{x}_\theta \\ \mathbf{x}_V \end{bmatrix} \text{ in polar form;} \\ \mathbf{x} &= \begin{bmatrix} \mathbf{u} \\ \mathbf{w} \end{bmatrix} = \begin{bmatrix} \mathbf{x}_u \\ \mathbf{x}_w \end{bmatrix} \text{ in rectangular form;} \\ \mathbf{f(x)} &= \begin{bmatrix} \mathbf{P(x)} - \mathbf{P} \\ \mathbf{Q(x)} - \mathbf{Q} \end{bmatrix} = \begin{bmatrix} \mathbf{f}_P(\mathbf{x}) \\ \mathbf{f}_Q(\mathbf{x}) \end{bmatrix} \end{aligned} \tag{2.25}$$

where the elements of $\mathbf{x}_\theta$, $\mathbf{x}_V$, $\mathbf{x}_u$, $\mathbf{x}_w$, $\mathbf{f}_P$, and $\mathbf{f}_Q$ are each defined at only a subset of the system buses, and the elements of $\mathbf{P(x)}$ and $\mathbf{Q(x)}$ are evaluated using (2.20) and (2.21) for

the polar form or (2.23) and (2.24) for the rectangular form. Note that **P** and **Q** are the sets of known nominal values of real and reactive bus power injections. The vector **f**(**x**), the set of power balance equations, is called the mismatch vector because it expresses the difference between the functional values of real and reactive power injections and the given information. The goal of the Newton-Raphson iteration is to drive these mismatches to zero. Then, all problem constraints will be satisfied.

The set of unknowns and constraints associated with each bus in a system hinges fundamentally on bus type. Since real and reactive power injections are allowed to vary at the slack bus to keep the voltage magnitude and angle fixed, the slack is not represented in either **f**(**x**) or **x**. At load bus *i*, since both real and reactive power injections are specified and bus voltage (represented in either polar or rectangular coordinates) is allowed to vary, then $f_i(\mathbf{x}) = \begin{bmatrix} P_i(\mathbf{x}) - P_i \\ Q_i(\mathbf{x}) - Q_i \end{bmatrix}$ and $x_i = \begin{bmatrix} \theta_i \\ V_i \end{bmatrix}$ or $\begin{bmatrix} u_i \\ w_i \end{bmatrix}$. Finally, at PV buses, where reactive power is allowed to vary within limits to hold bus voltage magnitude constant, $f_i(\mathbf{x}) = \left[P_i(\mathbf{x}) - P_i\right]$ and $x_i = \left[\theta_i\right]$ or $\begin{bmatrix} u_i \\ w_i \end{bmatrix}$. An additional constraint on bus voltage magnitude, expressed as $V_i^2 = u_i^2 + w_i^2$, is enforced when the rectangular formulation is used.

The Newton iteration step is given by (2.5). Since the objective is to find **x** such that **y** = **f**(**x**) = **0**, then

$$\mathbf{x}^{k+1} = \mathbf{x}^k - \left[\mathbf{J}(\mathbf{x}^k)\right]^{-1} \mathbf{f}(\mathbf{x}^k) \tag{2.26}$$

where

$$\mathbf{J}(\mathbf{x}^k) = \begin{bmatrix} \dfrac{\partial \mathbf{f}_P(\mathbf{x}^k)}{\partial \mathbf{x}_\theta} & \dfrac{\partial \mathbf{f}_P(\mathbf{x}^k)}{\partial \mathbf{x}_V} \\ \dfrac{\partial \mathbf{f}_Q(\mathbf{x}^k)}{\partial \mathbf{x}_\theta} & \dfrac{\partial \mathbf{f}_Q(\mathbf{x}^k)}{\partial \mathbf{x}_V} \end{bmatrix} \tag{2.27}$$

is the load flow Jacobian. Iterations continue until $\left\|\mathbf{f}(\mathbf{x}^k)\right\| < \varepsilon$, a tolerance.

As already shown, the Newton-Raphson power flow will converge to a solution quadratically, provided that the initial guess is good. Moreover, if a bus's load exhibits a voltage dependence of, for example, $P_{Li} = a_0 + a_1 V_i + a_2 V_i^2$, it is automatically incorporated into the problem through the Jacobian. Finally, the Newton-Raphson power flow generally exhibits a larger region of convergence than the Gauss-Seidel method. However, factoring the Jacobian is an expensive process, particularly for large systems, so each iteration requires more time to execute. Moreover, the boundaries of the regions of attraction tend to be fractal. This characteristic complicates the task of finding multiple low-voltage solutions.

2.3.3 Reactive power limits

PV buses vary their reactive power output to maintain a certain voltage level. However, they are limited in the amount of reactive power that they can provide for a given real power injection. When the reactive output of the generator reaches its limit, the generator no longer controls the local bus voltage, and the bus must be treated as a PQ bus, with reactive power injection fixed at the limiting value. Because the problem formulation changes with this type switching (an additional reactive power constraint is created, and the voltage at the former PV bus is now a variable), a nonlinearity is added to the linearized Newton-Raphson power flow equations. As this may affect the

convergence properties of the load flow, the manner in which var limits arise and the way in which they are handled must be carefully considered.

The reactive power output of each online generator is adjusted during power flow solutions to control the voltage of its local bus or of a remote bus. The amount of allowable variation in reactive power output is not unlimited, however, as fixed or variable limits Q_{max} and Q_{min} must be obeyed. These limits stem from the reactive capability curve, an example of which is shown in Figure 2.7. Each local-control generator holds the voltage of its local bus between the desired range V_{hi} and V_{lo} as long as its reactive power limit remains between Q_{max} and Q_{min}. Each bus controlled by a remote generator yields precedence to the var requirements of that generator's local bus when the local bus's voltage no longer falls inside the range defined by V_{hi} and V_{lo}, so that the remote bus is no longer controlled. When the reactive power limits are violated, neither the local bus nor the remote bus are controlled by the generator. The remote bus's reactive power requirements are then divided among its remaining remote-control generators.

Although var limits are usually treated as constants by power flow programs, they actually are functions of both the real power output and terminal voltage of the machine. The limits are governed by three factors [9], two of which affect machine currents. Armature current is limited to a value I_{amax} due to heat generated in the armature windings, and field current is limited to I_{fdmax} due to heat generated in the field windings. The third constant governs the heat generated by eddy currents in the stator laminations. If the generator is modeled as a constant voltage behind synchronous reactance jX_s, then the limits Q_f and Q_a due to field winding and armature winding heating may be expressed as

$$Q_f = \sqrt{\frac{X_d^2}{X_s^2} I_{fd\max}^2 V_t^2 - P^2} - \frac{V_t^2}{X_s} \tag{2.28}$$

$$Q_a = \sqrt{I_{t\max}^2 V_t^2 - P^2} \tag{2.29}$$

where V_t is the terminal voltage of the machine, P is the real power output of the machine, and X_d is the machine's d-axis transient reactance. These equations are derived in [9]. The limits Q_f and Q_a, as well as the limit Q_e caused by heating due to eddy currents, are identified in the reactive capability curve of Figure 2.7.

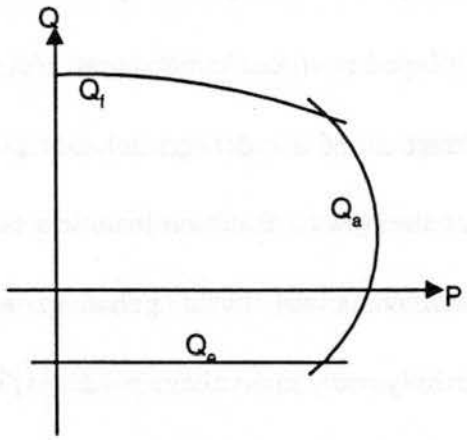

Figure 2.7: Reactive power capability curve

To prevent divergence during the first few iterations of the power flow, the var limits are usually relaxed. In subsequent iterations, if a var limit is violated, the offending PV bus is recast as PQ with its var injection set to the violated limit. The power flow calculation is performed to obtain a new set of voltages. If the formerly offending PV bus now possesses enough var capability to maintain the new bus voltage, then it will be returned to PV status. These actions affect the rate of convergence of the method. In fact, if the sensitivity of Q_{max} to changes in bus voltage is high, as is the case when Q_a becomes the limiting factor (see Figure 2.7), the rate of convergence decreases quite

noticeably [9], and the power flow may even fail to converge. Thus, proper enforcement of var limits in load flow calculations is a key concern.

2.4 Optimal Multiplier

When a power flow fails to converge, it is difficult to determine the reason for the divergence. It may be that the system cannot operate at the specified loading level and thus has no operating point for which the load demand can be satisfied. Alternatively, if the load flow fails to converge even though the system does have a real solution, the failure may perhaps be attributed to a poor initial guess. An initial guess is poor if it lies outside the region of attraction of the desired solution point. Since the regions of attraction encountered with the Newton-Raphson load flow have fractal, multidimensional boundaries, properly conditioning the initial guess to achieve a desired solution (particularly one of the possibly many low-voltage solutions) is impractical. Hence, when a load flow fails to converge, it is necessary to know the cause for the failure. Norm-reducing techniques offer a solution to this problem.

Norm-reducing techniques are modifications of Newton's method designed to prevent divergence. They entail scaling the correction vector $\Delta\mathbf{x}^k = \left[\mathbf{J}\left(\mathbf{x}^k\right)\right]^{-1}\mathbf{f}\left(\mathbf{x}^k\right)$ so that $\left\|\mathbf{f}\left(\mathbf{x}^{k+1}\right)\right\| < \left\|\mathbf{f}\left(\mathbf{x}^k\right)\right\|$ for $k = 0, 1, 2, \ldots$. This ensures that the solution guess $\mathbf{x}^k$ improves with each iteration, thus preventing divergence. Several possible norm-reducing techniques exist; they differ in how the modification of the correction vector is performed. One method is to scale the vector $\Delta\mathbf{x}$ by a scalar multiplier μ. Another method involves scaling each component of $\Delta\mathbf{x}$ by its own associated multiplier μ. Finally, $\Delta\mathbf{x}$ may be

modified by the addition of some vector that reduces the norm of the mismatch equations. While all three methods may find application in load flow calculations, the first technique is the most popular, and it tends to be used only with the rectangular load flow formulation. Its use in the rectangular-coordinate load flow calculation was first formulated in [10], from which the following discussion borrows.

The optimal multiplier is most conveniently developed if the load flow equations are formulated as follows. Let m be the number of buses in the system, and let $n = 2m$ be the number of unknowns. Define the vector of unknowns as $\mathbf{x} = \begin{bmatrix} x_1 & \cdots & x_n \end{bmatrix}^T$, the set of real and imaginary parts of all bus voltages. Let $\mathbf{S}$ be the specified values at all buses that include the real and reactive power injections at all PQ buses and the real power injection and square of the voltage magnitude at all PV buses. Thus, $\mathbf{S} = \begin{bmatrix} \mathbf{P}_s & \mathbf{Q}_s & |\mathbf{V}_s|^2 \end{bmatrix}^T$. Let $\mathbf{S}(\mathbf{x}) = \begin{bmatrix} \mathbf{P}(\mathbf{x}) & \mathbf{Q}(\mathbf{x}) & |\mathbf{V}(\mathbf{x})|^2 \end{bmatrix}^T$ be the functional values of the quantities defined in $\mathbf{S}$. The load flow problem then seeks a solution $\mathbf{x}$ such that $\mathbf{S} = \mathbf{S}(\mathbf{x})$. Because all terms of $\mathbf{S}(\mathbf{x})$ are quadratic, the load flow problem may be expressed as

$$\mathbf{S} = \mathbf{S}(\mathbf{x}) = \mathbf{A} \begin{bmatrix} x_1 x_1 \\ x_1 x_2 \\ \vdots \\ x_i x_j \\ \vdots \\ x_n x_n \end{bmatrix}. \tag{2.30}$$

This may be expanded in Taylor series about the current iteration's guess x^k to obtain the exact expression

$$\mathbf{S} = \mathbf{S}(\mathbf{x}^k) + \mathbf{J}(\mathbf{x}^k)\Delta\mathbf{x}^k + \mathbf{S}(\Delta\mathbf{x}^k). \tag{2.31}$$

Newton's method ignores the quadratic remainder term and thus obtains

$$\Delta \mathbf{x}^k = \left[\mathbf{J}\left(\mathbf{x}^k\right)\right]^{-1}\left(\mathbf{S} - \mathbf{S}\left(\mathbf{x}^k\right)\right) = \left[\mathbf{J}\left(\mathbf{x}^k\right)\right]^{-1}\mathbf{f}\left(\mathbf{x}^k\right). \tag{2.32}$$

Then,

$$\mathbf{x}^{k+1} = \mathbf{x}^k + \mu\Delta\mathbf{x}^k \tag{2.33}$$

where μ, a scalar called the optimal multiplier, is ordinarily unity. Hopefully, $\left\|\mathbf{f}\left(\mathbf{x}^{k+1}\right)\right\| < \left\|\mathbf{f}\left(\mathbf{x}^k\right)\right\|$, but this is not guaranteed.

Instead of choosing μ as unity, define it so as to guarantee that $\left\|\mathbf{f}\left(\mathbf{x}^{k+1}\right)\right\| < \left\|\mathbf{f}\left(\mathbf{x}^k\right)\right\|$. A convenient and effective way to do this is to minimize the square of the norm of $\mathbf{f}(\mathbf{x})$ along $\Delta\mathbf{x}^k$. In other words, choose μ to minimize the cost function

$$h = \frac{1}{2}\sum_{k=1}^{n}\left[\mathbf{S} - \mathbf{S}\left(\mathbf{x}^k + \mu\Delta\mathbf{x}^k\right)\right]^2. \tag{2.34}$$

The power flow calculation has thus been recast as a nonlinear programming problem whose goal is to minimize the quartic cost function of (2.34). Solution of the power flow problem has thus become a byproduct of the minimization.

In deriving the optimal multiplier, the first task is to scale $\Delta\mathbf{x}$ by μ in (2.31) and to recognize that $\mathbf{S}(\Delta\mathbf{x})$ is quadratic. Therefore,

$$\mathbf{S} - \mathbf{S}\left(\mathbf{x}^k\right) - \mu\mathbf{J}\left(\mathbf{x}^k\right)\Delta\mathbf{x}^k - \mu^2\mathbf{S}\left(\Delta\mathbf{x}^k\right) = \mathbf{0}. \tag{2.35}$$

Then, to make the notation more compact, three quantities are defined:

$$\begin{aligned}
\mathbf{a} &= \left[a_1 \quad \cdots \quad a_n\right]^T = \mathbf{S} - \mathbf{S}\left(\mathbf{x}^k\right) \\
\mathbf{b} &= \left[b_1 \quad \cdots \quad b_n\right]^T = -\mathbf{J}\left(\mathbf{x}^k\right)\Delta\mathbf{x}^k \\
\mathbf{c} &= \left[c_1 \quad \cdots \quad c_n\right]^T = -\mathbf{S}\left(\Delta\mathbf{x}^k\right).
\end{aligned} \tag{2.36}$$

Therefore, $\mathbf{a} + \mu\mathbf{b} + \mu^2\mathbf{c} = \mathbf{0}$. Then, the cost function of (2.34) becomes

$$h = \frac{1}{2}\sum_{i=1}^{n}\left(a_i + \mu b_i + \mu^2 c_i\right)^2 . \tag{2.37}$$

To minimize (2.37), set $\frac{\partial h}{\partial \mu} = 0$, thus obtaining the cubic equation

$$g_0 + g_1\mu + g_2\mu^2 + g_3\mu^3 = 0 \tag{2.38}$$

where

$$\begin{aligned} g_0 &= \sum_{i=1}^{n} a_i b_i \qquad g_1 = \sum_{i=1}^{n}\left(b_i^2 + 2a_i c_i\right) \\ g_2 &= 3\sum_{i=1}^{n} b_i c_i \qquad\quad g_3 = 2\sum_{i=1}^{n} c_i^2 . \end{aligned} \tag{2.39}$$

This cubic equation may have either three real roots or one real root and two complex conjugate roots. If only one real root μ exists, then (2.37) has only a single local extremum which, because (2.37) is quartic and positive, will be a minimum. If (2.38) has three real roots, then the smallest of the three, which shall be designated as μ, will lead to the closest local minimum of (2.37) along $\Delta\mathbf{x}$; the middle root (μ_2) will lead to the local maximum, and the largest root (μ_3) will lead to the further local minimum. Thus, μ always minimizes the norm of the power flow mismatch equations, thus ensuring that the next iteration's guess improves upon the previous iteration's estimate. In this way, use of the optimal multiplier μ prevents divergence of the power flow.

At a solution to the load flow problem, evaluating h in (2.37) yields zero. However, if no solution is found, h stays at a certain positive value. If μ approaches zero as the iterations proceed, a solution for the system does not exist, and the load flow Jacobian will become singular. Finally, if h remains nonzero, thus indicating that a solution has not been

found, but μ remains approximately unity, then a load flow solution does exist for the system but failed to converge there from the initial guess due to an arithmetic precision problem. Thus, use of the optimal multiplier has removed some of the guesswork involved in assessing the cause of power flow divergence. The optimal multiplier will play a key role in the formulation of the midpoint method.

It is interesting to consider the rate of convergence of the Newton-Raphson algorithm when the optimal multiplier is employed. To investigate this, (2.8) is rewritten as

$$\mathbf{J}(\mathbf{x}^k)(\mathbf{x}^{k+1} - \mathbf{x}^k) = \mu\mathbf{J}(\mathbf{x}^k)(\mathbf{x}^* - \mathbf{x}^k) + \mu\mathbf{R}(\mathbf{x}^* - \mathbf{x}^k). \tag{2.40}$$

Then,

$$\mathbf{x}^{k+1} - \mathbf{x}^k = \mu\mathbf{x}^* - \mu\mathbf{x}^k + \mu\left[\mathbf{J}(\mathbf{x}^k)\right]^{-1}\mathbf{R}(\mathbf{x}^* - \mathbf{x}^k) \tag{2.41}$$

$$\mathbf{x}^{k+1} - \mu\mathbf{x}^* + (\mu - 1)\mathbf{x}^k = \mu\left[\mathbf{J}(\mathbf{x}^k)\right]^{-1}\mathbf{R}(\mathbf{x}^* - \mathbf{x}^k) \tag{2.42}$$

$$\mathbf{x}^{k+1} - \mu\mathbf{x}^* = \mu\left[\mathbf{J}(\mathbf{x}^k)\right]^{-1}\mathbf{R}(\mathbf{x}^* - \mathbf{x}^k) + (1 - \mu)\mathbf{x}^k \tag{2.43}$$

$$\mathbf{x}^{k+1} - \mathbf{x}^* - (\mu - 1)\mathbf{x}^* = \mu\left[\mathbf{J}(\mathbf{x}^k)\right]^{-1}\mathbf{R}(\mathbf{x}^* - \mathbf{x}^k) + (1 - \mu)\mathbf{x}^k \tag{2.44}$$

$$\mathbf{x}^{k+1} - \mathbf{x}^* = \mu\left[\mathbf{J}(\mathbf{x}^k)\right]^{-1}\mathbf{R}(\mathbf{x}^* - \mathbf{x}^u) + (\mu - 1)(\mathbf{x}^* - \mathbf{x}^k) \tag{2.45}$$

Finally, in light of (2.7), Equation (2.45) may be rewritten as

$$\left\|\mathbf{x}^{k+1} - \mathbf{x}^*\right\| \le C'\left\|\mathbf{x}^* - \mathbf{x}^k\right\|^2 + D'\left\|\mathbf{x}^* - \mathbf{x}^k\right\|, \tag{2.46}$$

where C' and D' are constants. Note that if μ approaches unity at least linearly, then the quadratic convergence of the Newton-Raphson is preserved.

2.5 Non-Uniqueness of Load Flow Solutions

Because any practical load flow problem entails solving a system of nonlinear equations, generally more than one solution exists. The multiplicity of solutions arises as follows. If the voltages at all buses in the system are known, then all power injections are uniquely determined by a set of linear nodal equations of the form $S_i = V_i \sum_{k=1}^{n} Y_{ik}^{*} V_k$. However, if S_i is known at bus i instead of V_i, then the corresponding equation is quadratic in V_i, and the set of equations has two solutions. Finally, if all the voltages for the n-1 nonslack buses are unknown and all the power injections are known, then a quadratic equation may be written for each nonslack bus, each of which may have two solutions. If all possible combinations of solutions to these equations are counted, one finds that a maximum of 2^{n-1} solutions to the load flow equations may exist. The number of these solutions tends to decrease as system loading is increased [11]. While all solutions may be physically feasible, implying that the system could, in fact, operate at the point in question, only one of the solutions is practical. This is the solution with the highest voltages and lowest power losses [11].

An interesting way to view the existence of multiple power flow solutions was proposed in [11] in the form of what the authors termed "load flow functions." A load flow function is obtained by reducing the n nodal equations into one equation of order 2^n in one of the unknown voltages. Such a function is continuous and has a number of extrema and zeros. The zeros are the solutions to the load flow problem for that particular bus. A load flow function may be written for each bus in the system. The set of

possible solutions for the entire system is then the set of combinations of various zeros of each of the load flow functions. A key observation made in [11] is that the number of zeros for each load flow function decreases as loading is increased. Hence the number of solutions for the entire system also decreases as loading is increased.

Another way to visualize the existence of multiple solutions is to consider an analytical tool called the PV curve. A PV curve provides some insight into how power flow solutions vary with load. In particular, it shows how voltage magnitude V_i at bus i varies with real power load P_j at bus j, where it is often the case that $i = j$. With the reactive power load held constant, a series of power flow solutions is performed for varying P_j, and V_i is then plotted as a function of P_j. A typical PV curve, often called the nose curve because of its shape, is shown in Figure 2.8. One can readily see that corresponding to each active power level up to $P_j = P_{max}$, two solutions for V_i are possible, one of which is termed the high-voltage solution and the other the low-voltage solution. As loading is increased, these two solutions move closer together until they coalesce for $P_j = P_{max}$. This load level is called the point of maximum loadability. If the load being varied is modeled as constant power, then the PV curve thus drawn is a bifurcation diagram, and a saddle-node bifurcation occurs at the nose of the curve. This can be observed by inspecting the eigenvalues of the power flow Jacobian at solutions near the nose point and noting that one of them changes sign as the curve is traced around the nose. The point at which saddle-node bifurcation occurs is also called the fold point or turning point, and the power flow Jacobian is singular at this load level.

It is important to note that this analysis holds only when loads are modeled as constant power; that is, the PV curve is a bifurcation diagram and the nose point corresponds to a saddle-node bifurcation only when loads are modeled as constant power. The interpretation of PV curves for other load models will be discussed in a later section. Regardless of the type of load model, it is clear that beyond $P_j = P_{max}$, the system does not have a solution. In other words, the system simply cannot supply a real power load at bus j that exceeds P_{max}. Thus, this PV curve illustrates how, as loading increases, a high-voltage and a low-voltage solution move closer together until they merge into one solution and finally disappear. The implications of this behavior for voltage stability will be discussed shortly. QV curves, which plot bus voltage as reactive power at a bus or buses is varied while real power load is held constant, can be drawn in a similar manner. Finally, such curves can be drawn for all buses in the system. The union of all such curves forms an n+1-dimensional manifold which, if visualizable, would show how the system state approaches maximum loadability as loading is increased throughout the system.

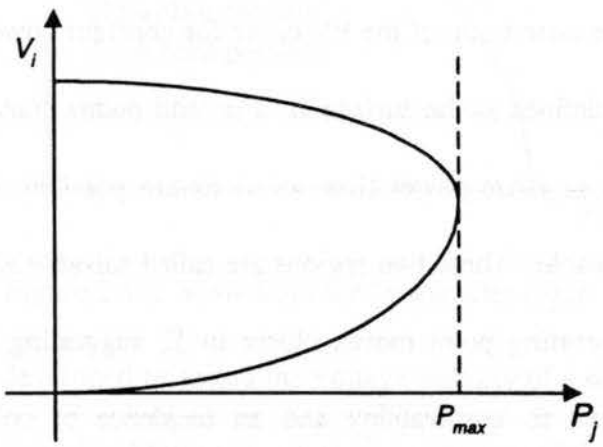

Figure 2.8: Typical PV curve

An interesting characteristic of PV curves is that generally they are not simple parabolas but may take a number of twists and turns. For example, the PV curve of Figure 2.9 was generated for the Stagg five-bus system when the real power load at bus 4 was varied from its starting value of 40 MW. In addition to the expected parabolic shape (the outer curve), there is a second portion which introduces two additional solutions for $P_4 < 160$ MW. Thus, for P_4 less than this load level, four solutions to the power flow equations exist. As loading is increased beyond this level, the two additional solutions vanish, leaving the high-voltage solution and a final low-voltage solution that approach each other until they coalesce at $P_{max} = 365$ MW. Similar curves may be drawn at the other system buses. Thus, it is clear from these diagrams that the number of power flow solutions decreases as loading is increased.

While PV and QV curves offer one perspective of the multiplicity of power flow solutions, a load parameter space representation such as the one sketched in Figure 2.10 can also be helpful. This figure plots the set of fold points in load parameter (MW, Mvar) space. Recall that a fold point is a parameter value for which the Jacobian is singular, and it is equivalent to the nose point of the PV curve for constant power loads. The set of all fold points shall be defined as the surface Σ. For load points contained within the region bounded by Σ, two or more power flow solutions are possible, while outside of Σ the power flow is unsolvable. These two regions are called solvable and unsolvable. As load is increased, the operating point moves closer to Σ, suggesting that increased loading might eventually lead to unsolvability and an incidence of collapse. A number of

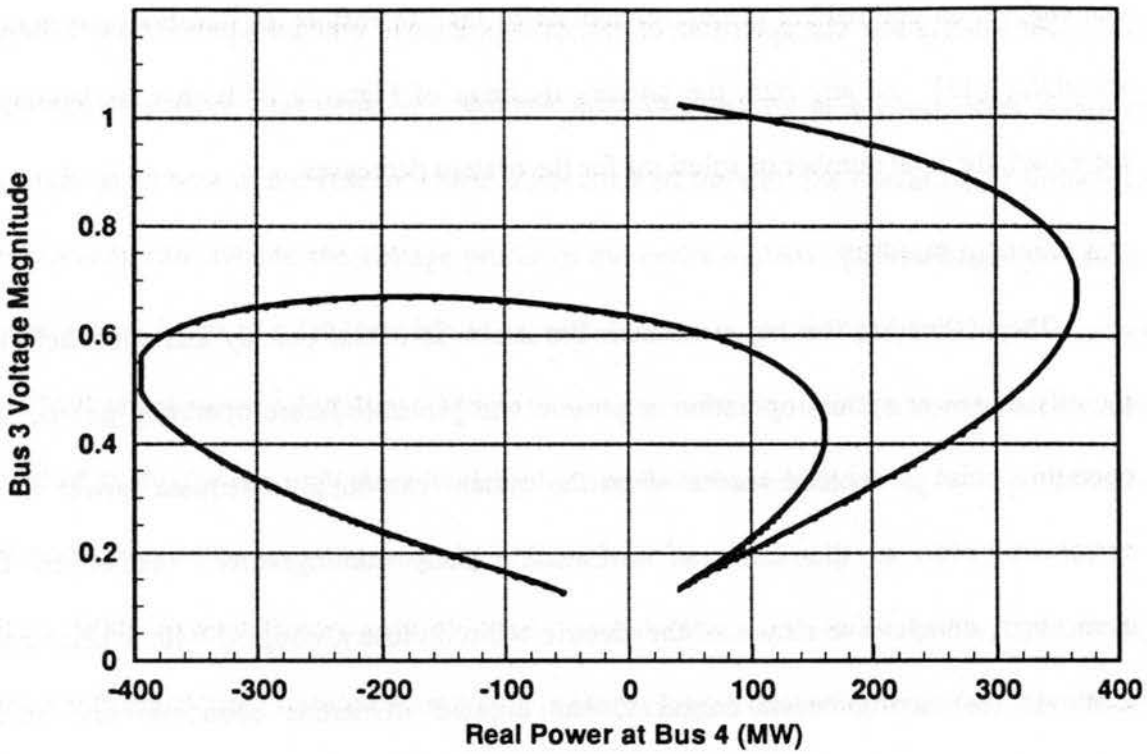

Figure 2.9: Example of a more complicated PV curve

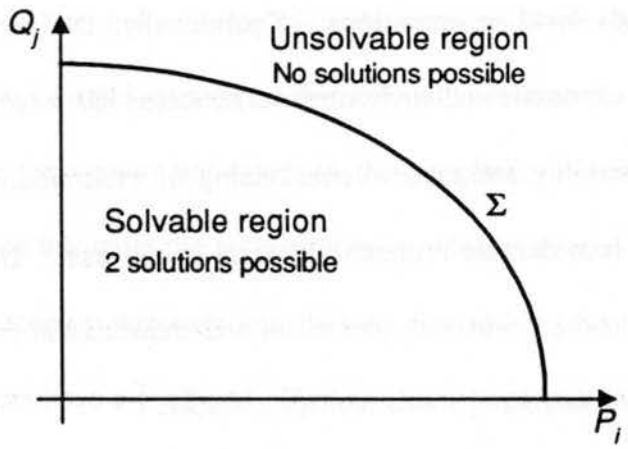

Figure 2.10: View from load parameter space

techniques have been developed to assess the voltage stability of a solvable system's state in terms of its proximity to Σ. Moreover, a technique for quantifying the unsolvability of points outside of Σ was recently presented in [12]. This method is promising because it

can suggest an optimal set of control actions to take to restore an unsolvable system to solvability [13]. At any rate, the primary message of Figure 2.10 is that, as loading is increased, the total number of solutions for the system decreases.

2.6 Voltage Stability

The motivation for this research is the desire to assess quickly and accurately the security of power system operation at present and probable future operating points. An operating point is deemed secure when the system can supply adequate power to all customers, even in the event of statistically likely contingencies. However, the increasingly competitive nature of the electric utility industry, coupled with a heightened sensitivity to environmental concerns, has created numerous economic and social constraints that restrict security enhancement efforts. No longer can a utility decide to install an additional generating unit or build new transmission lines without serious financial and perhaps legal repercussions. Traditionally, the need to balance system security issues with economic and environmental concerns has resulted in the problems of transient (angular) stability and thermal overloading of transmission system lines–topics that have attracted considerable research attention in the past. However, the growing imbalance between load growth and generation and transmission expansion has led to a new and increasingly fearsome nemesis, voltage collapse.

Voltage stability is the ability of a system to maintain voltage so that when load admittance is increased, load power also increases, so that both power and voltage are controllable [14]. To be judged voltage-stable, the system must maintain acceptable voltage levels at all buses, both in the steady state and following a disturbance. When a

system loses voltage stability, it no longer can maintain acceptable bus voltage levels and thus fails to serve load demand. Voltage instability results in a continuous decay of voltage in an area of the system which, if not isolated through the operation of protective equipment, can collapse the voltage profile of the entire system. This collapse can occur over a time frame of a few seconds to several minutes or even hours, making it a rather difficult phenomenon to analyze. Moreover, voltage stability is still a somewhat nascent field of study, for although there have been many disturbances involving voltage collapse over the last twenty years, the majority of these have occurred only since 1982.

While several factors may ultimately contribute to system insecurity, among the most influential causes are increased system loads, larger interutility transfers, and fewer additions to the transmission system. These factors may push a system to the point where either discrete contingencies such as an outage of a generating unit, or gradual parameter variation such as hourly load growth, may cause the system to lose stability. Interestingly, most reports of voltage instability suggest that the collapse was not immediately due to large disturbances in the system but rather to the progressive evolution of the system operating point [4]. In this case, the system moves gradually toward a state in which bus voltage magnitude becomes extremely sensitive to changes in load so that even minute fluctuations in load can have a profound effect on the voltage profile. Since system load exhibits only quasistatic behavior, the high sensitivity of bus voltages becomes a significant concern.

The effect of high sensitivity of bus voltage on changes in load may be conceptualized by studying the PV curve of Figure 2.8. As load admittance is increased,

load power increases rapidly at first, and then slowly, before reaching a maximum at the nose point. Before the maximum power transfer point is reached (that is, for operation on the top half of the PV curve), the load is supplied by high voltage and low current. Thus, little loss is incurred across the transmission lines. As load admittance is increased beyond the maximum power transfer point, however, load power begins to decrease as it is now supplied by low voltage and high current. The increased current flowing through the primarily reactive transmission lines incurs heavy reactive power losses, thus taxing the reactive power output capability of the generators. The generators, which use reactive power to maintain their voltage setpoints, quickly reach their limits and, therefore, no longer maintain their nominal voltages. Voltages decrease further, resulting in even heavier current flow through the transmission lines in order to serve load demand. This results in further losses, creating an uncontrollable decrease in voltage in an area of the system which, if not isolated by protective devices, will result in unacceptably low voltages throughout the system and consequent loss of load. Thus, it is clear that a deficit of reactive power is ultimately responsible for declining voltages, and increased system loading exacerbates this decline.

Because the move toward voltage collapse may occur over a diverse and unpredictable time frame, the voltage stability problem may be viewed in both a static and a dynamic sense. For example, in assessing voltage stability, one could be concerned with determining how much extra loading the system or its interconnections can tolerate before it can no longer serve load. This is tantamount to tracing the top of the PV curve as loading is increased and noting whether or not the system can still meet the demand. This

view treats voltage stability as a static problem, for it asks not how the system will react if it is suddenly perturbed from a given state, but rather just the identity of the state and its associated load capability. Alternatively, one might wonder whether a discrete outage such as a loss of a system component can be sustained by the system without causing an uncontrollable change in voltage. In other words, the system's response to perturbations about its current stable operating point is of interest. This amounts to investigating voltage stability in a dynamic sense. Both static and dynamic viewpoints have merit and each command a different set of analysis tools. Unfortunately, this dichotomy has fostered a great deal of confusion about the precise nature of voltage stability and how to quantify it. Thus, while the treatment of transient stability is fairly mature, present understanding of voltage stability is still somewhat limited.

Dynamic analysis of voltage stability is the less developed of the the two frameworks, primarily because it is the more abstruse and computationally challenging approach. The primary hurdle to understanding dynamic voltage stability has been that such an analysis requires dynamic models of load, generators, and other system devices [15]. While the state of generator dynamic models has evolved with the study of transient stability assessment, the inclusion of dynamic load models in transient stability studies of moderately loaded systems was seen to have little effect on stability results [16]. Therefore, the set of good aggregate, time-varying load models is deficient because of a lack of interest. Nevertheless, the need to identify the stability of the system's equilibrium points exists, so development of accurate load models is likely to accelerate.

Typically, power systems are represented by a set of differential-algebraic equations of the form

$$\begin{aligned} \dot{\mathbf{x}}(t) &= \mathbf{f}\big(\mathbf{x}(t), \mathbf{y}(t), \mathbf{u}(t)\big) \\ \mathbf{0} &= \mathbf{g}\big(\mathbf{x}(t), \mathbf{y}(t), \mathbf{u}(t)\big) \end{aligned} \tag{2.47}$$

where $\mathbf{x}(t)$ is the set of state variables, $\mathbf{y}(t)$ is the set of algebraic variables, and $\mathbf{u}(t)$ is the set of system inputs such as real and reactive power injections. This model may be as detailed as one desires, but typically for voltage stability studies, the structure-preserving or the internal-node classical models [5] suffice.

The manner in which $\mathbf{u}(t)$ is treated determines whether a static or a dynamic assessment of voltage stability is to be conducted. Ultimately, this decision depends on the type of load and generator models being used. Depending on these models, the set of inputs may be subdivided into various components as

$$\mathbf{u}(t) = \mathbf{u}^{\text{slow}}(t) + \mathbf{u}^{\text{small}}(t) + \mathbf{u}^{\text{fast}}(t) + \mathbf{u}^{\text{large}}(t). \tag{2.48}$$

The relative sizes of these components determine how well a particular static or dynamic stability assessment approach will work. If the effects of large disturbances such as line or generating unit outages are to be addressed, then a dynamic approach should definitely be adopted. The dynamic assessment framework provides two different approaches. For fast perturbations about the stable equilibrium point, small-signal analysis is employed, which involves inspecting the eigenvalues of the matrix $\mathbf{A}$ of the linearized system

$$\begin{bmatrix} \Delta\dot{\mathbf{x}} \\ \mathbf{0} \end{bmatrix} = \begin{bmatrix} \mathbf{A}_{11} & \mathbf{A}_{12} \\ \mathbf{A}_{21} & \mathbf{A}_{22} \end{bmatrix} \begin{bmatrix} \Delta\mathbf{x} \\ \Delta\mathbf{y} \end{bmatrix} + \begin{bmatrix} \mathbf{B}_1 \\ \mathbf{B}_2 \end{bmatrix} \Delta\mathbf{u} \tag{2.49}$$

and determining if any lie in the right-half plane. Under drastic assumptions about voltage

control and load characteristics, this small-signal analysis may be performed using solely the eigenvalues of the load flow Jacobian [14]. However, if $\mathbf{u}^{large}$ is substantial, then small-signal analysis does not apply. Moreover, if $\mathbf{u}^{slow}$ is significant, then the time frame of interest becomes long and linearized analysis may no longer provide an accurate picture. For both of these cases, time-domain simulation is the recommended, albeit computationally expensive, choice.

However, as has already been mentioned, the lack of an instigating fault is one of the main distinguishing characteristics of voltage collapse from transient stability problems. Instead, voltage stability assessment often focuses on the effects of gradual parameter variation and migration of the operating point. The components $\mathbf{u}^{large}$ and $\mathbf{u}^{fast}$ are no longer relevant and are thus neglected, leaving

$$\mathbf{u}(t) = \mathbf{u}^{slow}(t) + \mathbf{u}^{small}(t). \tag{2.50}$$

Typically one assumes that $\mathbf{u}^{small}$ is negligible and that $\mathbf{u}^{slow}$ is a slowly varying average load that can be approximated fairly well as a constant $\mathbf{u}(t) = \hat{\mathbf{u}} = \mathbf{u}^{slow}(t_0)$, where t_0 is some starting time. Under these assumptions, the differential-algebraic model of (2.47) may be rewritten as

$$\begin{aligned} \dot{\mathbf{x}} &= \mathbf{f}(\mathbf{x}(t), \mathbf{y}(t), \hat{\mathbf{u}}) = \hat{\mathbf{f}}(\hat{\mathbf{x}}, \hat{\mathbf{y}}) \\ \mathbf{0} &= \mathbf{g}(\mathbf{x}(t), \mathbf{y}(t), \hat{\mathbf{u}}) = \hat{\mathbf{g}}(\hat{\mathbf{x}}, \hat{\mathbf{y}}). \end{aligned} \tag{2.51}$$

This system does not depend on t and is hence autonomous. As a result, a point $(\mathbf{x}_0, \mathbf{y}_0)$, which is an equilibrium point for time t_0, is an equilibrium point for all time. Therefore, using the nomenclature of [17], the system can be approximated as being time invariant with fixed input $\hat{\mathbf{u}}$ and "frozen equilibrium" point $(\mathbf{x}_0, \mathbf{y}_0)$. The stability of this time-

invariant system is then used to gauge the stability of the original system about the frozen equilibrium point. In the absence of $\mathbf{u}^{small}$, provided that $\mathbf{u}^{slow}$ is indeed sufficiently laggard, the system state will reside in a vanishingly small area centered about the frozen equilibrium, and stability would then not be in question. This approach is the motivation for the use of load flow in voltage stability analysis, because the possible frozen equilibria are identified as the stable part of the PV curve is traced. However, because power systems are constantly subjected to minute parameter changes, the system state is continually pushed about the frozen equilibrium. This may place stability in jeopardy, particularly in the case of heavily stressed systems that may be identified as those frozen equilibria lying close to the bifurcation point on the PV curve. Static voltage stability analysis thus investigates how immune the system's stability is to these random parameter variations for operation at each of the various frozen equilibria. The stability characteristics of the frozen equilibria are judged according to where they lie on the PV curve.

The accuracy of the static approach to voltage stability assessment depends fundamentally on the way in which the system loads and the generator excitation loop are modeled. If the generator excitation loop is assumed to be stable, then static stability assessment is ideally suited to cases in which the load is modeled as constant power. For this topology, frozen equilibria on the upper half of the nose curve are stable, those on the bottom half are unstable, and the nose point is the state at which the system loses stability via a saddle-node bifurcation. If load is modeled as having a voltage dependence of the form $P(V) + jQ(V) = P_L V^{k_p} + jQ_L V^{k_q}$ where k_p and k_q are less than one, then the system

will again lose stability via a saddle-node bifurcation, although proximity to the nose point of the PV curve will no longer be an indicator of proximity to collapse because the nose point will no longer be the bifurcation point. If, on the other hand, k_p and k_q are greater than one, then the load models, when used in conjunction with an assumed stable exciter, never result in an unstable system. In this case, static stability assessment fails because of poor system models. Modeling deficiencies again plague static stability assessment when constant power loads are used with the IEEE Type I exciter [16]. In this case, the system loses stability via a Hopf bifurcation at low load levels and then regains stability shortly after a singularity induced bifurcation occurs fairly close to the nose of the PV curve, so that the entire lower half of the PV curve is predicted to be stable. These results are puzzling; they do not seem to reflect usual power system operation because they prematurely predict a loss of stability due to a Hopf bifurcation, an occurrence that cannot be detected using static stability techniques such as energy measures. This suggests that static load models are inadequate when generator dynamics are modeled. In [16] it was found that a load model of the form

$$\begin{aligned} T_{G_i}\dot{G}_i &= P_i - (V_i)^2 G_i \\ T_{B_i}\dot{B}_i &= Q_i - (V_i)^2 B_i \,, \end{aligned} \tag{2.52}$$

which features variable conductance and susceptance with a first-order delay, provided good results when used with generator dynamics models, particularly as T_{Gi} and T_{Bi} increase. As these time constants grow, indicating that the load responds more and more slowly, the point of Hopf bifurcation moves closer to the nose point of the PV curve until it no longer occurs; then, stability is lost via a saddle-node bifurcation involving an

eigenvalue related to load dynamics. This situation is ideally suited to the application of static voltage stability assessment because it mirrors the results of using constant power loads with stable exciters. Since much of a conventional system's load responds slowly, static stability assessment is a fairly reliable tool. However, with the advent of more electronic controls on power systems, this situation may change.

Methods that gauge the voltage stability of a system should indicate whether a system is stable or unstable, how close a stable system is to becoming unstable, and the mechanism by which an unstable system lost stability [9]. A number of techniques have been developed to address these issues in the static sense. These techniques may be categorized as depending either on a future assumed path to collapse or on the characteristics of the present operating point alone. Among those which belong to the first category is the point-of-collapse method [18], which solves the Newton-Raphson power flow repeatedly for a given variation in **u** with the explicit condition that the Jacobian be singular. With reference to Figure 2.10, the point-of-collapse method measures the distance along the path of a prescribed parameter variation from a point within the solvable region to the Σ boundary. Other methods that require a presumed path to collapse include those measuring how much additional real or reactive load can be added to a bus or buses before the operating point is driven to the nose of the PV or QV curves, and VQ sensitivity, which addresses the effect of additional reactive loading alone on bus voltage magnitudes. The disadvantage of this latter method is that it stresses the system in an unrealistic fashion. The major drawback of all these methods is they assume that future load variation is at least approximately known. However, this is not always the

case, particularly under the unusually stressed conditions associated with voltage collapse. The techniques that depend only on the current operating point, such as the use of the minimum singular value of the power flow Jacobian to indicate how close the Jacobian is to becoming singular [19], seek to mitigate these deficiencies. However, these techniques generally fail to indicate how or where an instability will occur and usually cannot take into account future changes in system parameters such as generators attaining their var limits.

A class of techniques which tries to marry the advantages of both these approaches utilizes the tendency of the load flow to have multiple solutions for a given loading. These methods do not require an assumed path to collapse, and they also can take future system changes, such as the enforcement of var limits, into account. The voltage instability proximity index (VIPI), introduced in [20], utilizes the angle between the vectors corresponding to two solutions in state space as an index. Another such technique, which is used extensively in this research, uses energy functions to quantify the distance between the operable solution and any of a number of type-one low-voltage solutions. This method was first presented in [4] and will be summarized here.

2.7 Energy Methods

A system of the form $\dot{\mathbf{x}} = \mathbf{f}(\mathbf{x},\alpha)$, with $\mathbf{f}$ a vector of possibly nonlinear functions having an equilibrium point $\mathbf{x}_e = \mathbf{0}$, is said to be asymptotically stable in a region Ω about $\mathbf{x}_e$ if there exists a positive definite function $V(\mathbf{x})$ such that $\dot{V}(\mathbf{x})$ evaluated along the system's trajectory is negative definite in Ω. This sufficiency theorem, an expression of Lyapunov's second method for assessing the stability of general systems, suggests that for

all trajectories originating within Ω, the state of the system will eventually return to the equilibrium point at the origin. One may thus think of Ω as defining a potential well whose valley is the equilibrium state. If the system originally resides at the bottom of the well and is perturbed slightly, it will behave much as a ball would if kicked up a hill. If the kick is small enough that the ball does not roll over the hill (meaning that the energy given the ball by the kick does not exceed the potential energy at the top of the hill), it will eventually return to the bottom. Similarily, a system that is perturbed slightly will return asymptotically to the equilibrium point if the energy with which it is imparted, say V, does not exceed the height of the potential well V^{cr}. However, if $V > V^{cr}$, the system state, like the overzealously displaced ball, will "roll" out of the equilibrium point's basin. The system is then said to be unstable. This ball-in-well analogy provides a good illustration for assessing system security via energy methods.

Energy methods generalize Lyapunov's second method to systems for which the negative definiteness for the chosen $V(\mathbf{x})$ cannot be guaranteed. Such techniques have proved quite useful in determining the transient stability of power systems [21]. In these applications, the energy well is fixed about the assumed stationary post-fault equilibrium, and as long as the energy of the post-fault trajectory is less than the energy associated with the potential energy boundary surface (that is, the height of the potential well), the system state will return to the post-fault stable equilibrium point (SEP). Note that the shape of the potential energy boundary surface is such that it connects all the various unstable equilibrium points (UEPs). These UEPs are located at saddle points of the energy function, which are values of $\mathbf{x}$ for which $\nabla V(\mathbf{x}) = \mathbf{0}$. At any rate, it is the depth of the

energy well that indicates the stability of the system. In voltage stability assessment, the situation is somewhat different. Here the equilibrium point is not fixed, but is slowly migrating with time as **u** varies. The shape of the energy well also varies, because the set of UEPs on the well's boundary varies with changes in **u**. As the system becomes more heavily stressed, the depth of the well decreases. When the system is on the verge of collapse, the well is shallow enough that even the random load variations can cause the state to escape, resulting in a quick decline of the voltage profile in all or part of the system. Hence, the depth of the well is the the figure of interest.

A scalar function $V(\mathbf{x})$ is developed for a multimachine power system in [17]. This energy function, which is not formally a Lyapunov function when losses are considered, may be expressed as

$$\begin{aligned} v(\mathbf{x}^u) = & -\frac{1}{2}\sum_{i=1}^{n}\sum_{j=1}^{n} b_{ij}V_i^u V_j^u \cos(\theta_i^u - \theta_j^u) + \frac{1}{2}\sum_{i=1}^{n}\sum_{j=1}^{n} b_{ij}V_i^s V_j^s \cos(\theta_i^s - \theta_j^s) \\ & - \left[\sum_{i=1}^{n}\int_{V_i^s}^{V_i^u} \frac{Q_i(\mathbf{x})}{\mathbf{x}}\, d\mathbf{x}\right] - \mathbf{P}^{\mathrm{T}}(\theta^u - \theta^s) - \sum_{i=1}^{n}\sum_{i=1}^{n} g_{ij}V_i^s V_j^s \cos(\theta_i^s - \theta_j^s)(\theta_i^u - \theta_i^s) \\ & - \sum_{i=1}^{n}[V_i^s]^{-1}\sum_{j=1}^{n} g_{ij}V_i^s V_j^s \sin(\theta_i^s - \theta_j^s)(V_i^u - V_i^s) \end{aligned} \tag{2.53}$$

where

$Y_{ij} = g_{ij} + jb_{ij}$ is the ijth element of the admittance matrix;

V_k^s, V_k^u denote bus k voltage magnitudes at the SEP and the UEP of interest, respectively;

θ_k^s, θ_k^u denote bus k angles at the SEP and UEP of interest, respectively; and

$S_k = P_k + jQ_k(\mathbf{x})$ denotes complex power injection at bus k.

In deriving this energy function, it was assumed that reactive power injection could be an arbitrary polynomial or exponential function of bus voltage magnitude, but that real power injection is independent of bus voltage magnitude in order to keep $\mathcal{V}(\mathbf{x})$ path independent and thus realizable in closed form. Also, it was assumed that the voltage control loop is stable and that the only modeling of voltage control is the inclusion of var limits to represent exciter saturation. This latter assumption is very important to note, because it indicates that the use of energy functions to predict vulnerability to voltage instability must be restricted to those situations where stability is lost through disappearance of the steady-state operating point through saddle-node bifurcation; the method will not be accurate when Hopf bifurcation is the culprit. Since proximity only to saddle-node bifurcation points can be monitored, the relevant UEPs to use with the energy measure are those whose associated Jacobian has a single positive eigenvalue. In other words, the energy function will be evaluated only at type-one UEPs. Since the Jacobian of the linearized dynamic system and the Jacobian of the power flow equations have the same number of eigenvalues with positive real part when the aforementioned assumptions are made [22], a UEP can be identified as type-one strictly on the basis of its load flow Jacobian.

The energy function approach has many useful features which make it an attractive choice for assessing the security of a system. As shown in [17], if energy measure contours are plotted in PQ space, they are primarily parallel to the maximum loadability boundary Σ and fairly evenly spaced. Hence, they can provide a relative stability ranking for a number of equilibrium points. Moreover, since the right eigenvector associated with the positive eigenvalue of a type-one UEP's Jacobian approximates the initial direction the

collapse would take if that particular UEP were the critical one [23], and since this eigenvector has relatively large components at only a subset of the system buses, then the energy measure corresponding to each UEP can be associated with a particular area of the system. For example, if a particular type-one UEP has a relatively large component at bus 1, then the corresponding energy measure would indicate proximity to collapse centered about bus 1. This is a useful interpretation. Finally, it was mentioned earlier that the energy function can take future system changes, particularly var limit enforcements, into account. This is true because var limits are enforced separately in calculating the high- and the low-voltage solutions. This characteristic is particularly advantageous because low-voltage solutions tend to drive generators to their limits, thus lowering the height of the potential well that the system state must overcome to collapse.

Thus, energy functions offer a smoothly varying, easily computed and interpreted measure of the proximity to collapse in an area of the system. Evaluating the function at a number of different type-one UEPs allows one to obtain and compare the security of different areas of the system and thereby identify the most stressed areas. Obviously, this requires that one somehow find this multitude of type-one solutions, a task which is far from straightforward. Moreover, one has no way of knowing which type-one solutions will be the critical ones as loading evolves. Consequently, the goal is to track a number of type-one low-voltage solutions in a manner independent of future load variation. These ideas will be illustrated in the next section.

2.8 The Need for Multiple Low-Voltage Solutions

Consider the lossless, symmetric three-bus system shown in Figure 2.11. Buses 1 and 2 are the load buses, while bus 3 is the slack bus. Such a system might model a large load center serviced by remote generation. At base loading, this system has four solutions, identified as solutions A, B, C, and D in Table 2.1. Solution A is the operable solution. The high voltage magnitudes assigned to buses 1 and 2 for solution A result in the least transmission losses and thus make solution A the desired operating point for the system. Solutions B and C are type-one low-voltage solutions, while solution D is a type-two low-voltage solution. Recall that under the assumption that the voltage control loop is stable, the system will lose stability via a saddle-node bifurcation. Therefore, only the type-one solutions will be of interest in this discussion.

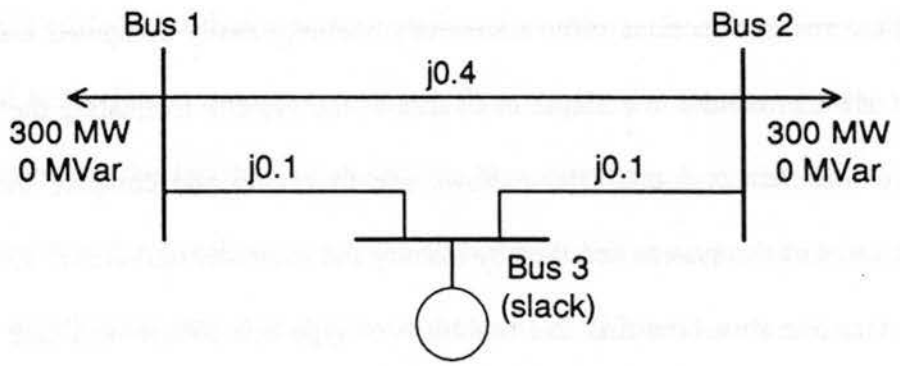

Figure 2.11: Simple three-bus system for illustrating load participation

Table 2.1: Solutions for three-bus system

Voltage	Solution A	Solution B	Solution C	Solution D
V_1	0.9487	0.2677	0.7477	0.3162
θ_1	–18.43	–77.52	–26.95	–71.56
V_2	0.9487	0.7471	0.2677	0.3162
θ_2	–18.43	–26.95	–77.52	–71.56

It is interesting to consider how these solutions change as system loading varies. Figures 2.12 through 2.14 show the positions of the four solutions in V_1-V_2 space as loading is increased from the base case using three different participation schemes. In Figure 2.12, as load increases, bus 1 absorbs twice as much of the additional load as bus 2. For this situation, B is the critical solution, since it is the one that coalesces with A in a saddle-node bifurcation and causes a loss of solution. This occurs for a total system loading of 965 MW. Note that solutions C and D also coalesce, but at a lower loading of 787 MW. On the other hand, when load participation at bus 2 is twice that at bus 1 (Figure 2.13), C coalesces with A and is thus the critical solution. Recall that type-one low-voltage solutions can be associated with a particular bus or area of the system by

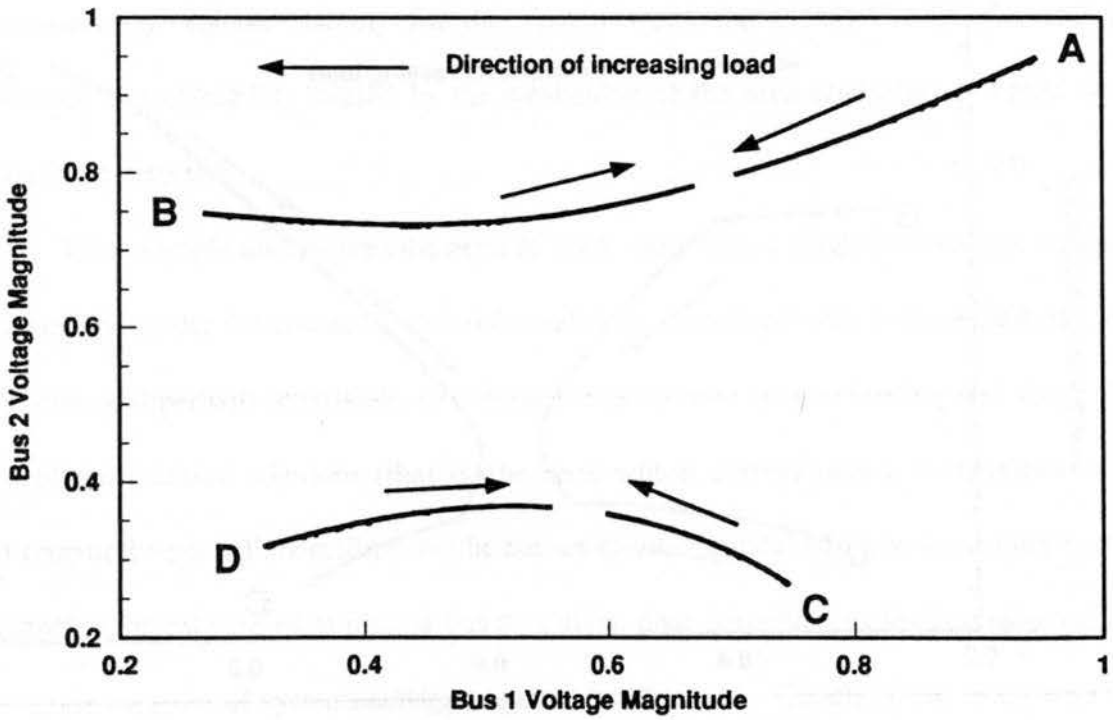

Figure 2.12: Maximum load participation at bus 1

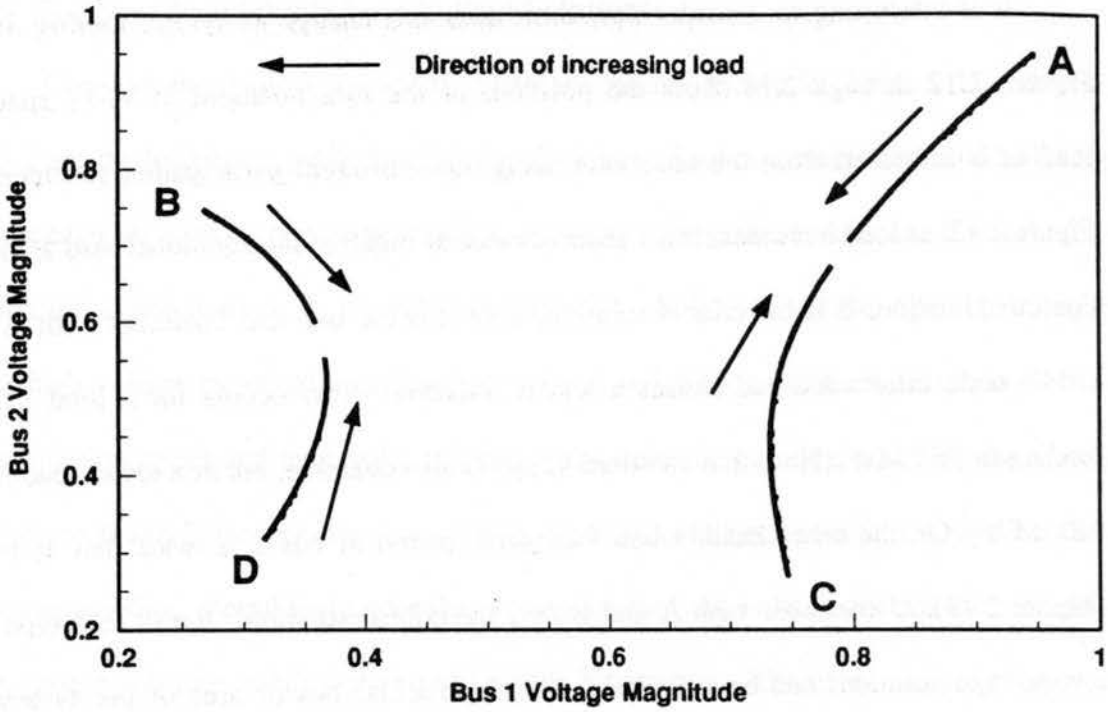

Figure 2.13: Maximum load participation at bus 2

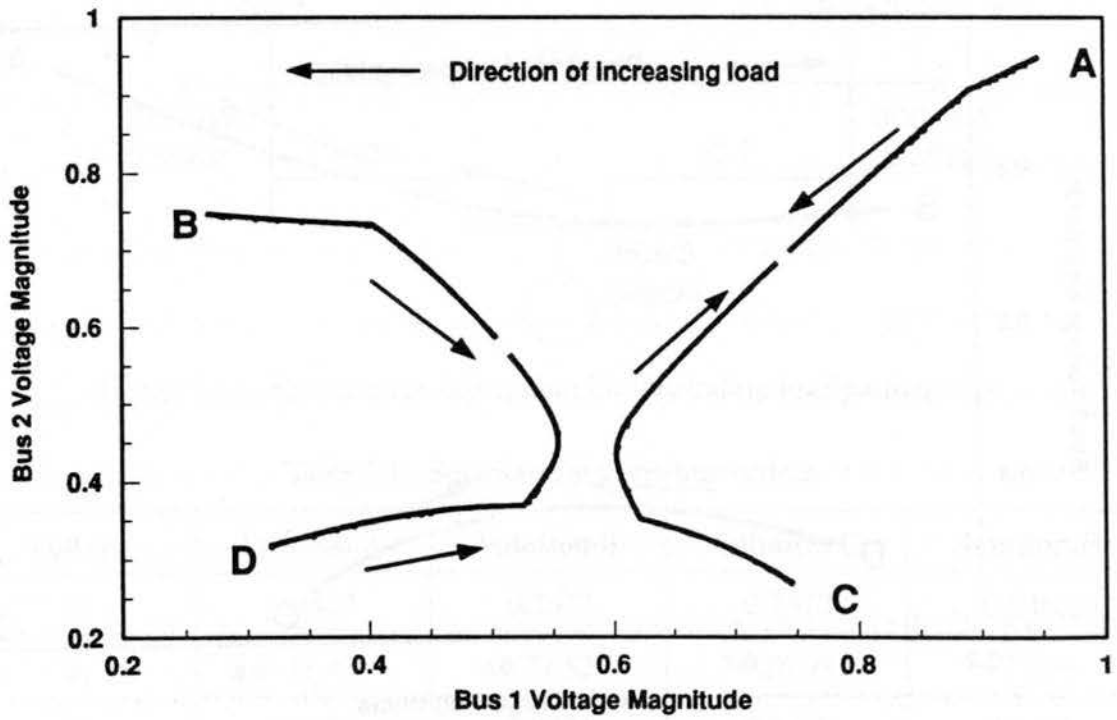

Figure 2.14: Varying load participation

looking at the eigenvectors corresponding to their positive eigenvalues. For this system, the eigenvectors indicate that B is the bus 1 low-voltage solution, while C is the bus 2 solution. This identification makes intuitive sense. Observe that a bifurcation involving solution B accompanies a stressing of the area about bus 1, while stressing bus 2 induces instability via solution C.

Now consider the more interesting case in which load participation is initially higher at bus 1, but, when the bus 1 load is 1.3 times the base value, participation is switched so that most of the additional load is absorbed by bus 2. The variation of the four solutions is shown in Figure 2.14. This time observe that although B is the solution initially moving toward A, it is ultimately C that is the critical one, coalescing with the operable solution and causing a loss of stability. It is clear that if only solution B had been followed, the assessment of voltage stability for the system would have been inaccurate, and the eventual loss of stability caused by the weakening of the area about bus 2 would never have been detected.

This example underscores the need to track more than a single low-voltage solution. Particularly under the unusually stressed conditions associated with voltage collapse, it is difficult, and perhaps impossible, to ascertain exactly how system loading will vary. The set of most critical solutions (that is, the ones whose corresponding energy measure is lowest) at time t_0 will most likely not be the set of most critical buses at some later time t_1. Therefore, if only the most critical bus at a given time is tracked as loading increases, an accurate measure of system stability may not be obtained. Clearly, then, more than one low-voltage solution must be monitored as loading is increased. This task, while easy to

justify, is far from simple to execute for the reasons already discussed. The remainder of this thesis explores various methods of accomplishing this goal and introduces a new method more suitable for online application.

CHAPTER 3

EXISTING TECHNIQUES FOR FINDING LOW-VOLTAGE SOLUTIONS

3.1 Introduction

The use of low-voltage solutions in assessing system voltage stability was described in the preceding chapter. There it was demonstrated that to gauge voltage stability reliably, one has to find a number of low-voltage solutions and to track them as the system evolves. However, this task can be quite computationally expensive, particularly when studying large systems, because a number of load flow solutions may have to be performed. Although it is important to identify the low-voltage solutions most critical to assessing the stability of the system, the need to assess voltage stability in an online setting, rather than solely in the planning stage, demands that this process be done efficiently. Thus, the goal of any low-voltage solution algorithm should be to compute all the most critical low-voltage solutions using as few full load flow solutions as possible. Given the nonlinearity of the power flow equations and the fractal regions of attraction of the various solutions, achieving this goal represents a formidable challenge.

A number of methods for computing low-voltage solutions have been introduced over the last fifteen years in the hope of bringing the goal of online voltage security assessment to fruition. These methods have achieved varying degrees of success, but all are considered either too computationally expensive for online application or too sparing in the number of low-voltage solutions they find. To provide a background for the development of the midpoint algorithm in Chapter 4, this chapter will survey a few of the

most popular existing techniques. The performance of each method will be evaluated in terms of computational efficiency and reliability.

3.2 Basic Algorithm of Tamura, Iba, and Iwamoto

Shortly after introducing the optimal multiplier to mitigate the divergence of the Newton-Raphson load flow, Tamura and his colleagues introduced two methods for finding low-voltage solutions in [3]. The motivation for these algorithms is the hope that by varying the initial guess, the Newton-Raphson iteration can be initialized within the region of attraction of different power flow solutions. The first of these techniques, which the authors referred to as the basic algorithm, is an exhaustive search routine designed to find a large number of solutions. Its computational expense renders it inapplicable to systems of realistic size, but is discussed here because it provides the basis for the authors' second approach, the popular simplified method. Both methods employ the rectangular form of the Newton-Raphson equations.

The basic algorithm can be summarized as follows:

(0) Solve the power flow in the usual way to obtain the stable operating $\mathbf{V}^s$, the vector of real and imaginary parts of all bus voltages.

(1) Calculate a value V_i^u for each load bus i that represents the low-voltage solution for that bus if all other bus voltages are kept constant. Recall from the discussion on multiple load-flow solutions in Chapter 2 that if the voltages are known at all buses except bus i, where P_i and Q_i are known quantities, then a quadratic equation may be written to find V_i. Solving this quadratic equation may yield not only V_i^s, the bus i voltage found in step (0), but also a

low-voltage solution estimate, V_i^{α}. This procedure is followed at all n-m load buses in the system.

(2) Construct the set of all initial guess vectors $\mathbf{V}^{\mathbf{u}}$. Each $\mathbf{V}^{\mathbf{u}}$ is formed by setting the starting voltage for bus i equal to either V_i^{s} or the newly computed V_i^{α}. Each $\mathbf{V}^{\mathbf{u}}$ has at least a single bus i for which V_i^{α} is used. Since V_i^{α} was calculated at all n–m load buses, there are $2^{n-m}-1$ vectors $\mathbf{V}^{\mathbf{u}}$ distinct from $\mathbf{V}^{\mathbf{s}}$.

(3) Compute full power flow solutions for each of the $2^{n-m}-1$ initial guesses $\mathbf{V}^{\mathbf{u}}$. Use the optimal multiplier to prevent divergence.

The quadratic equations that must be solved in (1) can be derived as follows [17]. The load flow equations in rectangular coordinates are written as

$$\begin{aligned} P_i &= \sum_{j=1}^{n}\left[u_i\left(u_j g_{ij} - w_j b_{ij}\right) + w_i\left(w_j g_{ij} + u_j b_{ij}\right)\right] \\ &= g_{ii}\left(u_i^2 + w_i^2\right) + u_i C + w_i D \end{aligned} \tag{3.1}$$

$$\begin{aligned} Q_i &= \sum_{i=1}^{n}\left[w_i\left(u_j g_{ij} - w_j b_{ij}\right) - u_i\left(w_i g_{ij} + u_j b_{ij}\right)\right] \\ &= -b_{ii}\left(u_i^2 + w_i^2\right) + w_i C - u_i D \end{aligned} \tag{3.2}$$

where

$$\begin{aligned} C &= \sum_{j=1,\, j\neq i}^{n}\left(u_j g_{ij} - w_i b_{ij}\right) \\ D &= \sum_{j=1,\, j\neq i}^{n}\left(w_i g_{ij} + u_j b_{ij}\right). \end{aligned} \tag{3.3}$$

Multiply (3.1) by b_{ii} and (3.2) by g_{ii} and add the equations to obtain

$$P_i b_{ii} + Q_i g_{ii} = u_i b_{ii} C + w_i b_{ii} D + w_i g_{ii} C - u_i g_{ii} D \ . \tag{3.4}$$

Solve this equation for w_i, thus obtaining

$$w_i = \alpha u_i + \beta \tag{3.5}$$

where

$$\begin{aligned} \alpha &= \frac{g_{ii} D - b_{ii} C}{b_{ii} D + g_{ii} C} \\ \beta &= \frac{P_i b_{ii} + Q_i g_{ii}}{b_{ii} D + g_{ii} C} \ . \end{aligned} \tag{3.6}$$

Plugging (3.5) into (3.4) yields a quadratic in u_i:

$$0 = g_{ii}\left(1 + \alpha^2\right) u_i^2 + \left(2\alpha\beta g_{ii} + C + \alpha D\right) u_i + \left(\beta^2 g_{ii} + \beta D - P_i\right). \tag{3.7}$$

One solution to these two equations will be the desired low-voltage guess component $V_i^{\mu} = u_i + j w_i$.

The basic algorithm was used to good advantage by the author on small systems [3]. In particular, two solutions were found for a heavily loaded Ward and Hale six-bus system, and 57 different solutions were found on a lightly loaded Klos and Kerner 11-bus system. However, use of the basic algorithm is prohibitively expensive. For example, to calculate the 57 solutions to the Klos and Kerner system required $(2^{11-1} - 1) = 1023$ power flow solutions. Obviously, for systems of realistic size, this inefficiency will be very problematic. The simplified method addresses this concern.

3.3 Simplified Method

The authors of [3] noted the initial guesses that most often converged to a solution were those for which only a single bus i was assigned V_i^{μ} and all other bus k voltage

guesses were set to V_k^s. In light of this, the simplified method was proposed. In the simplified method, only those $\mathbf{V}^u$ for which a single element i is set to V_i^u are used as initial guesses. Furthermore, PV buses are either omitted from the formulation (in which case, a total of $n-m-1$ different initial guesses is possible for an n-bus system with m PV buses), or they are recast as PQ, where the reactive power injections are set to their maximum var limits. For the latter case, $n-1$ different initial guesses are possible, so $n-1$ power flow solutions have to be performed, compared to $2^{n-m}-1$ with the basic algorithm; this affords the opportunity to compute the low-voltage solutions for systems of reasonable size. For example, the authors were able to find both solutions to a heavily loaded 43-bus case by solving only 19 load flows.

An encouraging characteristic of the simplified method is that the solutions obtained tend to correspond to type-one UEPs [17]. Recall from Section 2.6 that when a system loses stability, it does so through a bifurcation between the SEP and a type-one UEP. Thus, solving the $n-1$ power flows required by the simplified method provides a set of solutions which, depending on the future evolution of load, may coalesce with the operable solution and cause a loss of stability. It turns out that the energy measure associated with the bus i low-voltage solution (that is, the vector $\mathbf{V}^u$ for which $V_i = V_i^u$) provides a measure of voltage security in the area of bus i. Thus, the simplified method offers a convenient interpretation of the implications of each low-voltage solution obtained by using it. Of course, there is no guarantee that this method will find the single most critical solution, but the widespread adoption of the method suggests that it performs quite well in that regard.

However, the simplified method has two major drawbacks. First, although it offers a significant computational advantage over the basic algorithm, its requirement that $n-1$ power flow solutions be performed to calculate the critical energy measures for an n-bus system is still too expensive for the majority of real power systems. Furthermore, because the method relies on conditioning the initial guess in hope of visiting the regions of attraction of all UEPs, convergence cannot be guaranteed. Still, the simplified method is one of the most widely used low-voltage solution algorithms. Its performance will be compared with that of the midpoint method in Chapter 4.

3.4 Finding a Pair of Close Solutions

It is clear from the nose curve of Figure 2.8 that one indication of proximity to collapse could be the existence of high- and low-voltage solutions whose magnitudes are close to each other for a particular loading. A method developed by Iba et al. [6] seeks to detect this condition by exploiting a particular characteristic of the convergence of the rectangular Newton-Raphson load flow when solutions are close to each other. Numerical testing has shown that when a pair of load flow solutions $\mathbf{x}^s$ and $\mathbf{x}^u$ are close to each other, convergence to $\mathbf{x}^s$ tends to be along the line joining $\mathbf{x}^s$ and $\mathbf{x}^u$. In other words, the kth iteration step $\Delta\mathbf{x}^k$ used to compute $\mathbf{x}^{k+1} = \mathbf{x}^k + \Delta\mathbf{x}^k$ becomes more closely parallel to $\mathbf{x}^s - \mathbf{x}^u$. Iba's method takes advantage of this property through application of the optimal multiplier. Recall that the optimal multiplier was obtained by solving a cubic equation with three required roots, μ, μ_2, and μ_3. Iba's experience suggested that if all three of the multipliers μ, μ_2, and μ_3 were real, then a pair of closely located

solutions $\mathbf{x}^s$ and $\mathbf{x}^u$ existed. If $\mu < \mu_2 < \mu_3$, then, in iterating $\mathbf{x}^{k+1} = \mathbf{x}^k + \Delta\mathbf{x}^k$ to find $\mathbf{x}^s$, calculating $\mathbf{x}^0 = \mathbf{x}^k + \mu_3\Delta\mathbf{x}^k$ likely would provide a good approximation for $\mathbf{x}^u$, since $\Delta\mathbf{x}^k$ and $\mathbf{x}^s - \mathbf{x}^u$ are increasingly collinear. The authors used this technique to good advantage on systems of various sizes and found that the accuracy of the initial guesses was generally excellent, resulting in rapid convergence to $\mathbf{x}^u$.

Iba's method is particularly appealing because it involves very little additional computation. In fact, as the authors demonstrate, both $\mathbf{x}^s$ and $\mathbf{x}^u$ often can be determined using a single power flow calculation. However, it should be emphasized that this method finds a *single* low-voltage solution; it generally cannot find multiple low-voltage solutions, a serious a drawback in light of the discussion in Section 2.8. Moreover, its usefulness is suspect when the goal is to ascertain stability while still a reasonable distance from collapse. However, if one is primarily interested in detecting the condition in which only a single low-voltage solution remains, this algorithm provides an efficient vehicle.

3.5 Finding Low-Voltage Solutions by Tracing Manifolds

In [7], the authors introduce a method that seeks all the solutions to the power balance equations. The method focuses solely on the topological structure associated with the solution set to a particular system of equations and is theoretically guaranteed to find all the solutions because it does not depend on the convergence properties of the Newton-Raphson algorithm near the various solutions. The method assumes that one of the solutions is already known and that var limits on the generators are not enforced. This latter assumption is necessary so that the set of equations, and hence the topological

structures being investigated, do not change. The search for all solutions of the power flow equations can be restricted to a single quadrant of load parameter space. The key result is that any solution $\mathbf{x}^s$ is connected to at least another solution $\mathbf{x}_i^u$ by a manifold $\mathbf{M}^i$ and to some other solution $\mathbf{x}_j^u$ by another manifold $\mathbf{M}^j$. Consequently, from one solution, the algorithm finds all other solutions by tracing manifolds. The algorithm essentially traces the smooth curves of the manifolds using the continuation method.

Although this method calculates all the solutions to the power flow equations more efficiently than its chief predecessor, the application of the globally convergent probability-one homotopy method by Salam et al. [24], it still requires that a number of power flow solutions proportional to the product of $(n-1)$ and the number of solutions the system actually has be performed for an n-bus system, thus rendering it impractical for use in an online environment. Moreover, this author has some concern about the actual need for an exhaustive determination of low-voltage solutions. Since type-one low-voltage solutions are generally the ones of interest for voltage stability assessment, the determination of all the solutions to the power flow equations may be of more academic interest. The computational expense of the manifold-tracing method renders it unattractive for practical application.

3.6 Eigenvector Direction Method

Although not an existing method in the sense that it is currently employed to find low-voltage solutions, the eigenvector direction method, developed in the course of this research as the immediate predecessor of the midpoint method, will now be discussed.

The development of this technique is fairly similar to that of the midpoint method, so it should provide a good foundation for presenting that material in the next chapter.

3.6.1 Development

Consider two solutions in state space $\mathbf{x}^s$ and $\mathbf{x}^u$. Solution $\mathbf{x}^s$ is the stable or high-voltage solution, while $\mathbf{x}^u$ is an unstable or low-voltage solution of interest. Consider the midpoint $\mathbf{x}^m$ between them and the direction vector $\Delta\mathbf{x}$ joining all three solutions as shown in Figure 3.1. Expanding $\mathbf{f}(\mathbf{x}^s)$ and $\mathbf{f}(\mathbf{x}^u)$ in a Taylor series yields the expressions

$$\mathbf{f}(\mathbf{x}^s) = \mathbf{f}(\mathbf{x}^m + \Delta\mathbf{x}) = \mathbf{f}(\mathbf{x}^m) + \mathbf{J}(\mathbf{x}^m)\Delta\mathbf{x} + \mathbf{f}(\Delta\mathbf{x}) = \mathbf{0} \tag{3.8}$$

$$\mathbf{f}(\mathbf{x}^u) = \mathbf{f}(\mathbf{x}^m - \Delta\mathbf{x}) = \mathbf{f}(\mathbf{x}^m) - \mathbf{J}(\mathbf{x}^m)\Delta\mathbf{x} + \mathbf{f}(\Delta\mathbf{x}) = \mathbf{0}\,. \tag{3.9}$$

Subtracting (3.9) from (3.8) yields

$$2\mathbf{J}(\mathbf{x}^m)\Delta\mathbf{x} = \mathbf{0} \tag{3.10}$$

Clearly, unless $\Delta\mathbf{x} = \mathbf{0}$, $\mathbf{J}(\mathbf{x}^m)$ is singular, and $\Delta\mathbf{x}$ is the eigenvector corresponding to the zero eigenvector of $\mathbf{J}(\mathbf{x}^m)$. Since $\mathbf{x}^m$ is unknown, $\mathbf{J}(\mathbf{x}^m)$ and its eigenvectors are unknown, which is thus far inconsequential. However, if $\mathbf{x}^s$ and $\mathbf{x}^u$ are close to $\mathbf{x}^m$, then one may claim that $\Delta\mathbf{x}$ may be approximated by the eigenvector corresponding to the eigenvalue of $\mathbf{J}(\mathbf{x}^s)$ having the smallest magnitude. A similar claim is often made when assessing the initial effects of voltage collapse associated with a particular solution using the right eigenvector associated with the positive eigenvalue of a UEP rather than the right eigenvector associated with the zero eigenvalue at the unknown collapse point. In fact,

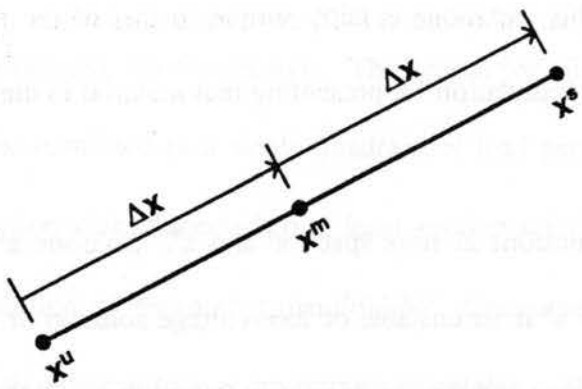

Figure 3.1: Orientation of the three solutions

several eigenvalues and eigenvectors for $\mathbf{J}(\mathbf{x}^s)$ may be calculated fairly efficiently using the inverse power method [25] or some other eigenvalue routine. Each of these eigenvectors may be interpreted as a search direction for finding low-voltage solutions, so one obtains a set of orthogonal directions to search in state space for low-voltage solutions.

Once these eigenvectors have been determined, the degree to which they approximate $\Delta\mathbf{x}$ may be improved through iteration. This can be understood by considering the Taylor expansion

$$\mathbf{f}(\mathbf{x}^u) = \mathbf{f}(\mathbf{x}^s + 2\Delta\mathbf{x}) = \mathbf{f}(\mathbf{x}^s) + 2\mathbf{J}(\mathbf{x}^s)\Delta\mathbf{x} + 4\mathbf{f}(\Delta\mathbf{x}) \tag{3.11}$$

and noting that $\mathbf{f}(\mathbf{x}^u) = \mathbf{f}(\mathbf{x}^s) = \mathbf{0}$. Thus,

$$-\mathbf{J}(\mathbf{x}^s)\Delta\mathbf{x} = 2\mathbf{f}(\Delta\mathbf{x}). \tag{3.12}$$

This is an exact relationship for $\Delta\mathbf{x}$. Thus, to improve the search direction offered by a particular eigenvector, substitute it for $\Delta\mathbf{x}$ in (3.12) and iterate once or twice. Call the resulting direction vector $\Delta\mathbf{x}^*$. Then, applying the optimal multiplier result discussed in

Section 2.4, in a manner to be addressed in more detail when the midpoint method is developed in the next section, quite possibly provides a good estimate for a low-voltage solution.

An interesting modification of this method is that, in addition to finding the eigenvector directions associated with $\mathbf{x}^s$, the algorithm may pursue the eigenvector directions calculated from each of the low-voltage solutions found. Thus, each subsequent solution gives rise to another set of orthogonal search directions, possibly uncovering additional low-voltage solutions with their own associated search directions. Unfortunately, as more search directions emerge, computational requirements burgeon. In fact, for an n-bus system with p solutions, a maximum of $2(n-1)p$ eigenvectors must be calculated, followed by $2(n-1)p$ power flows. Obviously, such requirements severely hinder the usefulness of this technique for reasonably sized systems. This method is of academic interest, however, so the results obtained by applying it to small systems will now be discussed.

3.6.2 Results of the eigenvector direction method

Consider first the application of the method to the Klos and Kerner three-bus system first described in [11]. This system is known to have high-voltage solution $\mathbf{x} = \left(1.000\angle 0°, 1.0782\angle -0.99°, 1.0500\angle -0.63°\right)$, and it also has three low-voltage solutions. The eigenvector method was used to find them. Table 3.1 demonstrates the process of finding these solutions. When one starts from the high solution $\mathbf{x}^s$, the smallest eigenvalue and the third smallest eigenvalue (in magnitude) correspond to eigenvectors that lead to unique low-voltage solutions; the second and fourth smallest eigenvalues

uncover the same solutions as the first and third eigenvalues, respectively. Denote these low-voltage solutions as $\mathbf{x}_a^u$ and $\mathbf{x}_b^u$. Then, the smallest magnitude eigenvalue of $\mathbf{J}(\mathbf{x}_a^u)$ corresponds to an eigenvector that uncovers the third low-voltage solution $\mathbf{x}_c^u$. Thus, all four solutions of the Klos and Kerner three-bus system have been found using five eigenvalue/eigenvector calculations and six power flow solutions.

Table 3.1: Application of eigenvalue method to Klos-Kerner system

Starting Solution	Eigenvalue # (1 = smallest)	Solution Found
$\mathbf{x}^s$	1	$\mathbf{x}_a{}^u$
	2	$\mathbf{x}_a{}^u$
	3	$\mathbf{x}_b{}^u$
	4	$\mathbf{x}_b{}^u$
$\mathbf{x}_a{}^u$	1	$\mathbf{x}_c{}^u$

The eigenvector direction method was then applied to the Stagg five-bus system. Table 3.2 shows the results of this endeavor. In the table, the various solutions are distinguished by the energy of the solutions to which they converge, and the eigenvector from which these solutions were found is identified by two digits. The first digit indicates the number of the low-voltage solution for which the corresponding eigenvalue/eigenvector pair was calculated. (The solutions are numbered in the order in which they are found, and the high-voltage solution is identifed as solution 0.) Call this solution the "source solution." The second digit indicates which eigenvalue/eigenvector pair of the source solution found the new low-voltage solution. Thus, if the source

solution digit is 2 and the eigenvalue number is 3, then the particular low-voltage solution, identified by its associated energy measure, was found from the eigenvector corresponding to the third smallest eigenvalue of the Jacobian evaluated at the second solution found for that particular loading. Data were collected over a wide load range, and loading was increased uniformly at all buses as a function of load parameter λ. The most noticeable characteristic of the method is that, as loading increases toward collapse at $\lambda = 3.035$, the critical low-voltage solution is found from the smallest eigenvalue/eigenvector of $\mathbf{J}(\mathbf{x}^s)$.

Table 3.2: Application of eigenvector method to Stagg five-bus system

λ	Source Solution #	Eigenvalue	Eigenvalue #	Energy of Solution	Solution Type
1.0	0	3.3296	1	3.4279	1
	0	13.0901	3	2.2722	1
	1	0.1964	1	3.4285	2
1.2	0	12.7454	3	1.9746	1
1.4	0	12.3798	3	1.6890	1
1.6	0	11.9899	3	1.4148	1
1.8	0	2.6529	1	1.1523	1
2.0	0	2.4528	1	0.9024	1
2.2	0	2.2324	1	0.6672	1
2.4	0	1.9824	1	0.4504	1
2.6	0	1.6853	1	0.2588	1
2.8	0	1.2962	1	0.1032	1
3.0	0	0.5682	1	0.0057	1
3.035	0	0.0617	1	0.0001	1

Moreover, although not shown in Table 3.2, for very low loading levels ($\lambda \leq 1.0$, where $\lambda = 1.0$ corresponds to base load), type-two and even type-three solutions were found. Again, the usefulness of this trait for static voltage stability assessment is somewhat suspect, and the computational expense of the method is prohibitive for larger systems.

3.7 Shortcomings of Existing Methods

This chapter has surveyed only a few existing methods for finding low-voltage power flow solutions. The treatment is by no means complete, but the selected algorithms represent the major classes of techniques available. They also elucidate some problems that plague all existing techniques, shortcomings that the midpoint method has been developed to mitigate.

Computational expense is the most obvious area in which many of these techniques need improvement, particularly if they are to be used for online studies. Table 3.3 summarizes the number of power flows that must be performed to find the set of lowest-energy solutions for each method. These statistics pertain to a system having n buses, m of which are PV, for which p low-voltage solutions exist. Because computational speed has increased dramatically over the last few years, the need to perform multiple load flows is not an impediment to online usage for small- and medium-sized systems. However, for larger bulk power systems typically studied in practice, the number of power flows to perform certainly must be kept to a minimum. The basic, simplified, manifold-tracing, and eigenvector direction methods fail to satisfy this requirement. Iba's method, though

Table 3.3: Computational requirements for the various methods

Method	# of Power Flows	Comments
Basic	2^{n-m-1}	Not limited to type-one solutions
Simplified	$n-1$	Finds type-one solutions only
Manifold Tracing	$(n-1)p$	Finds all power flow solutions
Eigenvector Direction	$2(n-1)p$	Also requires many eigenvector calculations
Iba	1	Applicable only to critically loaded systems

computationally thrifty, is inadequate because it fails to track multiple low-voltage solutions.

Another and perhaps more subtle malady plaguing some of these methods is their dependence on the rather capricious convergence characteristics of the Newton-Raphson load flow. The regions of convergence of the various solutions to the load flow equations possess fractal boundaries [2]. Figure 3.2 demonstrates the implications of this characteristic for the Stagg five-bus system. This plot was generated by varying the initial guess for voltage magnitude and angle over a 100-by-100 grid in bus 5 voltage-angle space and determining the solutions to which each initial guess converged. The different solutions are distinguished by their associated energy measures, which are plotted along the z-axis. Observe that the boundaries between the different convergence regions are extremely complex. Thorp and Naqavi [2] showed that these boundaries are actually fractal, for if they are inspected on increasingly smaller scales, they retain the same degree of complexity. This proves perilous for any algorithm whose success in finding low-voltage solutions depends upon its ability to find initial guesses sufficiently close to the

low-voltage solutions. Given the fractal nature of the regions of convergence, no matter how close an initial guess is to a particular low-voltage solution, it cannot be guaranteed that the initial guess lies within that solution's region of convergence. The basic, simplified, eigenvector direction, Iba's, and the soon-to-be-discussed midpoint method all seek good initial guesses to find low-voltage solutions and are thus plagued by this handicap; only Ma and Thorp's manifold-tracing method is immune. However, it certainly can be argued that the likelihood of an initial guess lying within the region of convergence of a solution increases as the initial guess becomes more accurate. This is the argument by which the midpoint method shall be promoted.

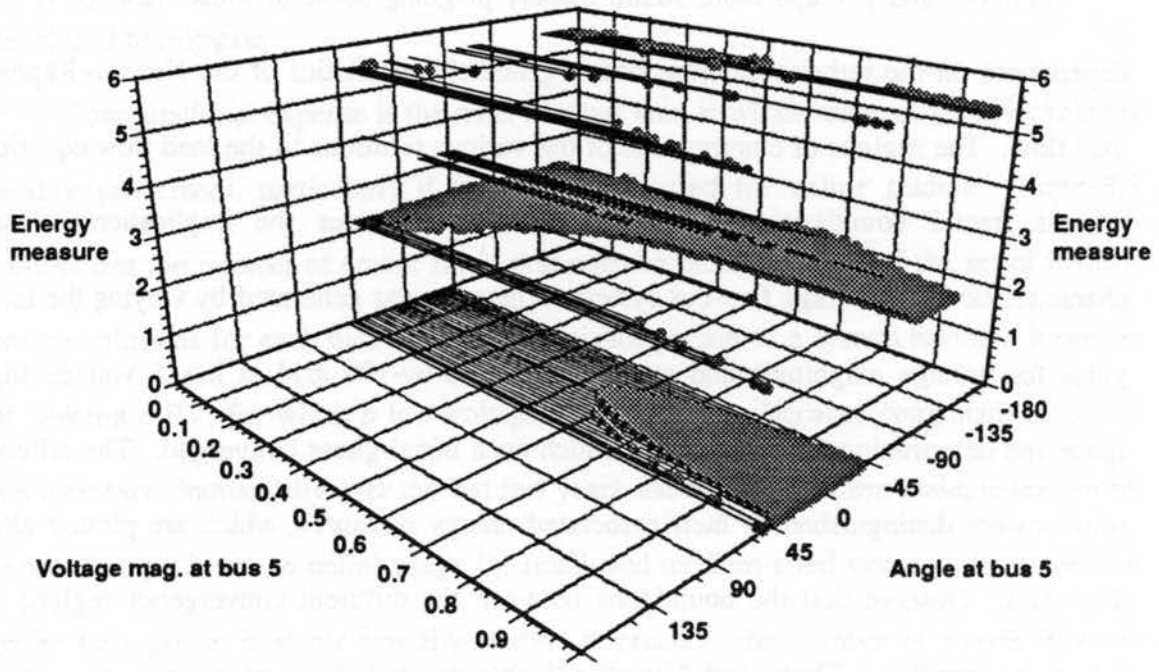

Figure 3.2: Fractal convergence regions for Stagg five-bus system

CHAPTER 4

DEVELOPMENT AND PERFORMANCE OF THE MIDPOINT METHOD

4.1 Introduction

This chapter will explore all aspects of the midpoint method for determining low-voltage solutions to the load flow problem. It will first develop the algorithm and demonstrate how it is derived largely from the structure of the power flow mismatch equations. It will thus become clear that execution of the algorithm requires little additional computation, a key advantage of the midpoint method. Then, the performance of the algorithm on three test systems of various sizes will be described. The ability of the algorithm to converge to multiple low-voltage solutions over a wide load range and with good initial guesses will be demonstrated. Since computational expense is a key concern, special attention will be paid to determining the set of buses at which to apply the midpoint method. Various screening methods may be applied, and the merits of each will be demonstrated.

To motivate the use of the algorithm in finding system UEPs, this chapter will compare the performance of the algorithm to that of the most popular existing method for finding low-voltage solutions, the simplified method discussed in Section 3.3. Comparisons will be drawn between each algorithm's ability to find critical low-voltage solutions, accuracy of each method's initial guesses, and number of iterations required for each to converge. Given the results of these comparisons, various possible enhancements of the midpoint method and its associated screening tools will be described.

Before delving into the derivation of the method, consider again the motivation for this research: existing methods for determining low-voltage power flow solutions either miss critical type-one UEPs or are too computationally expensive for online usage. The goal of the midpoint method is to provide a more robust and efficient method for determining the set of type-one low-voltage solutions closest to the operable solution.

4.2 Development of the Midpoint Method

Recall that the power balance constraints for an $(n+1)$-bus system (where bus $n+1$ is the slack) may be expressed as

$$\mathbf{S} = \mathbf{f}(\mathbf{x}^*) \tag{4.1}$$

where $\mathbf{S}$ is a vector of the constant real and reactive power injection (load minus generation) at all nongenerator buses and the real power and voltage-magnitude equality constraints at all PV buses except the slack. For convenience, assume that the first m buses are PV and that the remaining $n-m$ nonslack buses are PQ. Then, one may express $\mathbf{S}$ as

$$\mathbf{S} = \left[P_1,\ldots,P_m;\ V_1^2,\ldots,V_m^2;\ P_{m+1},\ldots,P_n;\ Q_{m+1},\ldots,Q_n\right]^T. \tag{4.2}$$

The unknown quantities are the real and imaginary parts of voltage at all buses:

$$\mathbf{x} = \left[u_1,\ldots,u_n;\ w_1,\ldots,w_n\right] \tag{4.3}$$

with $\mathbf{x}^*$ the value of $\mathbf{x}$ when a solution satisfying the constraints has been found. The vector of functions

$$\mathbf{f}(\mathbf{x}) = \left[f_{p1}(\mathbf{x}),\ldots,f_{pn}(\mathbf{x});\ f_{q1}(\mathbf{x}),\ldots,f_{qn}(\mathbf{x})\right] \tag{4.4}$$

provides the bus powers and voltages in light of the current iteration's solution vector.

Recall that the goal of the power flow is to find $\mathbf{x}^*$ so that $\mathbf{S} = \mathbf{f}(\mathbf{x}^*)$, that is, to find $\mathbf{x}$ so that the functional values match the known or regulated values for bus power injections and voltage magnitudes. For a PV bus, the constraints are real power injection and voltage magnitude, while for PQ buses the real and reactive power injections are constraints. Thus, for both PV and PQ buses, define

$$f_{\mathrm{pi}}(\mathbf{x}) = -\sum_{j=1}^{n}\left[u_i\left(u_j g_{ij} - w_j b_{ij}\right) + w_i\left(w_j g_{ij} + u_j b_{ij}\right)\right]. \tag{4.5}$$

For PV buses define

$$f_{\mathrm{qi}}(\mathbf{x}) = u_i^2 + w_i^2, \tag{4.6}$$

and at PQ buses define

$$f_{\mathrm{qi}}(\mathbf{x}) = -\sum_{j=1}^{n}\left[w_i\left(u_j g_{ij} - w_j b_{ij}\right) - u_i\left(w_j g_{ij} + u_j b_{ij}\right)\right]. \tag{4.7}$$

Because the power balance equations are quadratic with no first-order terms, we may express (4.1) exactly as the following Taylor expansion:

$$\mathbf{S} = \mathbf{f}(\mathbf{x}^*) = \mathbf{f}(\mathbf{x} + \Delta\mathbf{x}) = \mathbf{f}(\mathbf{x}) + \mathbf{J}(\mathbf{x})\Delta\mathbf{x} + \mathbf{f}(\Delta\mathbf{x}). \tag{4.8}$$

This equation will be the starting point for deriving the relationships between the operable solution and the low-voltage solutions.

Denote the operable solution is denoted as $\mathbf{x}^s$, where the superscript indicates that the operating point is stable. Moreover, designate any one of the low-voltage solutions as $\mathbf{x}^u$. Obviously, since $\mathbf{x}^u$ and $\mathbf{x}^s$ are solutions, then $\mathbf{S} = \mathbf{f}(\mathbf{x}^u) = \mathbf{f}(\mathbf{x}^s)$. Finally, as in Figure 3.1, define the midpoint of the line in state space that joins these two solutions as

$\mathbf{x}^m$, and the vector joining $\mathbf{x}^s$ to $\mathbf{x}^m$ (equivalent to the vector joining $\mathbf{x}^m$ to $\mathbf{x}^u$) as $\Delta\mathbf{x}^m$. Thus,

$$\Delta\mathbf{x}^m = \mathbf{x}^s - \mathbf{x}^m = \mathbf{x}^m - \mathbf{x}^u . \tag{4.9}$$

Now, from (4.8) and the fact that $\mathbf{f}(\mathbf{x})$ is quadratic, so that $\mathbf{f}(\mu\Delta\mathbf{x}) = \mu^2\mathbf{f}(\Delta\mathbf{x})$, it is clear that

$$\mathbf{f}(\mathbf{x}^s) = \mathbf{f}(\mathbf{x}^m + \Delta\mathbf{x}^m) = \mathbf{f}(\mathbf{x}^m) + \mathbf{J}(\mathbf{x}^m)\Delta\mathbf{x}^m + \mathbf{f}(\Delta\mathbf{x}^m) = \mathbf{S} \tag{4.10}$$

$$\mathbf{f}(\mathbf{x}^u) = \mathbf{f}(\mathbf{x}^m - \Delta\mathbf{x}^m) = \mathbf{f}(\mathbf{x}^m) - \mathbf{J}(\mathbf{x}^m)\Delta\mathbf{x}^m + \mathbf{f}(\Delta\mathbf{x}^m) = \mathbf{S} . \tag{4.11}$$

Subtracting (4.11) from (4.10) yields

$$\mathbf{0} = 2\mathbf{J}(\mathbf{x}^m)\Delta\mathbf{x}^m . \tag{4.12}$$

This statement suggests that $\mathbf{J}$ is singular at $\mathbf{x}^m$, so $\mathbf{x}^m$ is a point on the maximum loadability boundary Σ. Consequently, the change in load encountered while moving in state space along $\Delta\mathbf{x}^m$ can be considered one amount of load variation that collapses a system formerly operating at $\mathbf{x}^s$. As will be seen shortly, this collapse path tends to be associated more with an l_1 norm (that is, it tends to lie primarily along a single dimension) than with an l_2 norm. The vector $\Delta\mathbf{x}^m$ will be referred to as the midpoint direction.

Equation (4.12) also indicates that $\Delta\mathbf{x}^m$ is the right eigenvector associated with the zero eigenvalue of the Jacobian at $\mathbf{x}^m$. Hence, $\Delta\mathbf{x}^m$ indicates the inital direction of collapse from $\mathbf{x}^m$. Moreover, it is observed from (4.9) that $\mathbf{x}^m$, $\mathbf{x}^s$, and $\mathbf{x}^u$ are collinear and that $\mathbf{x}^m$ is equidistant from $\mathbf{x}^s$ and $\mathbf{x}^u$. Hence, $\mathbf{x}^m$ is the boundary point closest in solution space to both $\mathbf{x}^s$ and $\mathbf{x}^u$. Finally, it is clear that, starting from the operable solution $\mathbf{x}^s$, to find $\mathbf{x}^u$ it suffices to know $\Delta\mathbf{x}^m$. The remaining analysis seeks to approximate this vector.

Writing the Taylor expansion of (4.8) about $\mathbf{x}^m$ yields

$$\mathbf{f}(\mathbf{x}^m) = \mathbf{f}(\mathbf{x}^s - \Delta\mathbf{x}^m) = \mathbf{f}(\mathbf{x}^s) - \mathbf{J}(\mathbf{x}^s)\Delta\mathbf{x}^m + \mathbf{f}(\Delta\mathbf{x}^m). \tag{4.13}$$

By subtracting (4.10) from (4.13) and noting from (4.12) $\mathbf{J}(\mathbf{x}^m)\Delta\mathbf{x}^m = \mathbf{0}$, one finds that (4.13) may be rewritten as $\mathbf{J}(\mathbf{x}^s)\Delta\mathbf{x}^m = 2[\mathbf{f}(\mathbf{x}^m) - \mathbf{f}(\mathbf{x}^s)]$ or equivalently as

$$\Delta\mathbf{x}^m = 2[\mathbf{J}(\mathbf{x}^s)]^{-1}[\mathbf{f}(\mathbf{x}^m) - \mathbf{f}(\mathbf{x}^s)]. \tag{4.14}$$

This provides an analytical expression for the midpoint direction. The first term of the product, $[\mathbf{J}(\mathbf{x}^s)]^{-1}$, should be readily available since $\mathbf{J}(\mathbf{x}^s)$ is known in factored form provided that $\mathbf{x}^s$ was found using a Newton-Raphson load flow. The second term is more troublesome, however. The quantity $[\mathbf{f}(\mathbf{x}^m) - \mathbf{f}(\mathbf{x}^s)]$, which represents the difference in power injection (load minus generation) associated with $\mathbf{x}^s$ and $\mathbf{x}^m$, shall be called the midpoint mismatch, denoted by $\Delta\mathbf{S}$. This quantity is unknown since $\mathbf{x}^m$ is unknown. Otherwise, $\Delta\mathbf{x}^m$ could be evaluated directly in (4.14) and then used to find $\mathbf{x}^u$. Since $\mathbf{x}^m$ is unknown, an approximation must be employed.

To develop the approximation, first make use of the optimal multiplier result discussed in Section 2.4. Recall that the optimal multiplier is used to obtain the best possible update for the solution guess along a given direction $\Delta\mathbf{x}$. In other words, once $\Delta\mathbf{x}^k = -\mathbf{J}(\mathbf{x}^k)[\mathbf{S} - \mathbf{f}(\mathbf{x}^k)]$ has been calculated, evaluating $\mathbf{x}^{k+1} = \mathbf{x}^k + \mu\Delta\mathbf{x}^k$ rather than simply $\mathbf{x}^{k+1} = \mathbf{x}^k + \Delta\mathbf{x}^k$ minimizes a cost function, defined as the square of the norm of the power flow mismatch equations, along $\Delta\mathbf{x}^k$. The value of the optimal multiplier is obtained by solving the cubic equation

$$g_0 + \mu g_1 + \mu^2 g_2 + \mu^3 g_3 = 0. \tag{4.15}$$

This equation has three roots, with either one or all three roots real. If (4.15) has only one real root μ, then the cost function has a single minimum along $\Delta\mathbf{x}^k$. However, if three real roots μ, μ_2, and μ_3 exist such that $\mu < \mu_2 < \mu_3$, then $\mu\Delta\mathbf{x}^k$ uncovers the closest local minimum, $\mu_2\Delta\mathbf{x}^k$ uncovers a local maximum, and $\mu_3\Delta\mathbf{x}^k$ results in the more remote local minimum.

Consider the application of the optimal multiplier to the problem of finding an $\mathbf{x}^u$ from $\mathbf{x}^s$ without knowing $\Delta\mathbf{x}^m$. Clearly, (4.9) suggests that

$$\mathbf{x}^s + 2\Delta\mathbf{x}^m = \mathbf{x}^u \tag{4.16}$$

so that $\mathbf{x}^s$ and $\mathbf{x}^u$ lie along $\Delta\mathbf{x}^m$. In light of the optimal multiplier, precise knowledge of $\Delta\mathbf{x}^m$ is not necessary to find $\mathbf{x}^u$ from $\mathbf{x}^s$. Rather, suppose that a vector $\Delta\mathbf{x}^c$ that is collinear with $\Delta\mathbf{x}^m$ is found and that the optimal multiplier is applied to it. Since $\mathbf{x}^s$ is a power flow solution, the cost function is already zero, so $\mu = 0$. Whether μ_2 and μ_3 exist depends upon the g coefficients in (4.15). Specifically, if $g_2^2 < 4g_1g_3$, then μ_2 and μ_3 are real. Since μ_3 brings the new solution guess to the more remote local minimum of the cost function, and since $\mathbf{x}^u$ is a power flow solution and thus an absolute minimum of the cost function along $\Delta\mathbf{x}^m$, then

$$\mathbf{x}^u = \mathbf{x}^s + \mu_3\Delta\mathbf{x}^c. \tag{4.17}$$

Unfortunately, a collinear vector $\Delta\mathbf{x}^c$ is not known. However, this treatment of the optimal multiplier suggests that if a reasonably accurate approximation $\Delta\mathbf{x}^{c*}$ for $\Delta\mathbf{x}^c$ is obtained, then evaluating

$$\mathbf{x}^0 = \mathbf{x}^s + \mu_3 \Delta \mathbf{x}^{c*} \tag{4.18}$$

should provide a good initial guess $\mathbf{x}^0$ for $\mathbf{x}^u$. A good initial guess is one which is close in state space to $\mathbf{x}^u$. Quantitatively, this means that the initial mismatch

$$\rho = \left\| \mathbf{f}(\mathbf{x}^0) - \mathbf{S} \right\|_\infty \tag{4.19}$$

is small. The task now is to decide upon an adequate approximation for $\Delta \mathbf{x}^c$.

Because of the linearity of (4.14), it is clear that to approximate $\Delta \mathbf{x}^m$ by $\Delta \mathbf{x}^{c*}$, the midpoint mismatch $\Delta \mathbf{S} = \mathbf{f}(\mathbf{x}^m) - \mathbf{f}(\mathbf{x}^s)$ must be approximated. Recall that the midpoint solution $\mathbf{x}^m$ is the point on the maximum loadability boundary Σ closest in soluion space to both $\mathbf{x}^s$ and $\mathbf{x}^u$. Thus, $\Delta \mathbf{S}$ provides the parameter variation which collapses the system via this bifurcation point. Numerical examination has shown that $\Delta \mathbf{S}$ typically contains a relatively large component at only a single bus, and then only in the reactive component at that bus. Furthermore, this bus number corresponds to the bus number used to identify the solution (see Section 2.8).

For example, consider Figure 4.1 in which the real and reactive mismatches at the midpoint solution are plotted for each bus as load is increased uniformly at all buses of the Stagg five-bus system. These values are normalized with respect to the largest midpoint mismatch value at each particular loading. For this case, the midpoint $\mathbf{x}^m$ was calculated using $\mathbf{x}^m = 0.5 * (\mathbf{x}^s + \mathbf{x}^u)$ where $\mathbf{x}^u$ is the solution corresponding to bus 5 found using the simplified method. The figure shows that the reactive power mismatch at bus 5 is the dominant component of $\Delta \mathbf{S}$. In other words, the path to collapse via bifurcation at

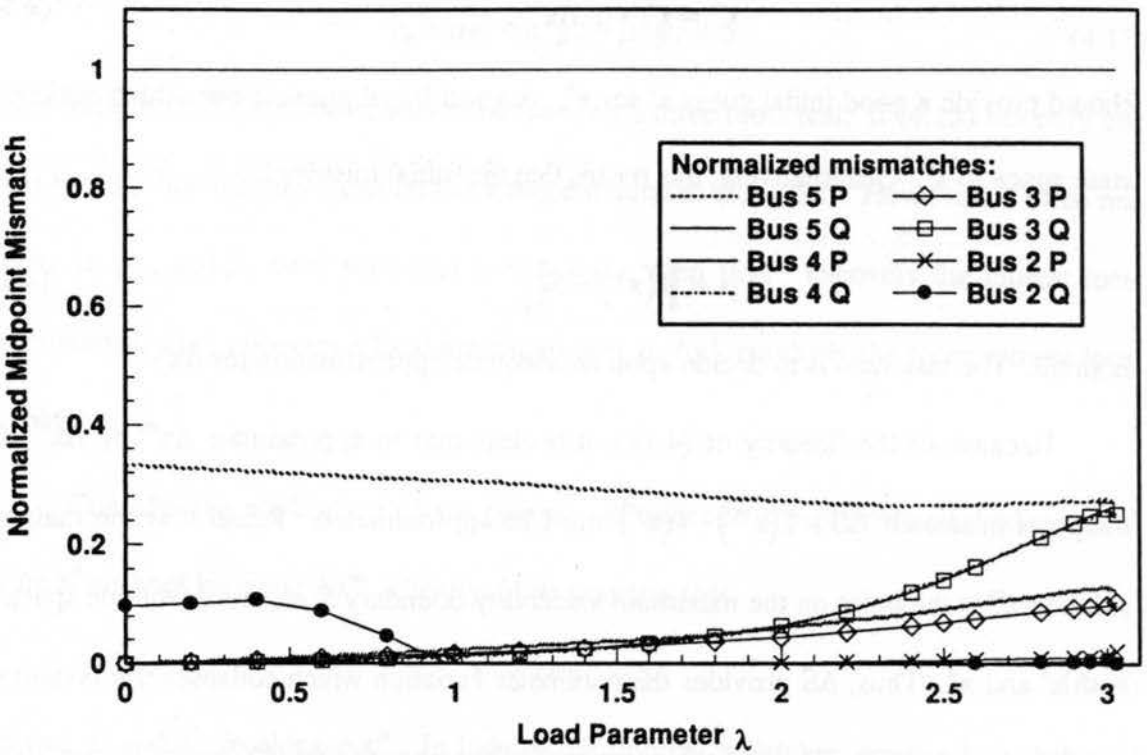

Figure 4.1: Midpoint mismatches for Stagg five-bus system

$\mathbf{x}^m$ is dominated by a change in reactive power at bus 5 alone. Since this path to collapse is by definition $\Delta\mathbf{S}$, it is clear that $\Delta\mathbf{S}$ may be approximated as a vector $\Delta\mathbf{S}^*$ consisting entirely of zero elements except for a single element corresponding to the bus for which an associated low-voltage solution is desired; that element is set to one. Again, because of the linearity of (4.14), the accuracy of this approximation determines the accuracy of $\Delta\mathbf{x}^{c*}$, which, in turn, is the approximation for $\Delta\mathbf{x}^m$. Applying the third optimal multiplier μ_3 as in (4.17) should then result in a correspondingly accurate initial guess $\mathbf{x}^0$.

4.3 Midpoint Method Low-Voltage Solution Algorithm

The above developments may now be summarized in the form of a computationally inexpensive algorithm. The algorithm is repeatedly applied to each bus k in a set $\mathbf{K}$ consisting of all buses for which potential low-voltage solutions are desired. It is assumed

that the operable solution $\mathbf{x}^s$ has already been found. For each bus k in $\mathbf{K}$, the following tasks are performed:

1) Set $\Delta\mathbf{S}^*$ with a single nonzero element at the position of the reactive power mismatch for bus k.

2) Calculate the search direction $\Delta\mathbf{x}^{c*}$ using (4.14) with $\Delta\mathbf{S}^*$ replacing $\mathbf{f}(\mathbf{x}^m) - \mathbf{f}(\mathbf{x}^s)$.

3) Attempt to apply the optimal multiplier technique. One of the three roots to the cubic equation will be zero. If the two remaining roots are complex conjugates, then a second local minimum of the square of the norm of the power flow mismatches does not exist along $\Delta\mathbf{x}^{c*}$, and the effort to find a low-voltage solution corresponding to that bus should be abandoned. If, however, the two additional roots are real, then the largest root μ_3 determines how far to move in the direction $\Delta\mathbf{x}^{c*}$. Set $\mathbf{x}^0 = \mathbf{x}^s + \mu\Delta\mathbf{x}^{c*}$ as the initial estimate of $\mathbf{x}^u$.

4) Solve the Newton-Raphson power flow using $\mathbf{x}^0$ as an initial guess for $\mathbf{x}^u$.

The main advantage that this method enjoys over those presented in Chapter 3 is that its computational requirements are quite reasonable. If the operable solution has been found using the Newton-Raphson method, then $\mathbf{J}(\mathbf{x}^s)$ is already available in factored form. Otherwise, it must be calculated and factored once for the entire set $\mathbf{K}$. Moreover, since $\Delta\mathbf{S}^*$ is a sparse vector, $\Delta\mathbf{x}^{c*}$ can be calculated very efficiently using sparse vector methods with fast-forward, full-backward substitution [26]. (Henceforth, $\Delta\mathbf{S}^*$ and $\Delta\mathbf{x}^{c*}$ will be denoted as $\Delta\mathbf{S}$ and $\Delta\mathbf{x}$ for notational simplicity.) Calculating μ_3 is a trivial task as well, requiring only a power flow mismatch calculation and a few operations of order n.

Finally, provided the initial guess $\mathbf{x}^0$ is good, which means that ρ in (4.19) is small, the second power flow solution should converge fairly quickly. The performance of the algorithm in this regard will be evaluated shortly.

The final issue to address is the determination of the set **K** of buses to check. This set should be general enough so that no critical low-voltage solutions are missed. Yet it should not be so inclusive that an excessive number of power flow solutions must be performed. Specifically, for the midpoint method to become preferable to the simplified method, the most critical low-voltage solutions should be identified using fewer than $n-1$ power flow solutions. A newly developed, easily computed linear sensitivity screening measure will be discussed in Section 4.6.

4.4 Performance of the Midpoint Method

This section explores the application of the midpoint method to systems of various sizes and complexities. Performance will be evaluated in terms of the method's ability to track several low-voltage solutions as loading is increased over a wide load range toward maximum loadability, as well as its ability to obtain accurate initial guesses. The effect of alternative load parametrizations and the enforcement of var limits will also be addressed.

4.4.1 Tracking low-voltage solutions

The symmetrical three-bus system used to illustrate the effect of load participation on the identity of the critical low-voltage solution was studied first to establish the ability of the midpoint method to track both of its type-one low-voltage solutions. Specifically,

Specifically, consider the case in which load participation at bus 1 is twice that at bus 2. Recall from Figure 2.12 that the low-voltage solution corresponding to bus 1 was critical, coalescing with the high-voltage solution at a total system load of 965 MW. The type-one solution associated with bus 2 vanished at a total load of 787 MW when it coalesced with the type-two solution. Figure 4.2 illustrates the ability of the midpoint method to track both of these solutions over the entire load range for which they exist. These curves were obtained by increasing load uniformly at both load buses and applying the midpoint method at these buses for each loading. The results are encouraging because they suggest that the method does fulfill its primary goal of finding type-one low-voltage solutions reliably, at least for this simple system.

The next system of interest was the Stagg five-bus system. The existence of low-voltage solutions for this system was previously studied using the simplified method in [27]. For extremely low loadings, the Stagg five-bus system has four low-voltage solutions, but beyond the base loading only one type-one solution has been found. Application of the midpoint method to this system accurately portrayed this behavior, as shown in Figure 4.3. Again, load was increased uniformly throughout the system, and the midpoint method was applied at all buses to find the low-voltage solution associated with each bus. Interestingly, for λ ranging between 1.9 and 2.8, the final low-voltage solution was discovered by applying the method at all four nonslack buses. This behavior illustrates the manner in which various areas of the system tend to merge as the load approaches critical levels. For a highly interconnected model such as the Stagg five-bus

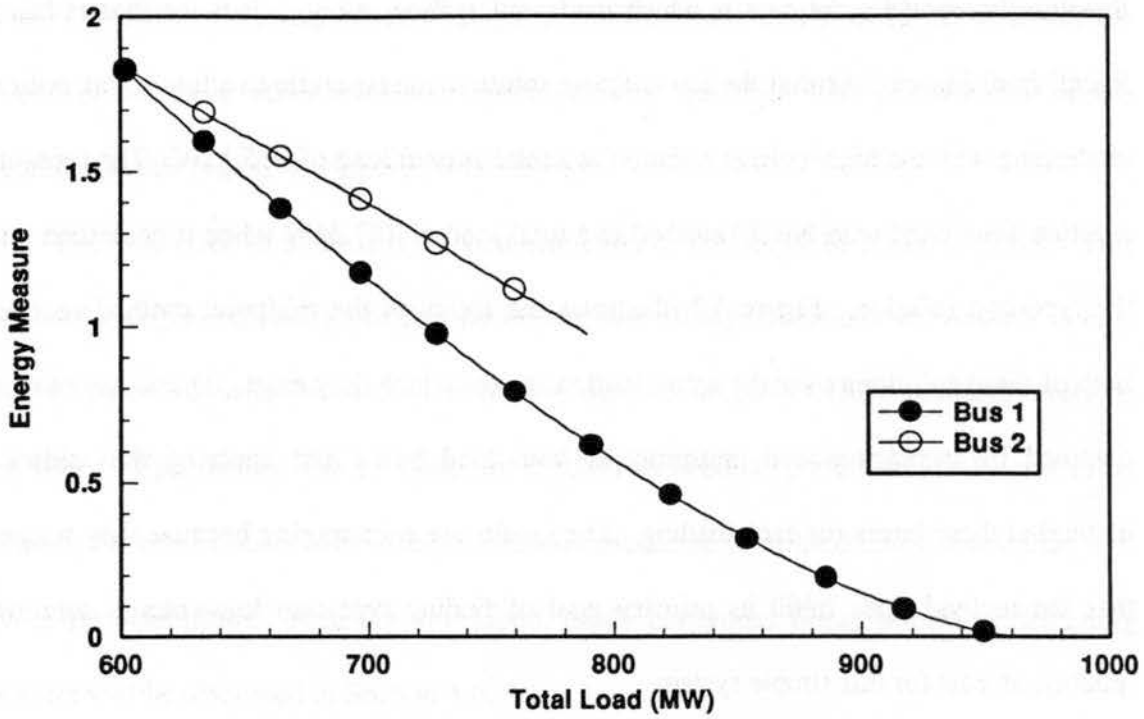

Figure 4.2: Convergence for symmetrical three-bus system

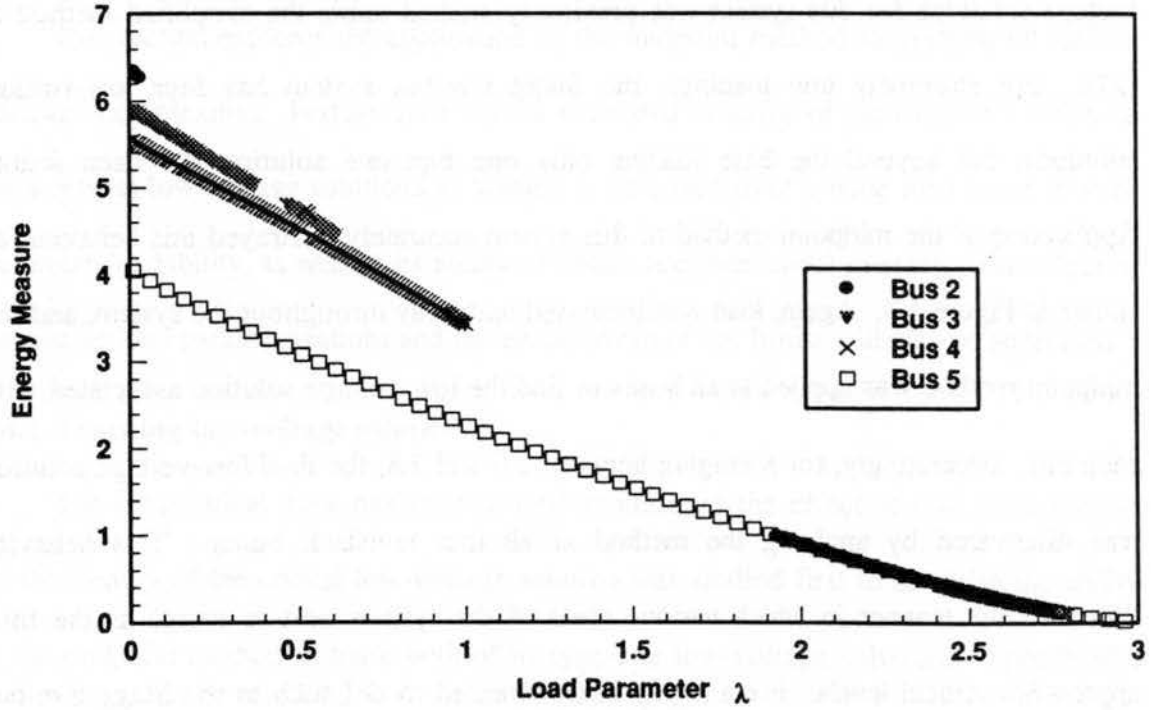

Figure 4.3: Convergence for Stagg five-bus system

system, the entire network tends to merge into a single area. An implication of areas merging for larger systems is that often only the weakest areas of the system need be identified; the associated low-voltage solutions may then be obtained by applying the midpoint method at the center bus for that area or at its nearest neighbors. Consequently, it is sometimes helpful to have some idea of the topology of the network when searching for low-voltage solutions.

The algorithm was then applied to the IEEE 118-bus system. Again, real and reactive loads were increased uniformly at all buses. Generator participation factors were obeyed, and var limits enforced. Violations of var limits were not checked until the power flows had converged. The 118-bus system has several low-voltage solutions, among the most critical of which are those corresponding to buses 1, 21, 43, 44, 53, and 95 [28]. Figure 4.4 illustrates the ability of the simplified method to track these solutions over the load ranges for which they exist. Bus 44 is the critical bus for this particular load parametrization, though a slight change in load participation may ultimately cause bus 95 to be critical because it appears to be extremely sensitive to load increases. Note that the point of maximum loadability corresponds to $\lambda = 2.92$. When the midpoint method was applied at these six buses and the energies of the resulting solutions were plotted as functions of load, the six curves of Figure 4.5 were produced. These profiles closely resemble those of Figure 4.4, with a few notable exceptions. For example, the midpoint algorithm failed to trace the most critical solution at bus 44 all the way to the point of collapse. Instead, applying the method at bus 45 for $\lambda > 2.87$ allows the most critical

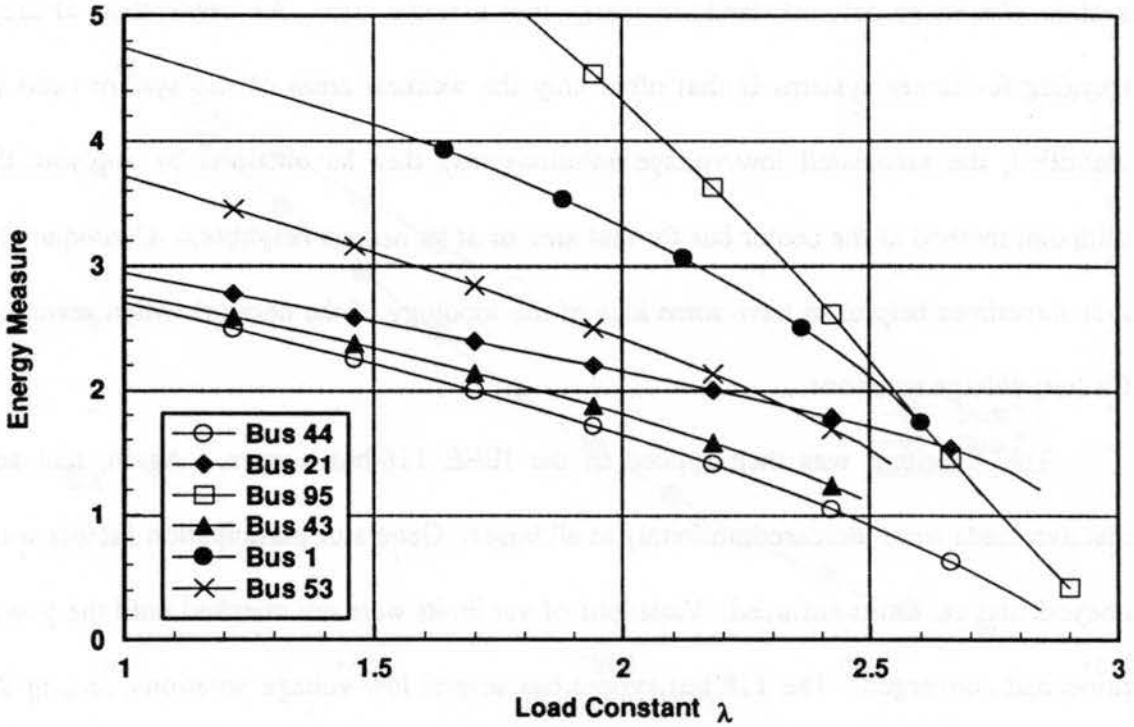

Figure 4.4: Critical low-voltage solutions for IEEE 118-bus system

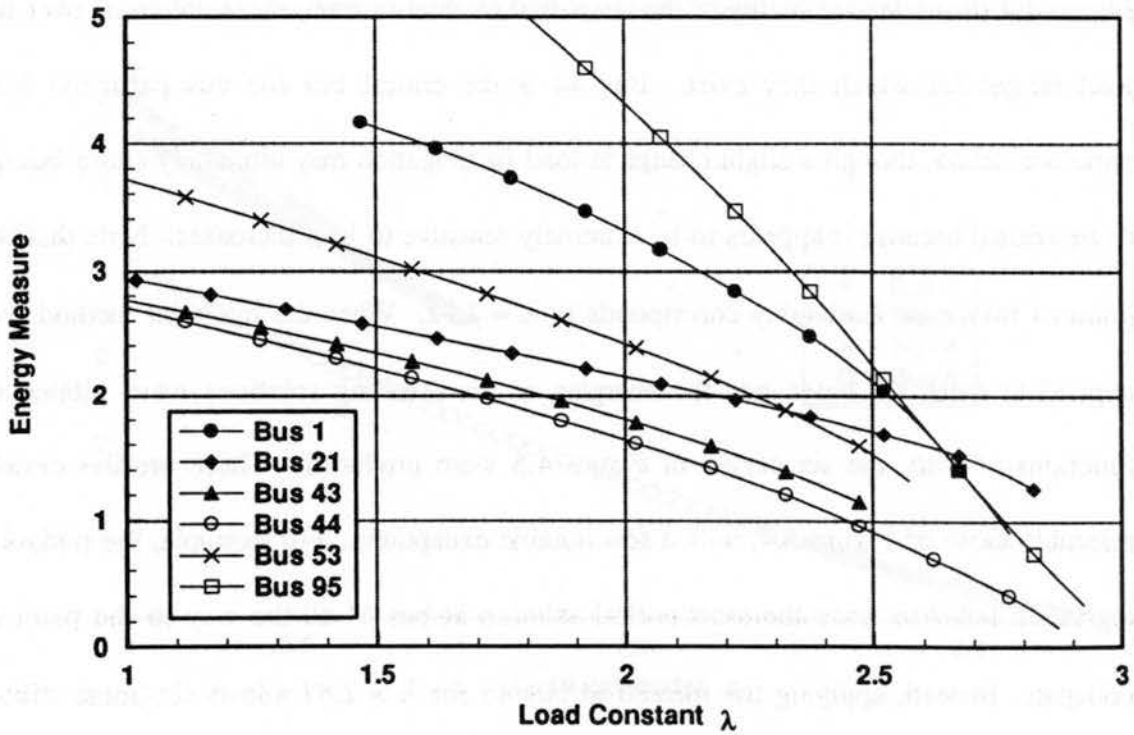

Figure 4.5: Convergence of midpoint method for IEEE 118-bus system

solution to be traced to the point of collapse. Another example of the merging of areas is offered by bus 52, whose associated low-voltage solution eventually merges with that of bus 53. Again, the importance of considering the nearest neighbors of critical buses is emphasized. The most important conclusion drawn from this exercise, however, is that the midpoint method exhibits good convergence properties, for it is able to track a number of low-voltage solutions over a wide load range.

This encouraging behavior is not specific to the case of uniform load parameterization. Figure 4.6 reveals that when load is increased only at buses 43 and 95 and at their sets of nearest neighbors (44, 34, 36, 37, 45 and 96, 82, 94, 80, 92, 100, 97), application of the midpoint method at these buses is successful in tracing the set of low-voltage solutions towards maximum loadability. Several other load parametrizations were investigated, and each was successfully handled by the midpoint method. Load voltage dependencies were not investigated, however. This is an issue of future research.

Another issue that has both present and future research implications is the effect of var limit enforcement on the performance of the midpoint method. In all the plots presented thus far, var limits were ignored until the norm of the power flow mismatches approached zero. Recall that when a var limit is seen to be violated, the PV bus is recast as a PQ bus with reactive load set at its maximum var limit, and the power flow must then be resolved. Obviously, the need to repeat the power flow calculation can have a profound impact on the quality of the initial guess obtained using the midpoint method, especially since low-voltage solutions tend to push var sources to their limits. Thus,

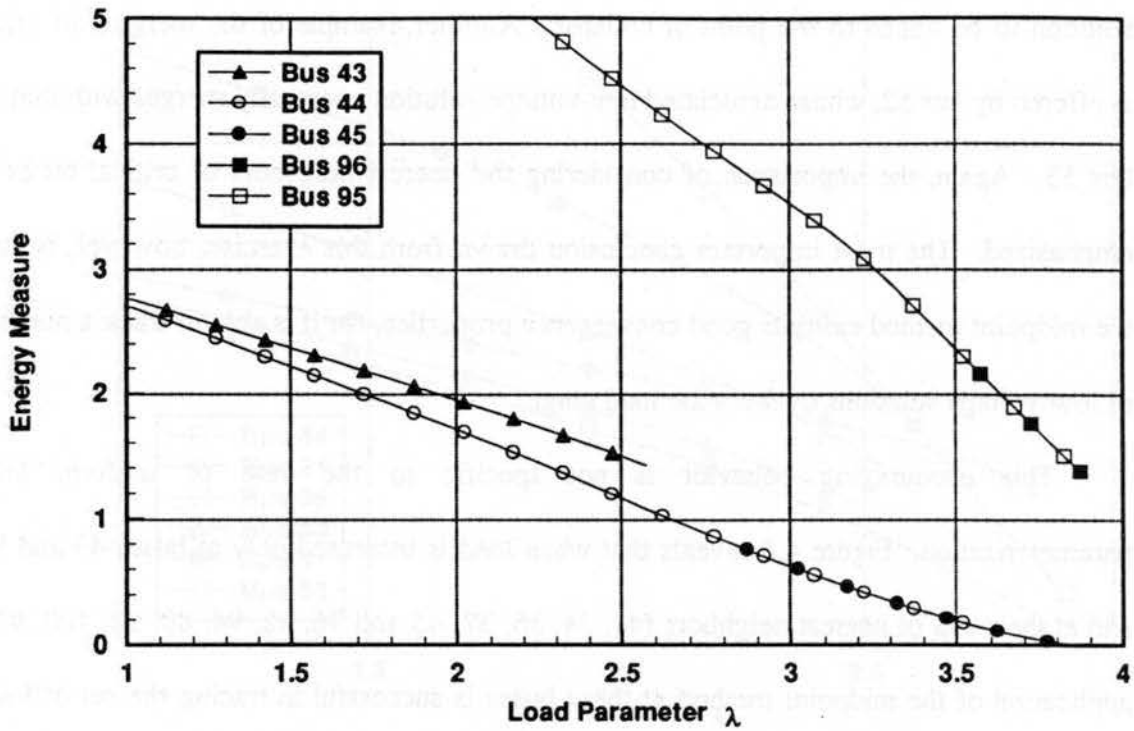

Figure 4.6: Convergence of midpoint method for different load participation

proper enforcement of generator var limits is a key concern. In this research, when the midpoint method was applied at generator buses, the generator buses were first recast as load buses set to their maximum var limits. This approach met with limited success, as will be shown in the following section. The point at which var limits were checked also has a profound impact on the performance of the algorithm, though not on its convergence properties. When var limits are checked as the norm of the power flow mismatches falls below 100 per-unit, no difference is noticed in the ability of the method to converge to low solutions. However, early enforcement of var limits does have a favorable effect on the number of iterations needed to converge to the low-voltage solution. This will be demonstrated shortly.

4.4.2 Accuracy of initial guesses

For the midpoint method to be a reliable low-voltage solution technique, it should provide initial guesses from which convergence to the low-voltage solution is efficiently accomplished. This means that the initial mismatches associated with the low-voltage guesses should be small and that the number of iterations required to converge should also be small. This section explores both of these issues.

Figure 4.7 plots the maximum element of the mismatch at the initial guesses associated with the two load buses of the symmetrical three-bus system as load is increased twice as fast at bus 1 as at bus 2. The curves show that as the load in the system is increased, so long as both solutions exist, the initial mismatches for each guess are quite low, thus increasing the likelihood that the low-voltage solution calculations will converge. This is particularly true of the initial guess for bus 1, which improves significantly as maximum loadability is approached. The increase in the maximum mismatch for the bus 2 initial guess also proves beneficial, for it suggests that the bus 2 low-voltage solution might no longer exist beyond a certain loading. This observation forms the foundation for screening buses by initial cost, a topic which will be addressed in Section 4.6. At any rate, the low initial mismatches suggest that the initial guesses are quite good.

A similar conclusion can be drawn for the method applied to the IEEE 118-bus system. Figure 4.8 indicates that the initial mismatches are again quite small for the most critical buses as loading is increased. The initial guesses improve significantly as the

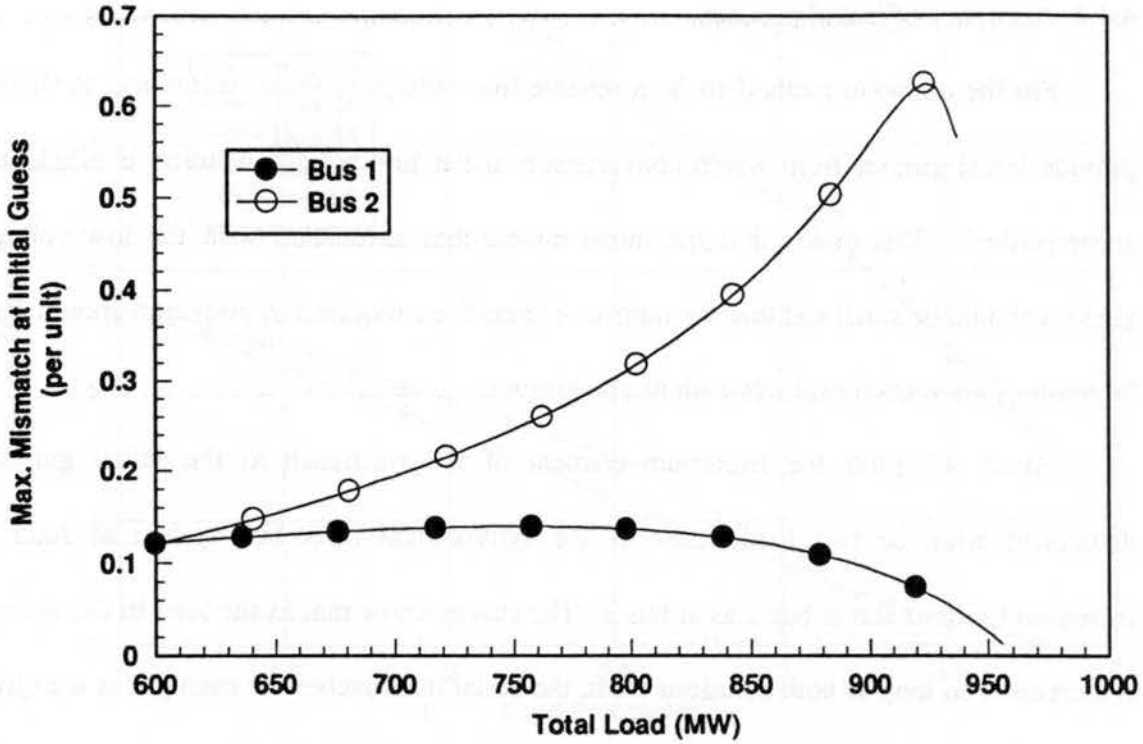

Figure 4.7: Accuracy of initial guesses for three-bus system

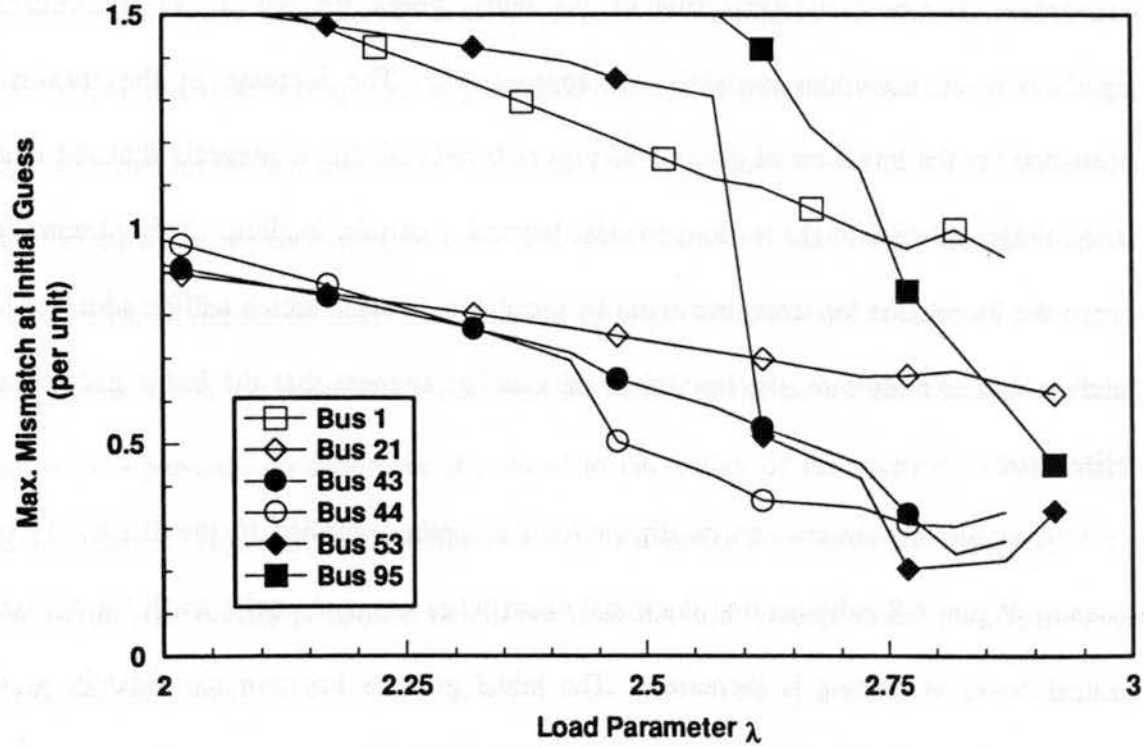

Figure 4.8 Accuracy of initial guesses for IEEE 118-bus system

system approaches maximum loadability, thereby ameliorating the convergence ability of the algorithm as the system becomes more stressed.

An interesting aspect of the mismatches at the midpoint method's initial guesses is that they tend to have as their largest elements the real power component corresponding to the bus at which the midpoint method was applied. This differs, for example, from the simplified method, whose initial guesses incur their greatest mismatches in the reactive power injection of a bus that is usually not the bus at which the method was applied. Curiously, this characteristic of the midpoint method changes as maximum loadability approaches, where the largest mismatches are then seen to be reactive in nature.

This behavior is chronicled in Table 4.1 for the Stagg five-bus system for five different loadings. In this table, "p" denotes real power and "q" denotes reactive power, while "n" indicates that no guess was possible. Thus, the notation "p2" suggests that the maximum mismatch of the initial guess corresponded to the real power injection at bus 2, while "n0" indicates that no initial guess was possible. Similar observations hold for the IEEE 118-bus system. These results intimate that perhaps the midpoint method could be improved by making the approximation of the midpoint mismatch slightly more flexible than simply defining it as a singleton. Some preliminary exploration of the concept of an adaptive $\Delta\mathbf{S}$ has been conducted, but it will receive greater attention in future research.

The last load entry of Table 4.1 suggests another important concept. Originally it was hoped that the computation expense of the method could be improved if the number of buses at which the midpoint method was unable to determine an initial guess increased noticeably as loading was increased. Recall that no initial guess is possible if only one root

Table 4.1: Location of maximum mismatches for Stagg five-bus system

λ	Bus #	Max. Mismatch	λ	Bus #	Max. Mismatch
0.500	2	p2	2.000	2	p2
	3	p3		3	p3
	4	p4		4	p4
	5	p5		5	p5
1.000	2	n0	2.500	2	q2
	3	p3		3	p3
	4	p4		4	q4
	5	p5		5	p5
1.500	2	p2	2.975	2	n0
	3	p3		3	n0
	4	p4		4	n0
	5	p5		5	q5

of the cubic equation used to find the optimal multiplier is real. Unfortunately, Figure 4.9 indicates that the benefits of losing initial guesses are felt only when the system is on the brink of losing solvability. Then, the number of no-guess buses increases dramatically. Prior to this point, the plot is not the anticipated monotonically increasing function.

Of course, the accuracy of an initial guess does not always translate into quick convergence to the low-voltage solution. This is due to the fractal convergence boundaries of the Newton-Raphson's solutions. However, the power flows performed to find the low-voltage solutions generally converged quickly, particularly when generator

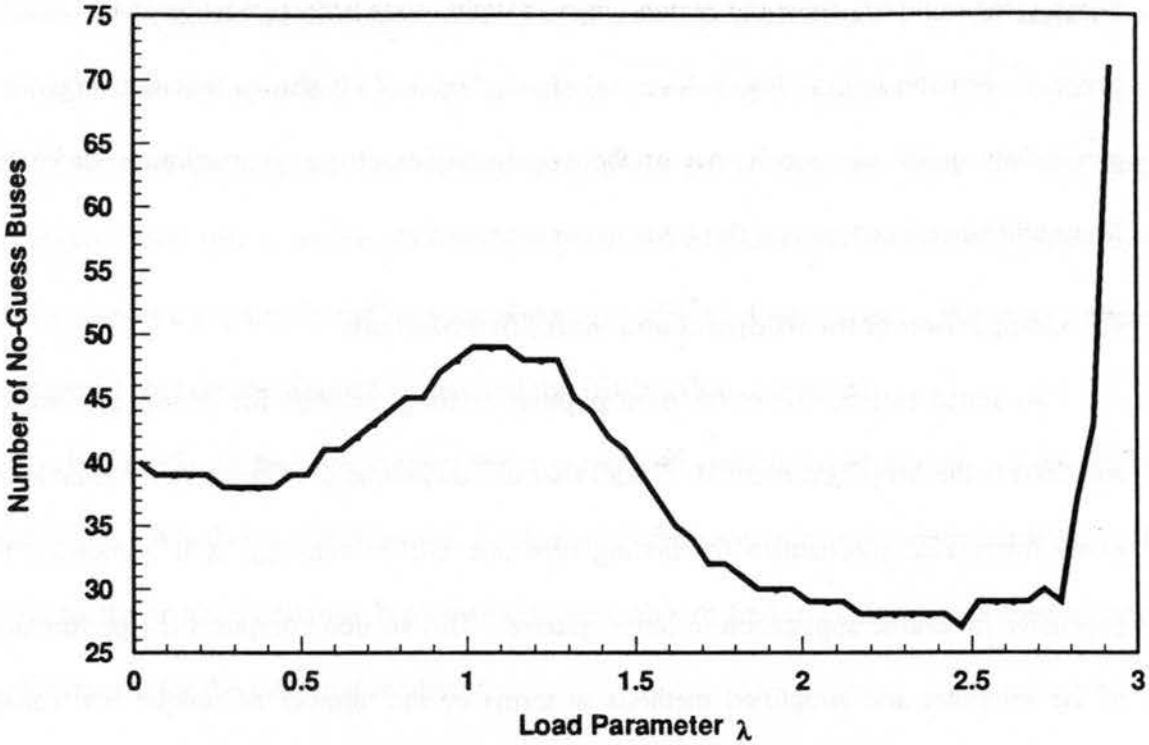

Figure 4.9: Number of no-guess buses for IEEE 118-bus system

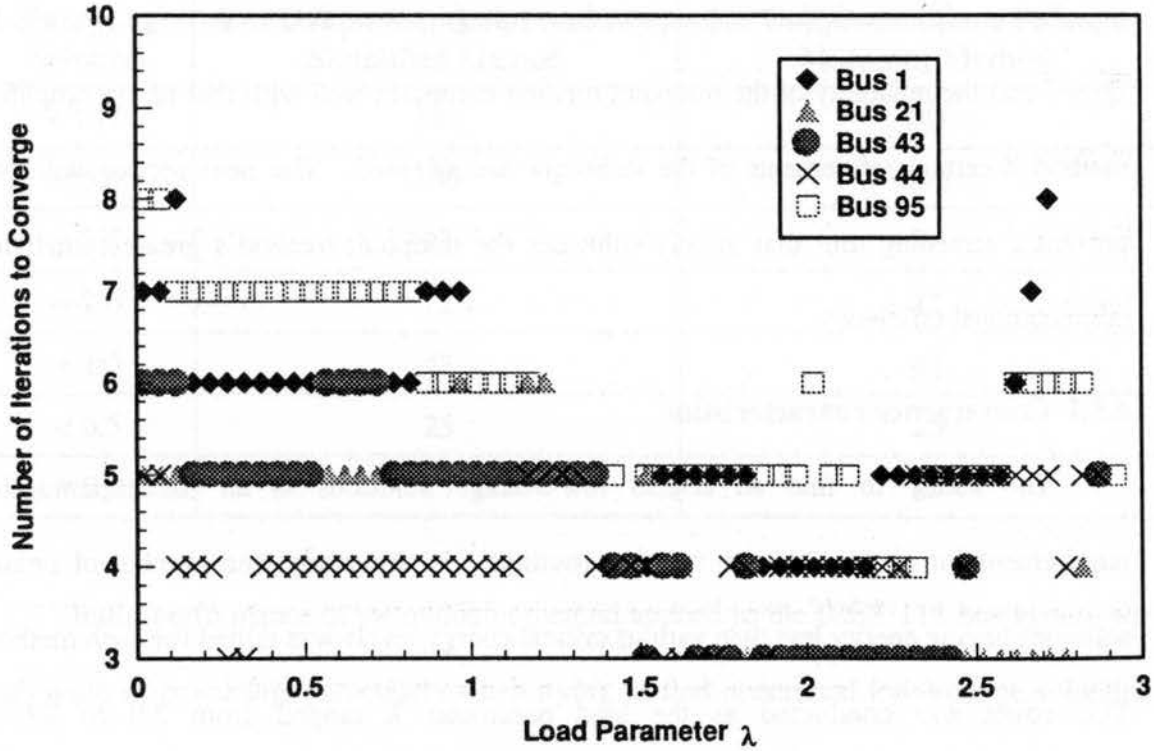

Figure 4.10: Number of iterations to converge for IEEE 118-bus system

buses were excluded from the search and var limits were enforced early in the solution process. For the critical low-voltage solutions, Figure 4.10 shows that convergence is particularly quick and accelerates as the system inches closer to maximum loadability. More will be said concerning this issue in the next section.

4.5 Comparison of the Midpoint and Simplified Methods

As stated earlier, one of the most popular existing methods for finding low-voltage solutions is the simplified method. Recall that this technique provides a fairly reliable and easily interpreted mechanism for finding type-one UEPs, although it is somewhat too expensive for online application to large systems. This section compares the performance of the midpoint and simplified methods in terms of the number of unique low-voltage solutions each is able to find, the accuracy of each method's initial guesses, and the expediency with which their subsequent low-voltage power flows converge. It will be shown that the reliability of the midpoint method compares well with that of the simplified method if certain refinements of the technique are adopted. The next section will then present a screening tool that greatly enhances the midpoint method's greatest attribute, computational efficiency.

4.5.1 Convergence characteristics

The ability to find all critical low-voltage solutions is an uncompromisable requirement for all low-voltage solution routines. In this study, the number of unique solutions having energy less than various critical energy levels was tallied for each method. This count was conducted as the load parameter λ ranged from 2.0 to 3.0 in

value. The intent was to obtain some idea of how the performances of the algorithms compare when trying to find solutions at various levels of system stress. In particular, this study focused on whether one method performed better than the other in detecting solutions while still a sizable distance away from maximum loadability, and how their performances compared in the more crucial stages of load development. These tests were performed for both the Stagg five-bus and the IEEE 118-bus systems.

For the Stagg five-bus system, the two methods performed identically, as shown in Table 4.2. Whether a solution was a substantial distance from maximum loadability or right on the brink of collapse, both methods were able to find it. This was an encouraging achievement for the midpoint method.

Table 4.2: Unique solutions found for Stagg five-bus system

Energy of Solution	**# of Unique Solutions Found by Simplified Method**	**# of Unique Solutions Found by Midpoint Method**
< 10.0	183	183
< 5.0	156	156
< 3.0	97	97
< 2.0	72	72
< 1.0	43	43
< 0.5	25	25
< 0.2	13	13

Initial performance of the midpoint method applied to the IEEE 118-bus system was not quite so promising, particularly when trying to find noncritical low-voltage solutions. Table 4.3 shows that the simplified method is much better in finding solutions with energy

measures from 3.0 to 10.0. The midpoint method found only 87% as many solutions with energy less than 10.0 as did its counterpart. However, the comparison is much more favorable when the focus is on low-energy solutions. The comparison becomes even more favorable if generator buses are excluded from the set of buses at which the simplified and midpoint techniques are applied. Table 4.4 shows that although the simplified method performs slightly better in finding the highest-energy low-voltage solutions when generators are not searched, the midpoint method is more adept at finding the more critical solutions. This suggests that the manner in which generator buses have been treated by the midpoint method is somewhat deficient. A better way to treat PV buses with the midpoint method will be pursued in future research. For now, a sound approach might be to apply the simplified method at generator buses and the midpoint method at load buses. However, adoption of this hybrid technique might be necessary only if one is interested in more than just the most critical low-voltage solutions. As indicated by Table 4.3, the two methods perform almost identically in finding the low-energy solutions.

Table 4.3: Unique solutions found for IEEE 118-bus system

Energy of Solution	**# of Unique Solutions Found by Simplified Method**	**# of Unique Solutions Found by Midpoint Method**
< 10.0	2012	1746
< 5.0	849	795
< 3.0	257	252
< 2.0	90	88
< 1.0	16	16
< 0.5	6	6
< 0.2	2	2

Table 4.4: Unique solutions for the IEEE 118-bus system with generators discounted

Energy of Solution	# of Unique Solutions Found by Simplified Method	# of Unique Solutions Found by Midpoint Method
< 10.0	1559	1536
< 5.0	629	639
< 3.0	202	211
< 2.0	68	74
< 1.0	13	15
< 0.5	6	6
< 0.2	2	2

Table 4.5: Unique solutions for IEEE 118-bus system with early var limit enforcement

Energy of Solution	# of Unique Solutions Found by Simplified Method	# of Unique Solutions Found by Midpoint Method
< 10.0	1703	1644
< 5.0	682	657
< 3.0	229	223
< 2.0	82	82
< 1.0	15	15
< 0.5	5	5
< 0.2	1	1

Another key issue is the timing of var limit enforcement. For the results in Tables 4.2 through 4.4, var limits were not checked until the power flow had converged. Now consider the case in which var limits are enforced when the norm of mismatch decreases below 100 per-unit. Table 4.5 shows that, with generators excluded from the set of buses to check, both methods find more higher-energy solutions than they were able to uncover

when the checking of var limits was delayed, although both miss a solution on the brink of collapse (at $\lambda = 2.92$). Once again, the simplified method outshines the midpoint method in determining higher-energy solutions. However, the two techniques are equally capable in finding solutions with energy measures less than 2.0.

4.5.2 Accuracy of initial guesses

A particularly strong advantage of the midpoint method is that it calculates initial guesses that generally have significantly smaller associated mismatches than those guesses produced by the simplified method. In this study, initial guesses were calculated by both methods as load was varied over the range $2.0 \leq \lambda \leq 3.0$, and the number of times mismatches of various magnitudes were encountered was tallied for each method. Results were collected for both the Stagg five-bus system and the IEEE 118-bus system.

Figure 4.11 corresponds to the Stagg five-bus system. The bar chart clearly demonstrates that the initial guesses calculated by the midpoint method significantly improve upon those of the simplified method. Note that about 40 solutions were found from initial guesses having all maximum mismatch components less than 1.0 per unit. The most accurate initial guesses obtained using the simplified method had maximum initial mismatch components in excess of 2.0 per unit.

Figure 4.12 presents equivalent results for the IEEE 118-bus system. Again, one finds that the midpoint method generally provides the more accurate initial guesses. Also clear from the chart is the existence of a great number of cases (731) in which no initial

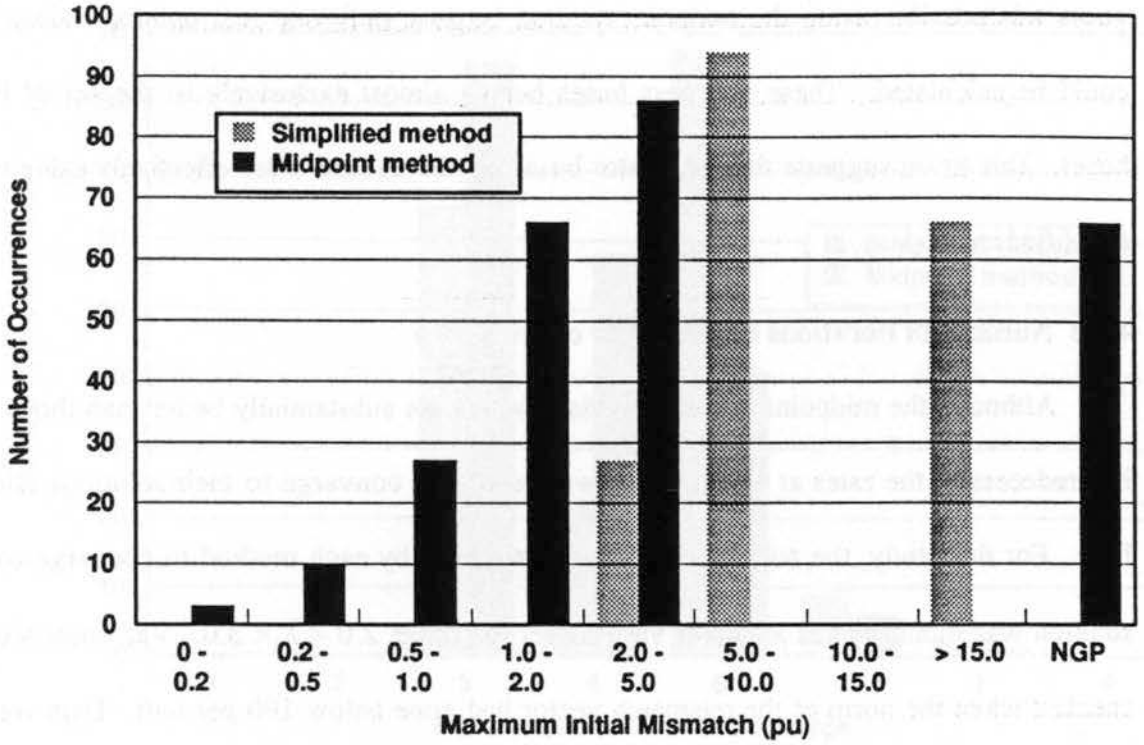

Figure 4.11: Mismatch comparison for Stagg five-bus system

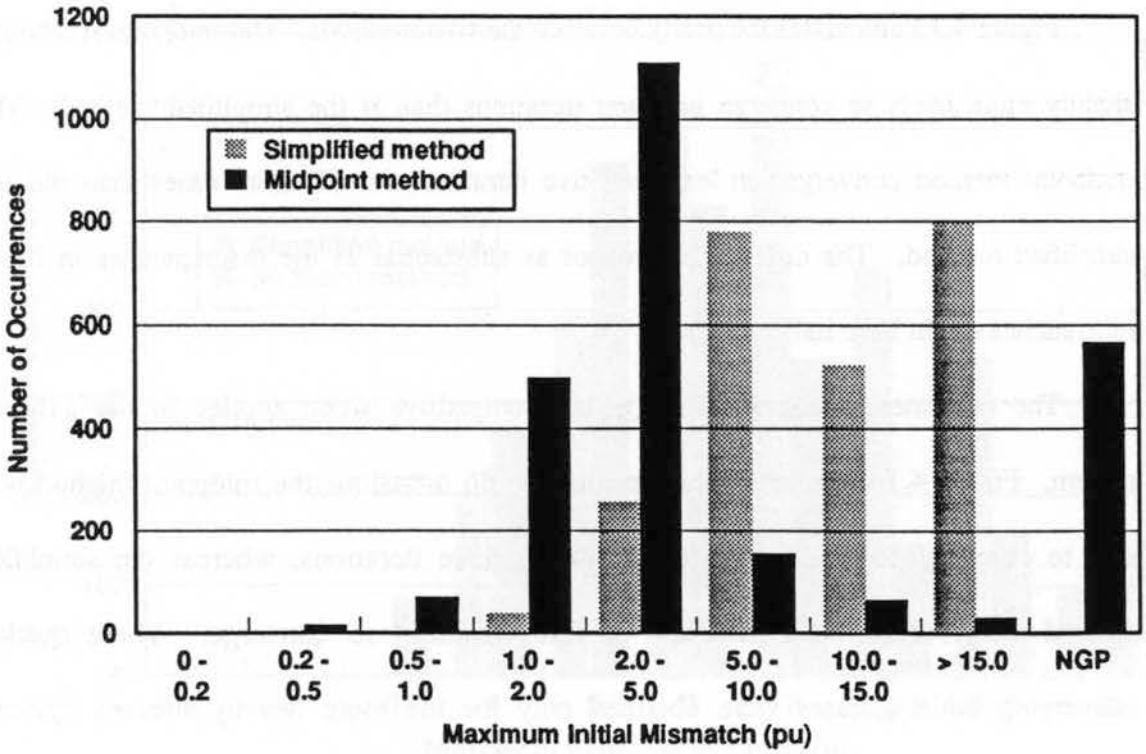

Figure 4.12: Mismatch comparison for IEEE 118-bus system

guess was possible using the midpoint method because only one real optimal multiplier could be calculated. These no-guess buses belong almost exclusively to the set of PV buses. This again suggests that generator buses can be treated more effectively using the simplified method.

4.5.3 Number of iterations required for convergence

Although the midpoint method's initial guesses are substantially better than those of its predecessor, the rates at which these two techniques converge to their solutions differ little. For this study, the number of iterations required by each method to converge to a solution was monitored as load was varied over the range $2.0 < \lambda < 3.0$. Var limits were checked when the norm of the mismatch vector had gone below 100 per unit. Data were collected for both the Stagg five-bus system and the IEEE 118-bus system.

Figure 4.13 elucidates the parity between the two methods. The midpoint method is slightly more likely to converge in fewer iterations than is the simplified method. The midpoint method converged in less than five iterations for 57 more cases than did the simplified method. The differences are not as substantial as the discrepancies in initial mismatches might have indicated.

The two methods again prove highly competitive when applied to the 118-bus system. Figure 4.14 presents these results. On 86 occasions the midpoint method was able to converge to a low-voltage solution in three iterations, whereas the simplified method always required a minimum of four iterations to converge. These quickly converging initial guesses were obtained only for the more heavily stressed systems

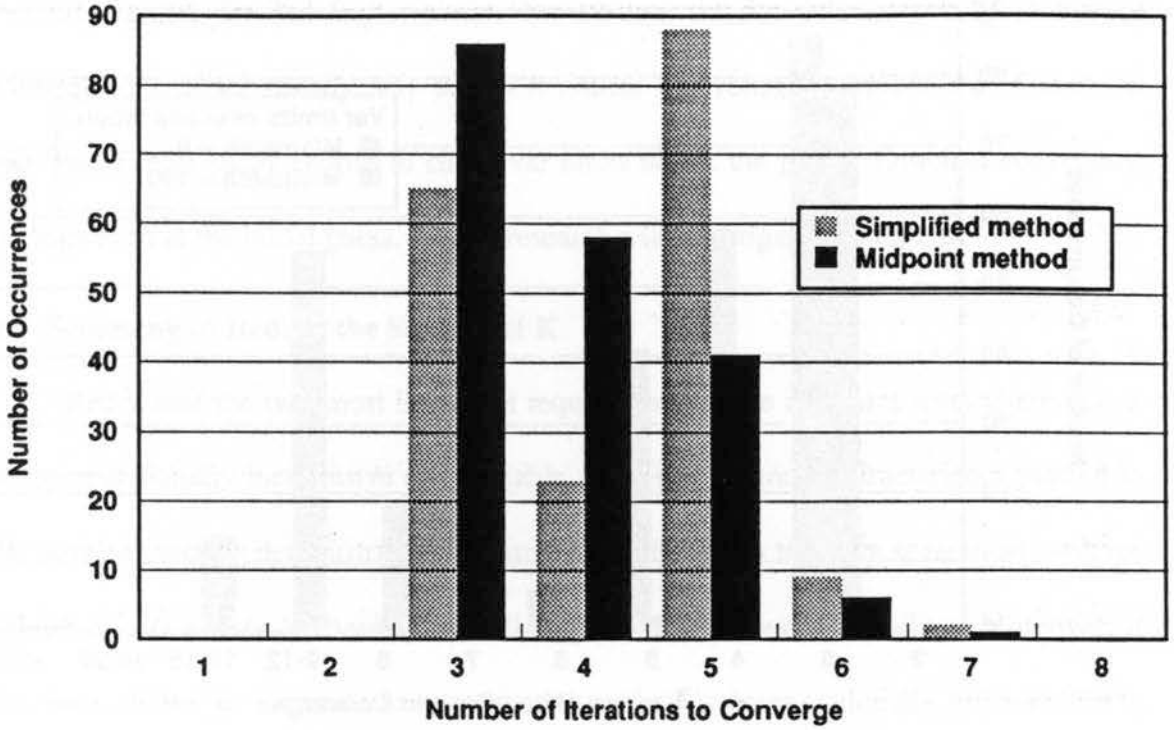

Figure 4.13: Iteration comparison for Stagg five-bus system

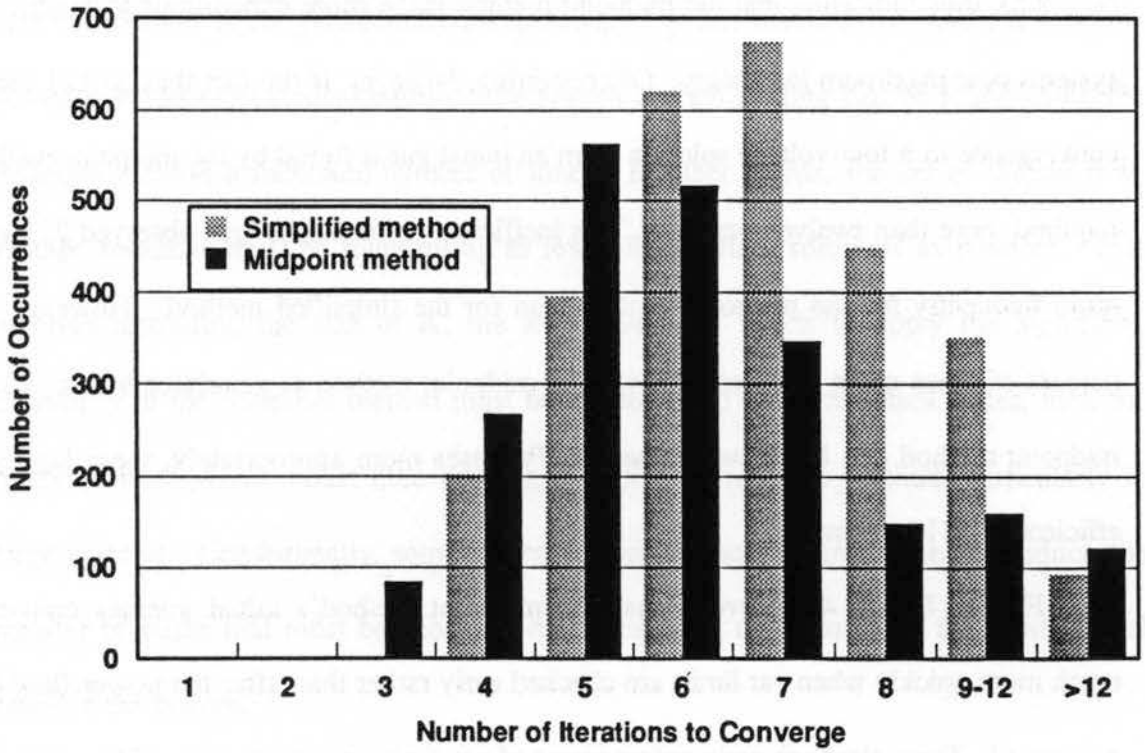

Figure 4.14: Iteration comparison for IEEE 118-bus system

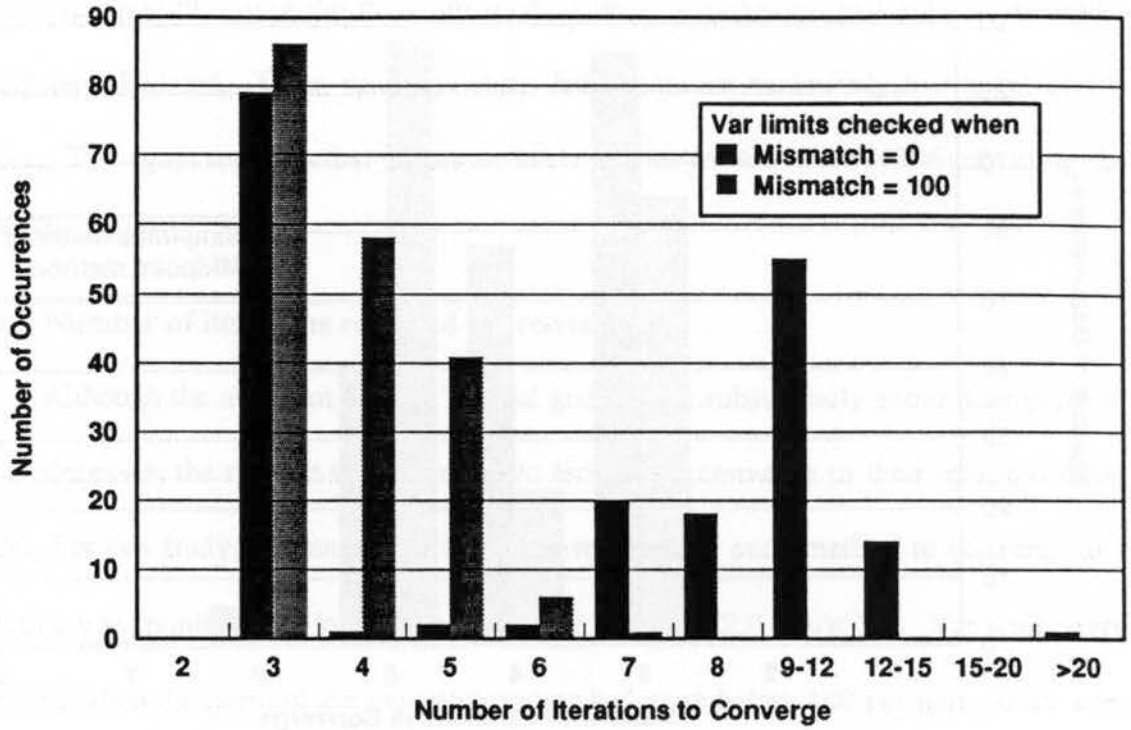

Figure 4.15: Effect of delaying var limit enforcement

($\lambda > 2.5$), thus indicating that the midpoint method is the more expeditious technique for systems near maximum loadability. Disconcerting, however, is the fact that, in 121 cases, convergence to a low-voltage solution from an initial guess found by the midpoint method required more than twelve iterations. This inefficient performance was observed 21 times more frequently for the midpoint method than for the simplified method. However, 85 percent of these cases involved applying the midpoint method at generator buses. If the midpoint method can be refined to handle PV buses more appropriately, these lapses in efficiency will be minimized.

Finally, Figure 4.15 reveals that the midpoint method's initial guesses converge much more quickly when var limits are checked early rather than after the power flow has converged. Thus, although early enforcement of var limits sacrifices some of the midpoint

method's ability to find higher-energy low-voltage solutions, it does help accelerate convergence. Since usually only the most critical low-voltage solutions are of interest, one would most likely choose to check var limits before the power flow had converged, perhaps even at the initial guess. Future research will investigate this further.

4.6 Screening to Reduce the Size of Set K

Recall that the two most important requirements of the midpoint method are that it be computationally inexpensive and realiable. The convergence characteristics plotted in the previous section demonstrate the algorithm's reliability in tracking several low-voltage solutions over a wide-load range toward the point of maximum loadability. Moreover, it has been shown to a certain extent that the method is computationally efficient, for it requires that little additional computation be performed. However, this has not established that the method is computationally inexpensive. For this claim to be made, it must be shown that the most critical buses of the system at each loading can be found using the midpoint method a minimum number of times. In other words, the set of critical low-voltage solutions must be found using as few full load flow solutions as possible. This involves restricting the size of **K**, the set of buses at which to apply the algorithm. Obviously, if the midpoint method must be applied at all $(n-1)$ nonslack buses, then the midpoint method can boast little advantage over the simplified method, particularly in large systems. Consequently, some screening method must be introduced to reduce the number of buses that must be checked while preserving the identity of the most critical buses in the system.

During the course of this research, a number of characteristics of the midpoint method and its low-voltage solutions were studied in the hopes of devising a suitable screening tool. This section chronicles the evolution of this task. While the resulting techniques are by no means foolproof, they are expeditious and thus suitable for online application.

4.6.1 Screening by initial cost

Because of the efficiency of the algorithm in obtaining initial guesses $\mathbf{x}^0$ for low-voltage solutions, for small- and medium-sized systems it would be practical to perform this calculation at all buses. Once all possible initial guesses have been computed, a cost function $\rho(\mathbf{x}^0)$ defined as the norm of $\mathbf{f}(\mathbf{x}^0) - \mathbf{S}$ could be calculated, and full load flow solutions could then be performed starting from the initial guesses associated with the least values of $\rho(\mathbf{x}^0)$. Figure 4.16 provides the motivation for this screening method. It shows how the cost function at the initial guess $\mathbf{x}^0$ varies with the energy measure corresponding to the type-one solution found from the initial guess. With few exceptions, it seems the initial guesses that incur the least initial costs will ultimately converge to the lowest-energy and, therefore, most critical, low-voltage solutions. Thus, once $\mathbf{x}^0$ has been determined efficiently for each bus in the system, the search for low-voltage solutions may originate from only the least-cost initial guesses.

Work with the Stagg five-bus and IEEE 118-bus systems elucidated the merits of this screening technique. For both systems, load was increased uniformly at all buses as the midpoint method was applied at each bus for each loading. The costs associated with each initial guess were averaged over the range $2.0 \leq \lambda \leq 3.0$ for both systems. In the

case of the Stagg system, the buses listed in order of decreasing initial cost are 2, 3, 4, and 5. This suggests that if the midpoint method is applied at these buses, the most critical low-voltage solution will correspond to bus 5, the second most critical solution will correspond to bus 4, and so on. Figure 4.2 validates these suggestions. For the 118-bus system, initial cost screening identifies the following set as the buses yielding the fifteen most critical solutions for $2.0 \leq \lambda \leq 3.0$: 43, 44, 21, 22, 20, 76, 52, 53, 45, 33, 86, 1, 98, 13, 95. Figure 4.17 plots the variation of the energy measures associated with these solutions as loading is increased. This suggests that screening by initial cost is successful in identifying the most stressed buses of the system.

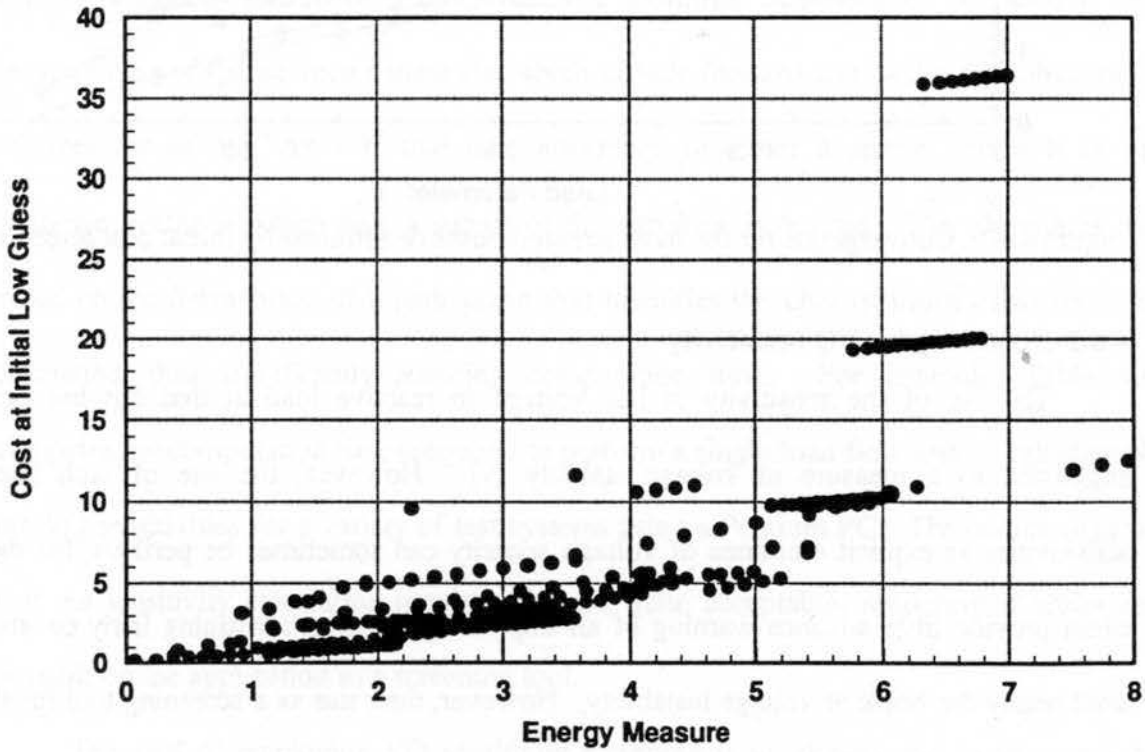

Figure 4.16: Initial cost screening properties for IEEE 118-bus system

Initial cost can provide an efficient screening tool for restricting the size of the set of buses to check for small- or medium-sized systems. However, because this screening tool entails calculating $\mathbf{x}^0$ through the midpoint method for every bus in the system, it is not

especially suited for large power systems. For this reason, the development of an alternative screening tool based on VQ sensitivity was pursued.

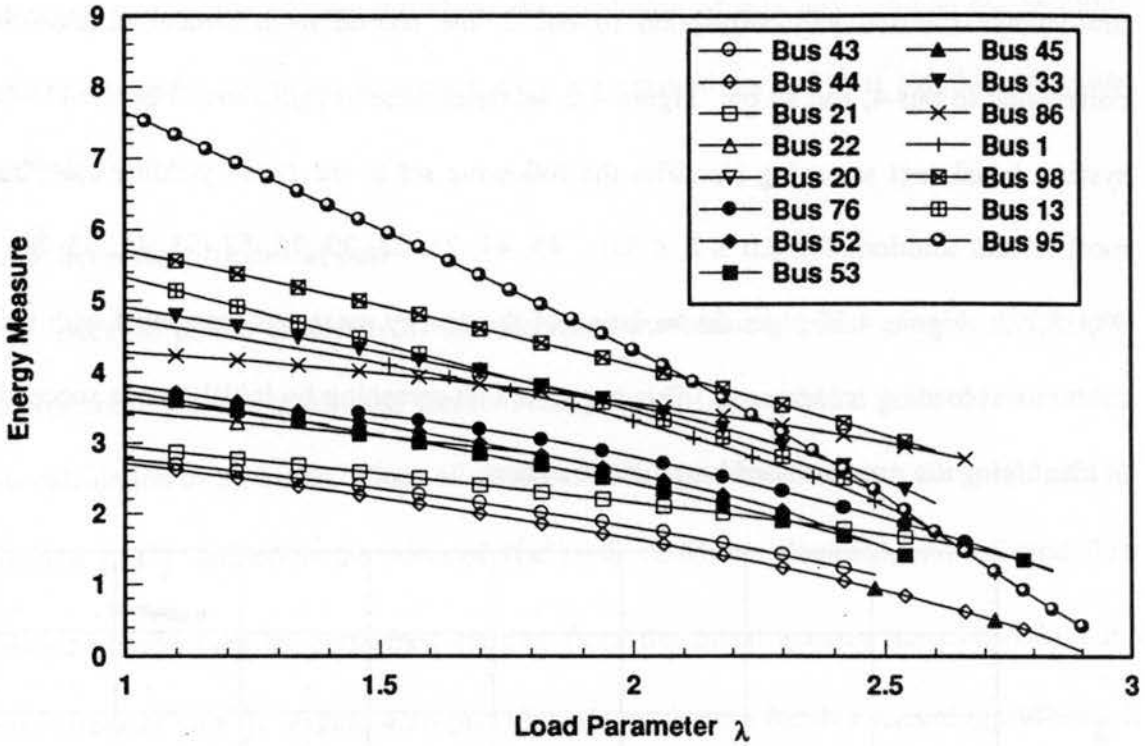

Figure 4.17: Convergence for the most stressed buses determined by initial cost screening

4.6.2 Screening by VQ sensitivity

The use of the sensitivity of bus voltage to reactive load at that bus has been suggested as a measure of voltage stability [9]. However, the use of such linear sensitivities as explicit measures of voltage security can sometimes be perilous, for they often provide little advance warning of an impending collapse, remaining fairly constant until nearly the brink of voltage instability. However, their use as a screening tool for the midpoint method has shown considerably more promise. This is particularly true for large systems for which the idea of calculating the costs associated with initial guesses at all buses is unattractive.

The calculation of VQ sensitivities for a system's load buses may be most easily understood by considering the following set of equations in which the relationship between changes in active and reactive power and changes in bus voltage angle and magnitude are clearly indicated:

$$\begin{bmatrix} \Delta \mathbf{P} \\ \Delta \mathbf{Q} \end{bmatrix} = \begin{bmatrix} \mathbf{J}_{P\theta} & \mathbf{J}_{PV} \\ \mathbf{J}_{Q\theta} & \mathbf{J}_{QV} \end{bmatrix} \begin{bmatrix} \Delta \theta \\ \Delta \mathbf{V} \end{bmatrix}. \tag{4.20}$$

Because the sensitivity of bus voltage magnitude at bus i to reactive power injection at bus i is of interest, the only nonzero element of the right-hand-side vector is $\Delta \mathbf{Q}_i$, and the only unknown of interest is $\Delta \mathbf{V}_i$. Hence, this calculation affords the opportunity to use sparse vector methods. Reference [26] provides a thorough treatment of the theory and programming of sparse vector methods, which include forward and backward substitution schemes for solving $\mathbf{Ax} = \mathbf{b}$ that take advantage of either a sparse vector $\mathbf{b}$ or an unknown vector in which only a subset of the variables is desired. The algorithms are based on the formulation of a path graph that identifies the only quantities that must be calculated, thus significantly reducing computation time. For example, Table 4.6 compares the computation times required to perform a single load flow and to calculate all the VQ sensitivities for a variety of test systems using a Pentium PC. The results suggest that the sensitivity calculation requirements are quite acceptable, rendering it useful for possible online application as a screening tool.

The goal of employing VQ sensitivity screening is to identify the locally weakest buses in the system. These will be the buses most likely to yield low-energy solutions.

Table 4.6: Computation times for VQ sensitivities

Test System	Power Flow Computation Time (sec)	VQ Sensitivity Computation Time (sec)
IEEE 118-Bus	0.3	0.1
IEEE 300-Bus	0.5	0.3
415-Bus Utility System	1.1	0.5
2000-Bus Utility System	14.3	23.6

Moreover, under certain conditions, it can be argued that the most sensitive bus in terms of VQ considerations will be the most advantageous ones to pursue with the midpoint method because they will incur the least initial mismatches. Consider the midpoint mismatch vector $\Delta\mathbf{S}$ with the single nonzero element ΔS_{Qi}. This element may be expressed functionally as

$$\begin{aligned}\Delta S_{Qi} &= f_{Qi}\left(\mathbf{x}^{\mathrm{m}}\right) - f_{Qi}\left(\mathbf{x}^{\mathrm{s}}\right) \\ &= \sum_{j=1}^{n} g_{ij}\left(-w_i^{\mathrm{m}}u_j^{\mathrm{m}} + u_i^{\mathrm{m}}w_j^{\mathrm{m}} + w_i^{\mathrm{s}}u_j^{\mathrm{s}} - u_i^{\mathrm{s}}w_j^{\mathrm{s}}\right) + b_{ij}\left(w_i^{\mathrm{m}}w_j^{\mathrm{m}} + u_i^{\mathrm{m}}u_j^{\mathrm{m}} - w_i^{\mathrm{s}}w_j^{\mathrm{s}} - u_i^{\mathrm{s}}u_j^{\mathrm{s}}\right).\end{aligned} \tag{4.21}$$

Assuming that all conductances g_{ij} are negligible, ΔS_{Qi} may be recast as generation minus load,

$$\Delta S_{Qi} = \sum_{j=1}^{n} b_{ij}\left(w_i^{\mathrm{s}}w_j^{\mathrm{s}} + u_i^{\mathrm{s}}u_{\mathrm{j}}^{\mathrm{s}} - w_i^{\mathrm{m}}w_{\mathrm{j}}^{\mathrm{m}} - u_i^{\mathrm{m}}u_j^{\mathrm{m}}\right). \tag{4.22}$$

After converting all voltages to polar form using

$$\mathrm{V}_i = u_i + \mathrm{j}\,w_i = V_i\cos\theta_i + \mathrm{j}\,V_i\sin\theta_i \tag{4.23}$$

and collecting like terms, one may rewrite (4.22) as

$$\Delta S_{Qi} = \sum_{j=1}^{n} b_{ij}\left[V_i^s V_j^s\left(\sin\theta_i^s \sin\theta_j^s + \cos\theta_i^s \cos\theta_j^s\right) - V_i^m V_j^m\left(\sin\theta_i^m \sin\theta_j^m + \cos\theta_i^m \cos\theta_j^m\right)\right].$$

(4.24)

Assuming that bus voltage angles are largely independent of reactive power injection, a plausible assumption because the elements of $\mathbf{J_{Q\theta}}$ are usually small, particularly when the system is more lightly loaded, we have

$$\sin\theta_i^s \sin\theta_j^s + \cos\theta_i^s \cos\theta_j^s \approx \sin\theta_i^m \sin\theta_j^m + \cos\theta_i^m \cos\theta_j^m = A \tag{4.25}$$

where A is a constant. Then,

$$\Delta S_{Qi} = \sum_{j=1}^{m} b_{ij} A\left(V_i^s V_j^s - V_i^m V_j^m\right). \tag{4.26}$$

The larger in magnitude the VQ sensitivity is at bus i, the smaller V_i^m will be relative to V_i^s, since an increase in reactive power load at bus i will incur a larger magnitude drop in V_i^m if the VQ sensitivity at bus i is high. Hence, from (4.26), ΔS_{Qi} will increase. The same will hold true if the sensitivity of the voltage magnitude at bus j to reactive power injection is high. Then, either a large $\left|\partial V_i/\partial Q_i\right|$ or a large $\left|\partial V_j/\partial Q_i\right|$ will cause ΔS_{Qi} to increase. These sensitivities should be greatest at bus i and its nearest neighbors, since VQ sensitivities identify the weakest areas in the system. Hence, a large $\left|\partial V_i/\partial Q_i\right|$ suggests that the approximation of the components of $\Delta\mathbf{S}$ has improved; thus, the initial mismatches associated with the low-voltage guesses should decrease accordingly. Consequently, the midpoint method should converge to the low-voltage solutions more reliably, as was suggested by Figures 4.16 and 4.17. Hence, under the assumptions that

transfer conductances are negligible and that voltage angles are largely independent of reactive power injection (approximations that are often employed in performing the fast decoupled load flow), the best initial guesses, and thus the most critical low-voltage solutions, will originate from either the most highly VQ-sensitive buses or their nearest neighbors. It should be noted, however, that this argument weakens as the system becomes more heavily stressed, because the approximations of the fast decoupled load flow become less valid.

For VQ sensitivities to be successful as a screening tool, they must provide a relative measure of the ability of buses to serve additional load. Figure 4.18 shows how VQ sensitivities fulfill this requirement for the symmetrical three-bus system. If this were a large system for which computational expense was a significant concern, the curves of Figure 4.18, which show how $|\partial V_i/\partial Q_i|$ varies as total system load increases, would suggest that bus 1 provides a lower-energy and, therefore, more critical low-voltage solution than bus 2, particularly as loading is increased. This result is encouraging, since it was found in Figure 4.2 that bus 1 does indeed lead to the critical solution and that bus 2 no longer provides a low-voltage solution beyond a total system load of 795 MW. Similiarly, appropriate indications are offered by Figure 4.19 for the IEEE 118-bus system investigated at the same set of buses as before. All the sensitivities increase as the load parameter increases, and the sensitivities corresponding to buses 43 and 44 increase most

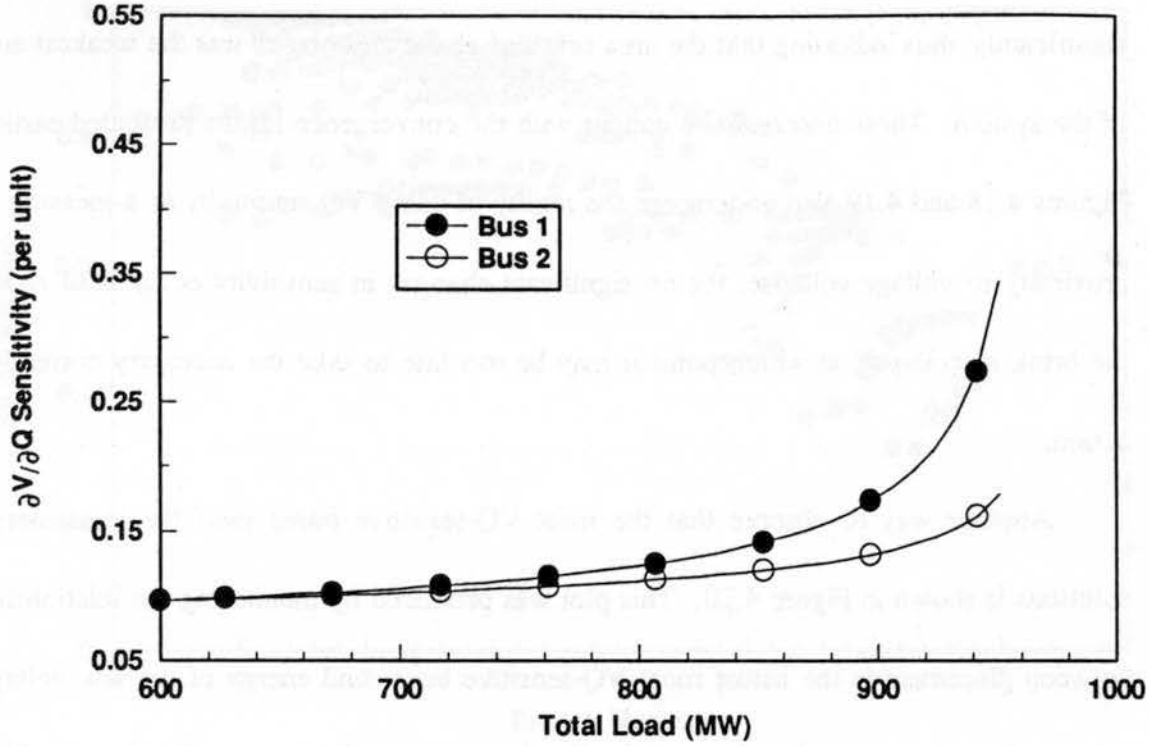

Figure 4.18: VQ sensitivities for three-bus system

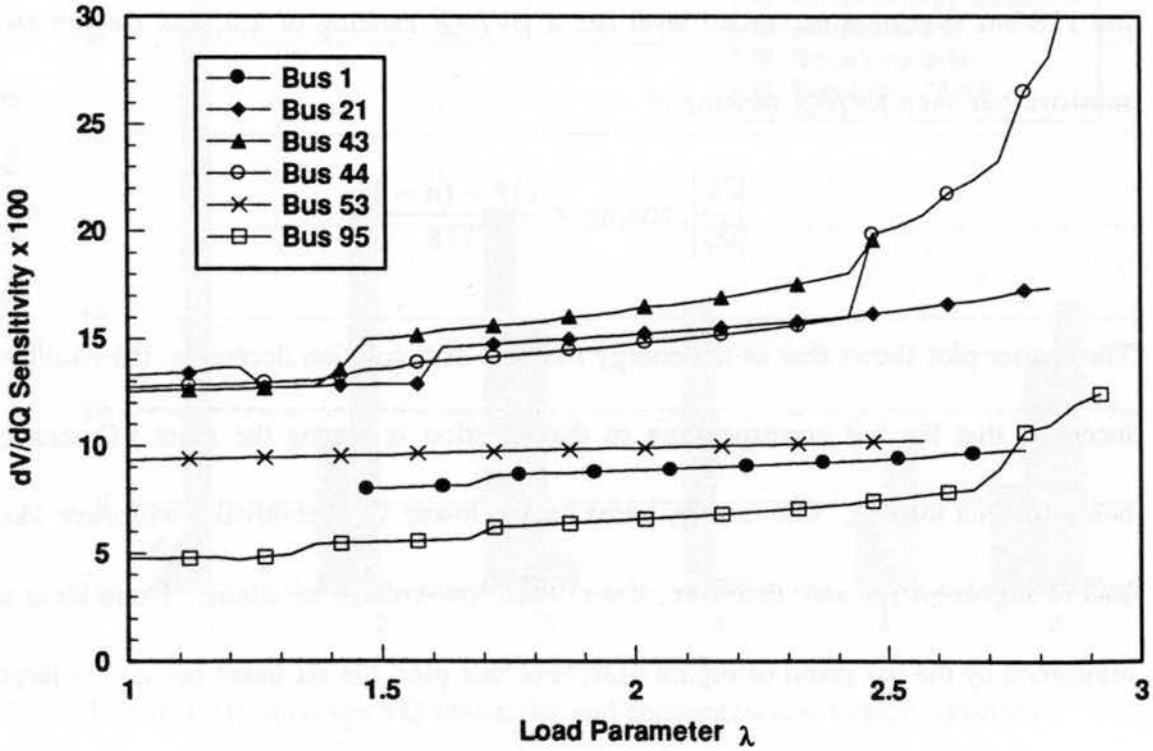

Figure 4.19: VQ sensitivities for IEEE 118-bus system

significantly, thus indicating that the area centered about these buses was the weakest area of the system. These observations concur with the convergence results presented earlier. Figures 4.18 and 4.19 also underscore the futility of using VQ sensitivity as a measure of proximity to voltage collapse, for no significant changes in sensitivity occur until nearly the brink of collapse, at which point it may be too late to take the necessary corrective action.

Another way to observe that the most VQ-sensitive buses yield the least-energy solutions is shown in Figure 4.20. This plot was produced by monitoring the relationship between placement in the list of most VQ-sensitive buses and energy of the low-voltage solution found from that bus for each loading between $\lambda = 2.0$ and $\lambda = 3.0$ for the IEEE 118-bus system. The vertical axis measures $|\partial V/\partial Q|$ ranking. The most sensitive bus of the 118-bus system at each load level has a $|\partial V/\partial Q|$ ranking of 1.0, and the nth most sensitive bus has a $|\partial V/\partial Q|$ ranking of

$$\left|\frac{\partial V}{\partial Q}\right| \text{ ranking} = \frac{118 - (n-1)}{118}. \tag{4.27}$$

The scatter plot shows that as the energy measure of a solution decreases, the likelihood increases that the bus corresponding to that solution is among the most VQ-sensitive buses for that loading. Conversely, buses having lower VQ sensitivities will more likely lead to higher-energy and, therefore, less critical, low-voltage solutions. These ideas are reinforced by the bar graph of Figure 4.21. For this plot, the six buses having the largest

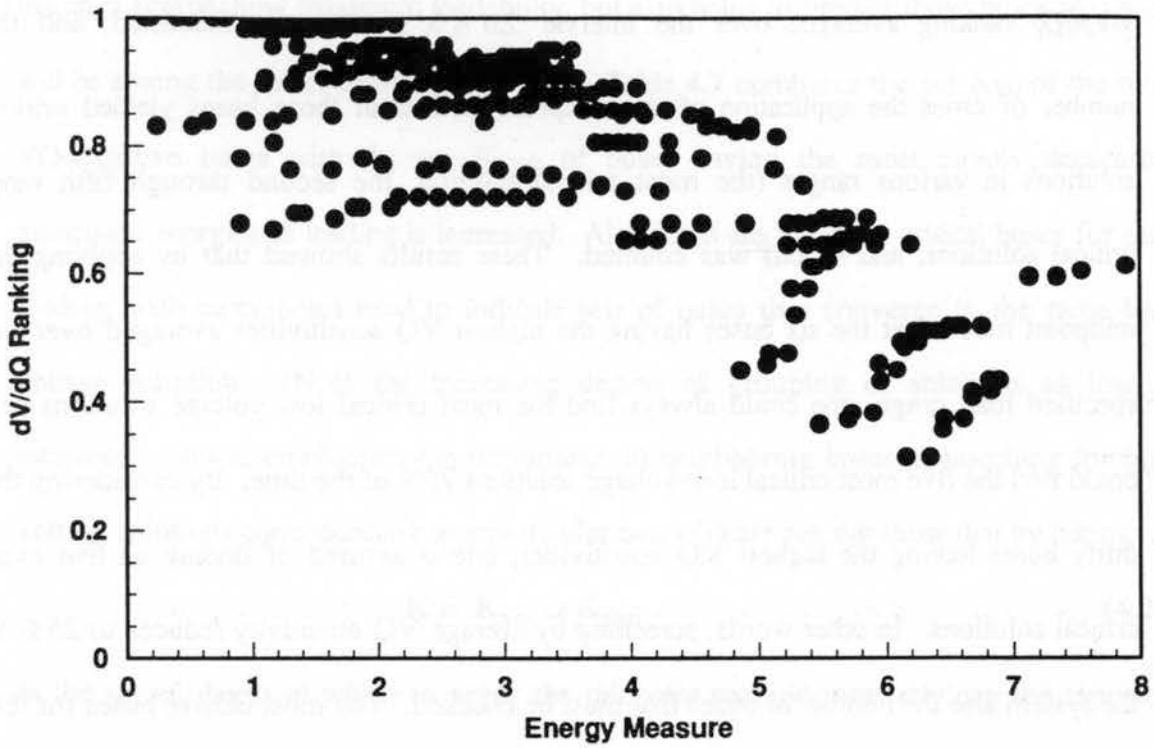

Figure 4.20: Relationship between VQ sensitivity and energy of solution

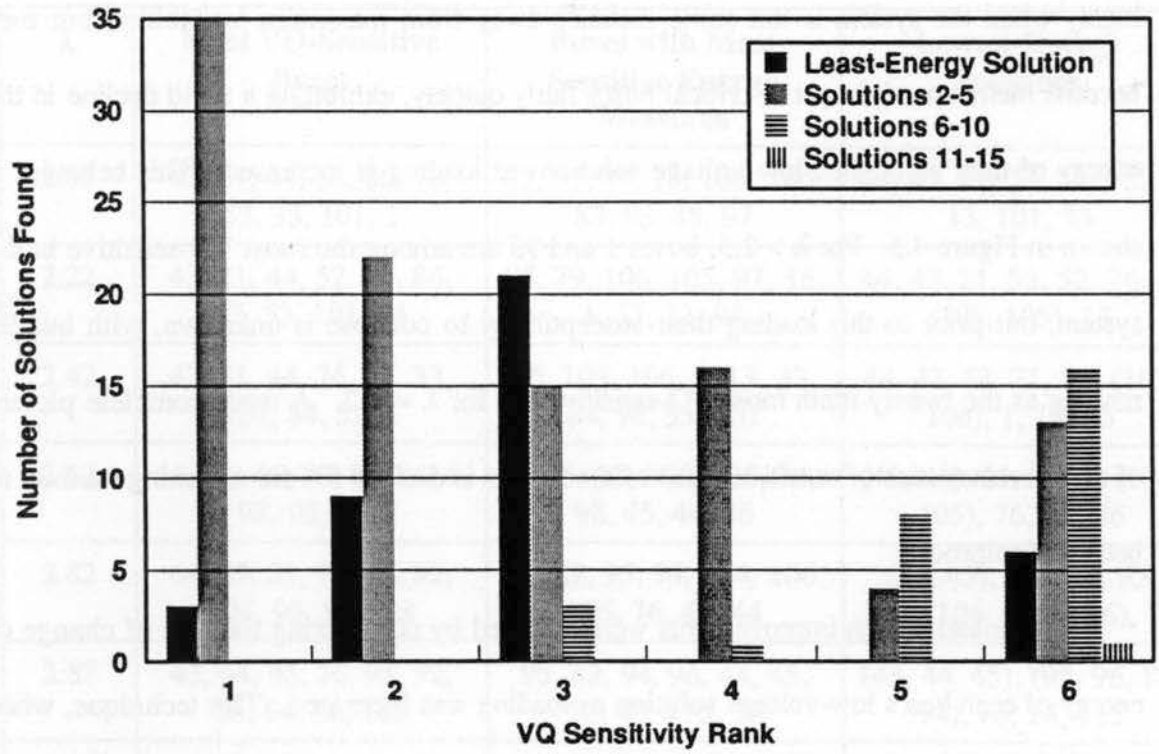

Figure 4.21: Average VQ sensitivity and convergence to critical solutions

$|\partial V/\partial Q|$ ranking averaged over the interval $2.0 \leq \lambda \leq 3.0$ were identified, and the number of times the application of the midpoint method at these buses yielded critical solutions in various ranges (the most critical solution, the second through fifth most critical solutions, and so on) was counted. These results showed that by applying the midpoint method at the six buses having the highest VQ sensitivities averaged over the specified load range, one could always find the most critical low-voltage solutions and could find the five most critical low-voltage solutions 75% of the time. By considering the thirty buses having the highest VQ sensitivities, one is assured of finding all five most critical solutions. In other words, screening by average VQ sensitivity reduces to 25% of the system size the number of buses that must be checked. The most elusive buses for this screening method are buses 1 and 95. The VQ sensitivity of these buses does not rank highly when the system is still some distance away from maximum loadability, but they become members of the set of critical buses fairly quickly, exhibiting a rapid decline in the energy of their associated low-voltage solutions as loading is increased. This behavior is shown in Figure 4.5. For $\lambda > 2.5$, buses 1 and 95 are among the most VQ-sensitive in the system, but prior to this loading their susceptibility to collapse is unknown, with bus 95 ranking as the twenty-ninth most VQ-sensitive bus for $\lambda = 2.2$. A more complete picture of the characteristics of sensitive areas of the system is desired for the screening method to become foolproof.

Fortunately, such improvements were afforded by considering the rate of change of energy of each bus's low-voltage solution as loading was increased. This technique, when combined with VQ-sensitivity considerations, not only identifies the most critical buses for

loadings approaching maximum loadability, but also helps to predict those buses that soon will be among the set of most critical buses. Table 4.7 compares the set $\mathbf{K}_{VQ}$ of the most VQ-sensitive buses with the set $\mathbf{K}_{ENG}$ of buses having the most rapidly decreasing associated energies as loading is increased. Also listed are the most critical buses for each loading, with parentheses used to indicate sets of buses that converge to the same low-voltage soltution. (Note the increasing degree of grouping of solutions as load is increased. This re-emphasizes the importance of neighboring buses in searching for low-voltage solutions corresponding to a particular bus.) These results show that by taking

$$\mathbf{K} = \mathbf{K}_{VQ} \cup \mathbf{K}_{ENG} \tag{4.28}$$

as the set of buses at which to apply the midpoint method, not only can the ten most

Table 4.7: Performance of the screening methods

λ	Most VQ-Sensitive Buses	Buses with Most Sensitive Energy Measures	Lowest-Energy Solutions
2.02	43, 21, 44, 52, 86, 76, 53, 33, 101, 1	82, 95, 79, 18, 106, 105, 83, 93, 88, 97	44, 43, 21, 53, 52, 76, 1, 13, 101, 33
2.22	43, 21, 44, 52, 76, 86, 33, 53, 101, 84	95, 79, 106, 105, 97, 16, 1, 13, 33, 98	44, 43, 21, 53, 52, 76, 1, (106, 105), 13
2.42	43, 21, 44, 76, 86, 33, 101, 84, 53, 1	95, 105, 106, 1, 13, 33, 84, 98, 53, 101	44, 43, 53, 21, 76, (105, 106), 1, 13, 95
2.62	44, 21, 45, 76, 33, 86, 1, 98, 95, 106	95, 1, 33, 106, 105, 76, 98, 45, 44, 86	(45, 44), 21, 95, 1, (106, 105), 76, 33, 86
2.82	44, 45, 21, 76, 95, 82, 104, 96, 106, 28	96, 82, 95, 94, 104, 106, 105, 76, 45, 44	(44, 45), (96, 94, 95, 82), (104, 105, 106), 76
2.87	43, 44, 45, 76, 95, 92, 86, 94, 28, 115	95, 82, 94, 96, 44, 45, 76, 43, 115, 28	(43, 44, 45), (95, 96, 82, 94), 76, 28, 115
2.92	95, 82, 96, 94, 28, 89, 115	93, 96, 94, 95, 82, 115, 28, 45	45, (95, 96, 94, 93, 82), 28, 115

sensitive buses at any given load be identified, but also the emerging weaknesses of buses 1 and 95 are noted in advance. In fact, bus 95 is identified when it is only the sixteenth most critical bus in the system. This can be very useful information, for it prompts the user to pay special attention to the area around bus 95 as loading is increased and to prepare to take corrective action in that area if necessary. Particularly encouraging is that, even when grouping of solutions is not considered, a maximum of sixteen power flows must be performed to find the ten most critical low-voltage solutions. Performance improves even further at higher loadings, where no more than twelve power flows are required to find the ten most critical solutions for $\lambda > 2.5$. When grouping of buses is considered, performance improves even more. Thus, the use of VQ-sensitivity screening, coupled with rate-of-change-of-energy considerations, is an expeditious and fairly reliable screening tool that greatly enhances the online application potential of the midpoint method.

CHAPTER 5

CONCLUSIONS

5.1 Introduction

The objective of this research has been to develop an improved method for determining type-one low-voltage power flow solutions that is sufficiently computationally inexpensive to be used in an online environment. The major contributions of this work and the future directions it will pursue are summarized in this chapter.

5.2 Contributions

The quest for low-voltage solutions is motivated by the desire to assess the voltage stability of a system far enough in advance that any necessary corrective actions may be taken. A class of assessment tools takes as its stability measure the distance in state space between the operable solution and various UEPs. In the case of static security assessment, only type-one UEPs are of interest, and each of these may be identified with a particular bus in the system, thus readily identifying the areas most prone to collapse and most in need of assistance. Given the wealth of material concerning voltage stability in the literature, it is somewhat difficult for the neophyte to identify some of the key components of the theory. Consequently, a great effort has been made to compile an extensive, cohesive review of some of the more significant aspects of voltage stability assessment, particularly as they relate to this work. A thorough understanding of this material should elucidate the motivation for conducting this research and thus grant more meaning to its results.

Moreover, a great number of pages have been devoted to presenting the theory of load flow computation and to demonstrating some of its idiosyncrasies and subtleties. Naturally, as this is not a formal treatise on the subject, some related issues, most notably the fast decoupled load flow, have been excluded from the discussion so as to focus on those issues most germane to the work's objectives. Since the midpoint method borrows liberally from the structure of the power flow equations, a detailed presentation of the development of the power balance equations was deemed essential. The benefit of this treatment has been that a variety of issues pertaining to the power flow have been consolidated in this work.

A number of techniques have been introduced during the past few years to find low-voltage solutions. A few such techniques are surveyed in this document. Though not a complete account of the great amount of work done on this subject, this discussion identifies a few methods that represent the wide variety of approaches. All the methods were found to be either too computationally expensive to be practical for online usage or lacking in the number of solutions they find. One interesting innovation introduced by this research is the eigenvector direction method which, although laborious to apply, illustrates some of the fundamental ideas incorporated into the midpoint method.

The midpoint method represents the key contribution of this research effort. Derived primarily from the structure of the power flow mismatch equations and employing a lone approximation on the manner in which systems approach collapse, the method was found to introduce little additional computation and to obtain initial guesses that generally reside quite close to the actual low-voltage solutions arising from them. The method

exhibits good convergence properties in tracking multiple load flow solutions over a wide load range toward the point of collapse; convergence to the solutions tends to occur within a reasonable number of power flow iterations, although this ability is somewhat suspect when the method is applied at generator buses. Its ability to track solutions was found to be invariant to load parametrization and the timing of var limit enforcement. Moreover, its convergence ability, initial guess accuracy, and rate of convergence compared quite favorably with those characteristics of one of the most popular low-voltage solution schemes, the simplified method, particularly when var limits were checked prior to convergence of the low-voltage power flow and when generator buses were excluded from the search. In light of these results, it was suggested that perhaps a reasonable approach would be to employ the simplified method at generator buses and the midpoint method at load buses, at least until a better approach is devised.

The final stage of this research focused on developing a screening technique to limit the number of buses at which the midpoint method must be applied to guarantee that all the critical low-voltage solutions had been determined. Using the square of the norm of the power flow mismatch equations at the initial guess as a screening quantity was seen to work well for small- to medium-sized systems because of the efficiency with which the midpoint method obtains initial guesses. For larger systems, for which the employment of the midpoint method at every bus becomes impractical, the use of VQ sensitivity as a screening tool was suggested. This parameter identifies the locally weakest buses in the system. When coupled with information regarding the rate at which buses are approaching collapse, VQ-sensitivity screening was able to compile a concise yet complete

list of buses to check for critical low-voltage solutions. Use of this screening tool greatly enhances the value of the midpoint method.

5.3 Future Directions

A number of issues concerning the midpoint method remain to be addressed. First, the performance of the algorithm when dependent load models are employed should prove rather interesting, particularly since the optimal multiplier, a key element of the midpoint algorithm, has difficulty when constant-current loads are present. Moreover, the performance of the algorithm at generator buses, which proved to be somewhat of an impediment in this research, should be improved. Addressing this issue will ultimately focus on the question of how var limits should be treated, for it seems doubtful that simply recasting PV buses as PQ buses set at maximum var limits is an adequate solution.

A novel idea that may hold promise both for the proper handling of var limits and for improving the rate of convergence is the concept of employing a variable approximation of the midpoint mismatch. The current approach always defines the approximation as a singleton. However, a better technique may be to define the elements of the vector according to what the actual midpoint mismatch had been for a previous low-voltage solution. This likely will result in more accurate initial guesses. More important, if a PV bus was found to be in violation of a var limit at the midpoint for a previous loading, it should be treated as var limited in the present solution; otherwise, type switching should be avoided. This is the kind of valuable information that adoption of a variable midpoint mismatch approximation may yield, thus meriting exploration in further pursuit of this work.

REFERENCES

[1] R. L. Devaney, *A First Course in Chaotic Dynamical Systems*. Reading, MA: Addison-Wesley, 1992.

[2] J. S. Thorp and S. A. Naqavi, "Load flow fractals," *Proc. 28th IEEE Decision and Control*, Tampa, FL, Dec. 1989, pp. 1822-1827.

[3] Y. Tamura, K. Iba, and S. Iwamoto, "A method for finding multiple load-flow solutions for general power systems," *Proc. IEEE 1980 PES Winter Meeting*, A80 043-0, New York, NY, Feb. 1980.

[4] C. L. DeMarco and T. J. Overbye, "An energy-based measure for assessing vulnerability to voltage collapse," *IEEE Trans. Power Syst.*, vol. PWRS-5, pp. 419-427, May 1990.

[5] P. W. Sauer and M. A. Pai, *Power System Dynamics and Stability*. Urbana, IL: University of Illinois, 1994.

[6] K. Iba, H. Suzuki, M. Egawa, and T. Watanabe, "A method for finding a pair of multiple load flow solutions in bulk power systems," *IEEE Trans. Power Syst.*, vol. PWRS-5, pp. 582-591, May 1990.

[7] W. Ma and J. S. Thorp, "Solving for all the solutions of power system equations," *Proc. 1992 ISCAS*, San Diego, CA, May 1992.

[8] G. W. Stagg and A. H. El-Abiad, *Computer Methods in Power System Analysis*. New York: McGraw-Hill, 1968.

[9] Electric Power Research Institute, "Voltage Stability: Basic Concepts, Analysis Objectives, and Existing Tools", Project RP3040-1, 1992.

[10] S. Iwamoto and Y. Tamura, "A load flow calculation method for ill-conditioned power systems," *IEEE Trans. Power Appar. & Syst.*, vol. PAS-100, pp. 1736-1743, April 1981.

[11] A. Klos and A. Kerner, "The nonuniqueness of load flow solution," *Proc. PSCC-5*, 3.1/8, Cambridge, 1975.

[12] T. J. Overbye, "A power flow measure for unsolvable cases," *IEEE Trans. Power Syst.*, vol. 9, pp. 1359-1365, Aug. 1994.

[13] T. J. Overbye, "Computation of a practical method to restore power flow solvability," *IEEE Trans. Power Syst.*, vol. 10, pp. 280-287, Feb. 1995..

[14] M. A. Pai and V. Ajjarapu, "Voltage Stability in Power Systems - An Overview," in *Recent Advances in Control and Management of Power Systems*, D. P. Sen Gupta, Ed. Bangalore, India: Interline Publishing, 1993.

[15] T. J. Overbye, M. A. Pai, and P. W. Sauer, "Some aspects of the energy function approach to angle and voltage stability analysis in power systems," *Proc. 31st IEEE Decision and Control*, Tuscon, AZ, Dec. 1992, pp. 2941-2946.

[16] T. J. Overbye, "Effects of load modelling on analysis of power system voltage stability," *Electric Power & Energy Systems*, vol. 16, no. 5, pp. 329-337, Jan. 1994.

[17] T. J. Overbye, "Application of an energy based security method to voltage instability in electrical power systems," Ph.D. dissertation, Univ. of Wisconsin, Madison, WI, 1991.

[18] F. L. Alvarado and T. H. Jung, "Direct detection of voltage collapse conditions," *Proceedings: Bulk Power System Voltage Phenomena - Voltage Stability and Security*, EPRI Report EL-6183, Jan. 1989.

[19] A. Tiranuchit and R. J. Thomas, "A posturing strategy against voltage instabilities in electric power systems," *IEEE Trans. Power Syst.*, vol. PWRS-3, pp. 87-93, Feb. 1988.

[20] A. Yokoyama and Y. Sekine, "A static voltage stability index based on multiple load flow solutions," *Proceedings: Bulk Power System Voltage Phenomena - Voltage Stability and Security*, EPRI Report EL-6183, Jan. 1989.

[21] M. A. Pai and P. W. Sauer, "Power system analysis by Lyapunov's direct method," *IEEE Control Syst. Mag.*, Jan. 1989.

[22] H. Chiang and J. S. Thorp, "The closest unstable equilibrium point method for power system dynamic security assessment," *IEEE Trans. Circuits & Syst.*, vol. CAS-36, pp. 1187-1200, Sept. 1989.

[23] I. Dobson and H. Chiang, "Towards a theory of voltage collapse in electric power systems," *Syst. Control Lett.*, pp. 253-262, June 1989.

[24] F. M. A. Salam, L. Ni, S. Guo, and X. Sun, "Parallel processing for the load flow of power systems: the approach and applications," *Proc. 28th Conf. Decision and Control*, Tampa, FL, Dec. 1989, pp. 2173-2185.

[25] W. H. Press, B. P. Flannery, S. A. Teukolsky, and W. T. Vetterling, *Numerical Recipes in Pascal*. Cambridge: Cambridge University Press, 1989.

[26] W. F. Tinney, V. Brandwajn, and S. M. Chan, "Sparse vector methods," *IEEE Trans. Power Appar. & Syst.*, vol. PAS-104, pp. 295-301, Feb. 1985.

[27] T. J. Overbye and C. L. DeMarco, "Improved techniques for power system voltage stability assessment using energy methods," *IEEE Trans. Power Syst.*, vol. 6, pp. 1446-1452, Nov. 1991.

[28] T. J. Overbye, "Use of energy methods for on-line assessment of power system voltage security," *IEEE Trans. Power Syst.*, vol. 8, pp. 452-458, May 1993.